

**THE INFLUENCE OF LEAF PIGMENTS, PHENOLOGY, AND SOLAR  
RADIATION REGIME ON REMOTELY SENSED ESTIMATES OF  
PHOTOSYNTHETIC EFFICIENCY AND PHOTOSYNTHETIC POTENTIAL,  
CANOPY PHOTOSYNTHESIS, AND NET ECOSYSTEM EXCHANGE**

A Dissertation

Presented in Partial Fulfillment of the Requirements for the

*Degree of Doctor of Philosophy*

with a

Major in Natural Resources

in the

College of Graduate Studies

University of Idaho

by

Steven R. Garrity

May 2010

Major Professor: Lee A. Vierling, Ph.D.

UMI Number: 3414286

All rights reserved

**INFORMATION TO ALL USERS**

The quality of this reproduction is dependent upon the quality of the copy submitted.

In the unlikely event that the author did not send a complete manuscript and there are missing pages, these will be noted. Also, if material had to be removed, a note will indicate the deletion.



UMI 3414286

Copyright 2010 by ProQuest LLC.



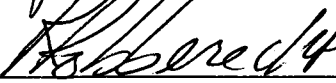
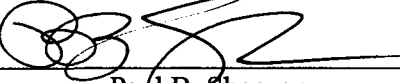
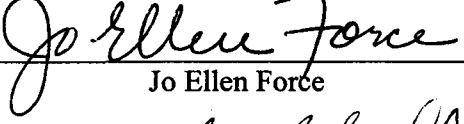
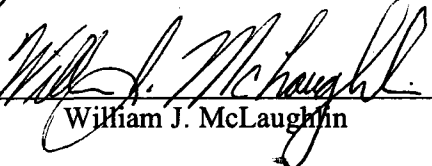
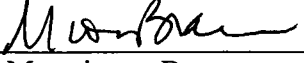
All rights reserved. This edition of the work is protected against unauthorized copying under Title 17, United States Code.



ProQuest LLC  
789 East Eisenhower Parkway  
P.O. Box 1346  
Ann Arbor, MI 48106-1346

## AUTHORIZATION TO SUBMIT DISSERTATION

This dissertation of Steven R. Garrity, submitted for the degree of Doctor of Philosophy with a major in Natural Resources and titled, "The Influence of Leaf Pigments, Phenology, and Solar Radiation Regime on Remotely Sensed Estimates of Photosynthetic Efficiency and Photosynthetic Potential, Canopy Photosynthesis, and Net Ecosystem Exchange", has been reviewed in final form, as indicated by the signatures and dates given below. Permission, as indicated by the signatures and dates given below, is now granted to submit final copies to the College of Graduate Studies for approval.

Major Professor	 Lee A. Vierling	Date <u>5/7/2010</u>
Committee Members	 Jeffrey A. Hicke	Date <u>5/7/10</u>
	 Ronald R. Robberecht	Date <u>5-7-10</u>
	 Paul B. Shepson	Date <u>5/11/10</u>
Department Administrator	 Jo Ellen Force	Date <u>5-13-2010</u>
Discipline's College Dean	 William J. McLaughlin	Date <u>5-14-2010</u>
Final Approval and Acceptance by the College of Graduate Studies		
	 Margrit von Braun	Date <u>5/18/10</u>

## ABSTRACT

### THE INFLUENCE OF LEAF PIGMENTS, PHENOLOGY, AND SOLAR RADIATION REGIME ON REMOTELY SENSED ESTIMATES OF PHOTOSYNTHETIC EFFICIENCY AND PHOTOSYNTHETIC POTENTIAL, CANOPY PHOTOSYNTHESIS, AND NET ECOSYSTEM EXCHANGE

Understanding the interactions between plant canopies and the environment is important for elucidating past, current, and future carbon cycle dynamics. Developments in instrumentation and modeling present new opportunities for quantifying the processes controlling photosynthesis at a variety of spatial and temporal scales, and thus are vital for estimating terrestrial carbon assimilation globally. The remote sensing based photochemical reflectance index (PRI) represents one such methodological advance. Leaf- and canopy-level PRI observations were combined with leaf optical and radiative transfer simulation models to elucidate the interactions between phenological changes in canopy structure, pigments, and physiology and reflectance-based estimates of photosynthetic radiation use efficiency. Simulation modeling results demonstrated that the PRI is significantly influenced by the carotenoid/chlorophyll ratio, photosynthetic acclimation, and changes in canopy structure. Equations describing the relationship between leaf pigments and spectral vegetation indices were developed with simulation models and used for prediction of carotenoid content. Empirically-based relationships between sky diffuse fraction and forest carbon assimilation were used to estimate the potential consequences of changing global radiation regimes on biosphere-atmosphere exchange of CO<sub>2</sub>. Simulations showed that a 1% increase/decrease in forest carbon assimilation occurs for every 1% increase/decrease in shortwave radiation that results from changes in sky diffuse fraction. Simulation results also showed no significant advantage of moderately diffuse skies compared to clear skies for total growing season carbon assimilation. The results of this dissertation demonstrate that the PRI should be considered to be more broadly useful for understanding photosynthetic efficiency and photoprotection than previously assumed. Such measurements may be useful for national efforts to understand the influence of climate change on terrestrial ecosystem carbon cycling.

## ACKNOWLEDGMENTS

I would like to acknowledge my major professor, Dr. Lee A. Vierling, for his guidance and encouragement throughout my graduate program. I would like to thank Dr. Vierling for giving me the freedom to pursue my ideas regardless of the risks involved, and for providing numerous opportunities for me to grow and succeed. I would also like to acknowledge my committee members, Drs. Ronald Robberecht, Jeffrey Hicke, and Paul Shepson. Dr. Robberecht has been a continual source of personal and professional guidance. His influence on both my personal pedagogy and research philosophy will undoubtedly prove to be indelible. Dr. Hicke has asked challenging questions that have forced me to see things from a different perspective. Finally, I am grateful for Dr. Shepson's incessant encouragement to publish my work. 'If it isn't published, it didn't happen' has been a continual source of motivation as I wrote the manuscripts that eventually formed this dissertation.

I would like to acknowledge the University of Michigan Biological Station's Biosphere-Atmosphere Research and Training (BART) program, which provided funding for a large portion of my research. I am grateful for my fellow BART students and BART-associated faculty and scientists who provided helpful suggestions that improved my research or who aided in field-based data collection. I am especially indebted to BART faculty members Hans Peter Schmid and Steve Bertman who greatly enriched my experience as a BART student, and to BART students Brady Hardiman, Kim Mueller, and Alan Talhelm who were always willing to lend a helping hand or engage in critical discussion of all things occurring at the biosphere-atmosphere interface. Finally, I am greatly indebted to Dr. Christoph Vogel for promptly answering countless requests for data, and for providing assistance with portions of my field work.

Several individuals have provided data, assistance with data analysis, critical evaluation of my work, encouragement, and helpful discussion at various stages of my graduate program. Most notable among these have been Peter Curtis, Anthony Davis, Danilo Dragoni, Jan Eitel, Michael Falkowski, Thomas Hilker, John Marshall, Sebastian Martinuzzi, Alistair Smith, and Andrew Turnipseed. I would also like to

acknowledge Keith Bickford and Jan Eitel for coauthoring portions of this dissertation.

This research was funded by an NSF IGERT fellowship (NSF grant DGE-0504552) awarded by the University of Michigan Biosphere-Atmosphere Research Training (BART) program to S. Garrity (BART), NSF grant DBI-0537040 (L. Vierling, PI), an NSF-EPSCoR grant to the State of Idaho, and US Department of Energy Cooperative Agreement No. DE-FC03-90ER610100.

## DEDICATION

I wish to dedicate this dissertation to my wife and good friend Keely Garrity, and to my two children Brock and Madison. The love, patience, encouragement, and motivation they provided throughout my graduate program have been an invaluable resource to me. I look forward to continuing this adventure alongside each of you. I also wish to thank my parents, Michael and Cynthia, for their support throughout my entire educational journey.

## TABLE OF CONTENTS

Title page .....	i
Authorization to submit dissertation .....	ii
Abstract.....	iii
Acknowledgements.....	iv
Dedication.....	vi
Table of contents.....	vii
List of Tables .....	xi
List of Figures.....	xiii
Introduction.....	1
References .....	5

### CHAPTER 1. TEMPORAL ASSESSMENT OF PRI FROM A DECIDUOUS FOREST CANOPY: THE ROLE OF PHENOLOGICAL CHANGES IN PIGMENTS AND PHOTOSYNTHETIC POTENTIAL AND DIURNAL CHANGES IN PHOTOSYNTHETIC RADIATION USE EFFICIENCY

Abstract .....	14
Introduction.....	15
Methods.....	16
Site description.....	16
CO <sub>2</sub> fluxes and calculation of radiation use efficiency.....	17
Reflectance measurements.....	18
Leaf and canopy reflectance modeling .....	19
Statistical analysis.....	21
Results.....	21



Seasonal trends.....	21
Leaf and canopy level simulations.....	22
Discussion.....	23
Acknowledgements.....	27
References.....	27
Tables.....	35
Figures.....	37

## CHAPTER 2. INFLUENCE OF LEAF CHLOROPHYLL AND CAROTENOID CONTENT ON THE PHOTOCHEMICAL REFLECTANCE INDEX

Summary.....	46
Introduction.....	47
Materials and methods.....	49
Leaf measurements.....	49
Model simulations.....	51
Leaf pigment content prediction.....	52
Statistical analysis.....	52
Results.....	53
Leaf pigments.....	53
Influence of pigments on PRI.....	53
Combined index carotenoid prediction.....	53
Discussion.....	54
Acknowledgments.....	57
References.....	58
Figures.....	63

## CHAPTER 3. A SIMPLE FILTERED PHOTODIODE INSTRUMENT FOR CONTINUOUS MEASUREMENT OF NARROWBAND NDVI AND PRI OVER VEGETATED CANOPIES

Abstract.....	73
Introduction.....	74
Background theory.....	74
Instrument design and technical specifications.....	78
Photodiodes.....	78
Narrow bandpass filters .....	78
Data logging.....	79
Circuit design.....	80
Housing.....	81
Irradiance and radiance instrumentation.....	81
Spectrometer comparison.....	83
Instrument performance.....	83
Discussion and conclusions .....	84
Acknowledgements.....	86
References.....	86
Figures.....	93

#### CHAPTER 4. ESTIMATING THE INFLUENCE OF CHANGING SKY DIFFUSE FRACTION ON GROSS AND NET CARBON ASSIMILATION

Abstract.....	102
Introduction.....	103
Materials and methods.....	104
Site description.....	104
Meteorological and CO <sub>2</sub> flux measurements.....	104
Light response curves .....	106
Modeling the response of GPP and NEE to changes in sky condition .....	106
Results.....	107
Meteorological variables.....	107

Response of RUE, NEE, and GPP to SDF.....	108
Variation in carbon assimilation under simulated changes in SDF ...	109
Discussion.....	110
Acknowledgments.....	113
References.....	113
Tables.....	118
Figures.....	122
 CONCLUSIONS AND FUTURE WORK.....	 130

## LIST OF TABLES

### CHAPTER 1

**Table 1.** Leaf chlorophyll and carotenoid content for deciduous tree species from the LOPEX database, Guo and Trotter (2004), and Liu et al. (2009). Pigment values reported by Liu et al. (2009) were obtained across a developmental gradient: juvenile (J), young (Y), mature (M) and senescent (S). .....35

**Table 2.** Slope and intercept of the linear least squares relationship between incident PPFD and the PRI and changes in canopy quantum efficiency ( $\alpha$ ) and canopy photosynthetic potential ( $\beta$ ) derived from fitted light response curves for three time periods, where 1 = days 140-145, 2 = days 146-153, and 3 = days 198-219. Numbers in parentheses are the 95% confidence intervals of the regression coefficients. ....36

### CHAPTER 2

**Table 1.** Summary of CO<sub>2</sub> exchange and environmental conditions during the study period. Values are reported as the mean  $\pm$  95% confidence interval of hourly averaged values measured under each sky diffuse fraction (SDF) classification. ....118

**Table 2.** Estimates of canopy quantum efficiency ( $\alpha$ ), canopy photosynthetic potential ( $\beta$ ), and the coefficient of determination from least squares regression ( $r^2$ ). .....119

**Table 3.** Percent change in biosphere-atmosphere exchange of CO<sub>2</sub> that would be expected with uniform brightening or dimming of the sky. Results are reported as the percent change from the baseline. The 95% confidence interval for all estimates is  $\pm$  0.5%. .....120

**Table 4.** Percent change in biosphere-atmosphere exchange of CO<sub>2</sub> with simulated changes in the proportion of each SDF class, where Sunny = SDF < 0.35, Partly cloudy = SDF > 0.35 & < 0.65, and Cloudy = SDF > 0.65. Results are reported as the % deviation from the baseline. The 95% confidence interval for all estimates is ± 0.5%. .....121

## LIST OF FIGURES

### CHAPTER 1

- Figure 1.** Mean daily values of (a) PRI, (b) RUE, and (c) LAI. Error bars represent the standard deviation of each daily mean. The break in the x-axes signifies the difference between data collected in 2006 (left) and 2007 (right).....37
- Figure 2.** Regression results for the relationship between daily averaged RUE and PRI. Error bars represent the standard deviation for daily averages of the PRI. ....38
- Figure 3.** Regression results for the relationship between PRI and APPFD during the fully leafed out period (closed circles), and between the residuals from the PRI-LAI regression and APPFD during the green up period (open circles).....39
- Figure 4.** Regression between the BRDF isotropic kernel weight and the strata for (a) LAI, (b) RUE, and (c) SDF. The coefficient of determination was significant for LAI and RUE, but not significant for SDF. ....40
- Figure 5.** Prospect simulation results, where (a) is the response of simulated PRI to carotenoid content (closed circles) or chlorophyll content (open circles). In each case one pigment was increased from 0 to 100  $\mu\text{g cm}^{-2}$  at 5  $\mu\text{g cm}^{-2}$  increments while the other was held constant at 0  $\mu\text{g cm}^{-2}$ . (b) The response of simulated PRI to increasing Chl content, where Car content was varied as a constant fraction Chl content. (c) The response of simulated PRI to increasing Chl/Car ratios, where the vertical lines represent the range of resulting values for each ratio that occurred due to variability in Chl content, and closed circles represent the mean for each ratio. Chlorophyll content was varied between 1 and 120  $\mu\text{g cm}^{-2}$  for each ratio simulation.....41

**Figure 6.** PROSAIL simulated canopy level PRI values with increasing (a) LAI or (b) Chl/Car ratio, where the vertical lines represent the range of resulting values for each ratio that occurred due to variability in Chl content, and closed circles represent the mean for each ratio. Chlorophyll content was varied between 1 and 120  $\mu\text{g cm}^{-2}$  for each ratio simulation .....43

**Figure 7.** Results from PROSAIL simulations where envelopes represent the range of PRI values expected as LAI increased for a range of Chl/Car ratios (a-f) .....44

**Figure 8.** Conceptual diagram of the expected seasonal PRI trend for a deciduous forest canopy based on the results of our study. The size of the arrow next to the variable (LAI, Chl, Car, or Chl/Car ratio) indicates the magnitude of change in that variable during the time period in which it occurs (green up, mature, or senescence). The symbols to the right of the variable names indicate the influence that each will have on the PRI, where (+) indicates an increase, (-) indicates a decrease, and (x) indicates no effect. The subset figure represents a typical diurnal trend, where the PRI response is primarily a function of changes in xanthophyll pigments .....45

## CHAPTER 2

**Figure 1.** Least square regression between chlorophyll and carotenoid content from leaves sampled in this study (closed circles) and from the LOPEX database (open circles).....63

**Figure 2.** Least squares regression between the carotenoid/chlorophyll ratio and chlorophyll content (a) and carotenoid content (b) for leaves sampled in this study (closed circles) and from the LOPEX database (open circles). Solid lines are the least squares fit for the leaf data and dashed lines are the least squares fit for the LOPEX data .....64

**Figure 3.** Least squares regression of leaf-derived (measured) PRI and PROSPECT-simulated (simulated) PRI versus chlorophyll content (a, d), carotenoid content (b, e), and the carotenoid/chlorophyll ratio (c, f). Closed circles represent leaves sampled for this study and closed circles represent data from the LOPEX database. In panels (a), (b), (d), and (e) solid lines are the least squares fit for the leaf data and dashed lines are the least squares fit for the LOPEX data. In panels (c) and (f) a single least squares line was fit to all data .....65

**Figure 4.** Response of PROSPECT-simulated PRI to carotenoid content (closed circles) or chlorophyll content (open circles). In each case one pigment was increased from 0 to 100  $\mu\text{g cm}^{-2}$  at 5  $\mu\text{g cm}^{-2}$  increments while the other was held constant at 0  $\mu\text{g cm}^{-2}$  .....66

**Figure 5.** PROSPECT-simulated PRI versus the carotenoid/chlorophyll ratio. The curvilinear model fitted to these data was used to predict the leaf carotenoid/chlorophyll ratio using leaf measurements of PRI .....67

**Figure 6.** PROSPECT-simulated CI versus chlorophyll content. The linear model fitted to these data was used to predict leaf chlorophyll content using leaf measurements of CI .....68

**Figure 7.** Fitted values of PROSPECT-simulated CI versus chlorophyll content across a range of carotenoid contents. Carotenoid content did not significantly influence the CI-chlorophyll relationship .....69

**Figure 8.** Predicted carotenoid content (PRI(c<sub>lm</sub>) x CI(l<sub>m</sub>)) versus measured carotenoid content. Closed circles represent data measured for this study and open circles represent data obtained from the LOPEX database. The dashed line represents the 1:1 relationship. Slope = 0.93, intercept = 0.46  $\mu\text{g cm}^{-2}$ , RMSE = 1.43  $\mu\text{g cm}^{-2}$  ..70



**Figure 9.** The carotenoid prediction equation ( $PRI(c_{lm}) \times CI(lm)$ ) versus carotenoid content across a range of chlorophyll contents. Chlorophyll content did not significantly influence the predicted versus measured relationship. The dashed line represents the 1:1 relationship .....71

**Figure 10.** The carotenoid/chlorophyll ratio versus either chlorophyll content (closed circles) or carotenoid content (open circles). The solid line represents the least squares fit for chlorophyll content and the dashed line represents the least squares fit for carotenoid content. Data from Nakaji et al. (2006).....72

### CHAPTER 3

**Figure 1.** Photosensitivity of the silicon photodiode used in the QuadPod instruments (data from Hamamatsu Corporation). The wavelengths used to calculate vegetation indices from the photodiode sensors in this study are denoted by vertical gray lines at 532, 568, 676 and 800 nm.....93

**Figure 2.** Photodiode voltage response using four different narrow bandpass filters. These data were generated using an ellipsometer set at a 1 nm wavelength sampling interval as a light source. The full width half maximum and peak transmissivity values of the bandpass filters (as specified by the manufacturer) are denoted by gray and dashed lines, respectively.....94

**Figure 3.** Electrical schematic of the current to voltage converter, including amplification circuit necessary for use with Hobo data loggers .....95

**Figure 4.** (A) Image of QuadPod instrument complete with irradiance and radiance sensor heads and data logger housing. (B) Image of QuadPod radiance and irradiance sensor heads mounted at a field-based study location .....96

<b>Figure 5.</b> Housing and parts schematic of QuadPod irradiance and radiance sensor heads .....	97
<b>Figure 6.</b> (A) Comparison of the normalized ideal cosine response and the normalized response between a LI-COR quantum sensor (LI-190) and a 676 nm and 800 nm filtered photodiode from the QuadPod fitted with a Teflon <sup>®</sup> diffusing disc. (B) The percent deviation of each detector's response from the ideal cosine response .....	98
<b>Figure 7.</b> Comparison of transmitted radiation through bare bandpass filters and bandpass filters with a Teflon diffuser.....	99
<b>Figure 8.</b> Regression between UniSpec instrument and the QuadPod at (a) 532 nm, (b) 568 nm, (c) 676 nm, and (d) 800 nm. Coefficients of determination were 0.992, 0.989, 0.997, and 0.994 respectively. Deviations from a 1:1 relationship are a function of the fixed integration time for the UniSpec instrument .....	100
<b>Figure 9.</b> Comparison of flux-tower measured Net Ecosystem Exchange (NEE) of CO <sub>2</sub> and a) NDVI and b) PRI for three days immediately prior to a precipitation event at a desert grassland ecosystem (Julian dates 181-183 of 2009) and three days immediately following the precipitation event (Julian dates 187-189). The sign convention for NEE is such that negative values indicate a net flux to the ecosystem. Data courtesy of M. Litvak and A. Fox .....	101

## CHAPTER 4

<b>Figure 1.</b> Light response curves of (a) NEE under sunny (SDF < 0.5) and cloudy (SDF > 0.5) sky conditions, and (b) GPP under sunny (SDF < 0.35), partly cloudy (SDF > 0.35 and < 0.65), and cloudy (SDF > 0.65) sky conditions .....	122
--	-----

**Figure 2.** Response of hourly (a) NEE, (b) GPP, and (c) RUE to SDF. Data are from daylight hours (600 – 1800) during the growing season.....123

**Figure 3.** The relationship between SDF and NEE during (a) midday, (b) mid-morning and mid-afternoon, and (c) early morning and late afternoon. Solid circles represent data collected prior to solar noon and open circles represent data collected after solar noon. Vertical lines represent the optimal SDF for the time period prior to solar noon (solid line) and after solar noon (dashed line).....124

**Figure 4.** The response of sky condition-averaged NEE to incident PPFD during (a) midday prior to solar noon, (b) midday after solar noon, (c) mid-morning, (d) mid-afternoon, (e) early morning, and (f) late afternoon. The numbers beside each data point represent the sky condition class, where 1 = sunny, 2 = partly cloudy, and 3 = cloudy. The solid line is the light response curve fit to the data within each given time period, and the dashed line is the light response curve of all the data pooled together .....125

**Figure 5.** The relationship between SDF and GPP during (a) midday, (b) mid-morning and mid-afternoon, and (c) early morning and late afternoon. Solid circles represent data collected prior to solar noon and open circles represent data collected after solar noon. Vertical lines represent the optimal SDF for the time period prior to solar noon (solid line) and after solar noon (dashed line).....126

**Figure 6.** The response of sky condition-averaged GPP to incident PPFD during (a) midday prior to solar noon, (b) midday after solar noon, (c) mid-morning, (d) mid-afternoon, (e) early morning, and (f) late afternoon. The numbers beside each data point represent the sky condition class, where 1 = sunny, 2 = partly cloudy, and 3 = cloudy. The solid line is the light response curve fit to the data within each given time period, and the dashed line is the light response curve of all the data pooled together .....127

**Figure 7.** Estimated response of total growing season (a)  $A_n$ , and (b)  $A_g$  to simulated uniform brightening (closed circles) and dimming (open circles) scenarios. Data points are the mean from 100 bootstrapped estimates and error bars represent the 95% confidence interval. The horizontal dashed lines represent the upper and lower 95% confidence bounds on the bootstrapped estimate of the mean of the observed data .....128

**Figure 8.** Estimated response of total growing season (a)  $A_n$ , and (b)  $A_g$  to simulated changes in the proportion of each sky condition class. Data points are the mean of 100 simulations and error bars represent the 95% confidence interval. The horizontal dashed lines represent the upper and lower 95% confidence bounds on the bootstrapped estimate of the mean of the observed data .....129

## INTRODUCTION

Globally, terrestrial ecosystem photosynthesis and respiration significantly influence patterns of atmospheric carbon dioxide (CO<sub>2</sub>) concentration (Randerson et al., 1997; Fan et al., 1998; Houghton, 2000), and thus are important processes to understand for quantifying and modeling past, current, and future trends in the carbon cycle (Schimel, 1995; Schlesinger, 1997). Broad scale (temporal and spatial) variability in plant canopy photosynthesis is often attributed to factors such as climate, species composition, leaf area and growing season length (Asner et al., 1998; White et al., 1999; Knapp & Smith, 2001; Hicke et al. 2002; Law et al., 2002; Lindroth et al., 2008; Duursma et al., 2009). However, localized and short-term (i.e., daily to seasonal) variability in plant canopy photosynthesis is predominantly influenced by the amount and quality of photosynthetically active radiation (PAR) absorbed by plant canopies (Hollinger et al. 1999; Gu et al., 2003; Oliphant et al., 2006) as well as the efficiency with which absorbed radiation is used to convert CO<sub>2</sub> into carbohydrates (Monteith, 1972, 1977). Absorbed PAR is a function of (a) incident PAR and (b) the fraction of PAR (fPAR) absorbed by a plant canopy, where incident PAR is dependent on latitude, topographical features, and atmospheric aerosols and clouds (Dubayah & Vankatwijk, 1992; Grant et al. 1996; Oliphant et al., 2006), and fPAR is largely determined by the amount of green biomass within a plant canopy and to a lesser extent by characteristics such as leaf angle distribution, leaf cellular structure, and leaf biochemistry (Sellers, 1985; Clearwater & Gould, 1995; Campbell & Norman, 1998; Ustin et al., 2009). Diurnal and seasonal variation in canopy radiation use efficiency (RUE (mol C mol photon<sup>-1</sup>)) is primarily a result of physiological responses to short-term variations in environmental conditions (Hari & Makela, 2003; Richardson et al., 2007; Polley et al., 2010). Several studies have demonstrated the importance of accurately describing RUE when estimating canopy-atmosphere exchange of CO<sub>2</sub> (e.g., Asner et al., 2004; Bradford et al. 2005; Yuan et al. 2007). Therefore, the ability to quantify canopy structure, biomass, and physiology is essential for understanding the role of plant canopy productivity in carbon cycle dynamics.

Advances in theory, modeling, and instrumentation have provided significant contributions to our ability to quantify plant canopy photosynthesis across a wide range of spatial and temporal scales. For example, the eddy covariance method provides high temporal resolution measurements of biosphere-atmosphere CO<sub>2</sub> exchange across spatial scales of approximately 1 km, depending on atmospheric boundary layer conditions (Baldocchi et al., 1988, Baldocchi, 2003). This method has been an integral component of international efforts to understand processes controlling terrestrial ecosystem productivity (Aubinet et al., 2000; Baldocchi et al., 2001). However, one obstacle to linking the processes controlling photosynthesis at the leaf level with the canopy level and beyond is the mismatch in sampling scale between cuvette- and meteorological-based approaches (Moncrieff et al., 1996; Gamon et al. 2006). The development and use of optical remote sensing methods has provided opportunities for quantifying both structural and physiological components of plant canopies across a nearly limitless range of spatial and temporal scales. For example, the normalized difference vegetation index (NDVI) and similar spectral vegetation indices have been used broadly to estimate several leaf and plant canopy characteristics including chlorophyll content (*e.g.*, Gamon and Surfus 1999), leaf area index (*e.g.*, Carlson and Ripley 1997), fPAR (*e.g.*, Sims et al. 2006), and green biomass (*e.g.*, Sellers 1985). These 'greenness' vegetation indices are a vital component of several biosphere-atmosphere models, which are used to estimate global primary productivity (*e.g.*, CASA, Potter et al., 1993; 3PGS, Coops et al., 1998; MOD-17, Running et al., 2004). Although these vegetation indices are well suited for quantifying canopy structural variables that determine the absorption of PAR, they lack the ability to describe the physiological changes in radiation use efficiency that is necessary for accurate estimation of ecosystem productivity.

Recent developments have produced optical remote sensing methods for quantifying leaf-level radiation use efficiency. The photochemical reflectance index (PRI) and its response to changes in the de-epoxidation state of the xanthophyll cycle was first described by Gamon et al. (1990, 1992). Xanthophylls are a type of

carotenoid pigment that have been shown to play a crucial role in down regulating photosystem II (PSII) activity, which is an important photoprotective strategy observed in all higher plant species (Young, 1991; Frank & Cogdell, 1996; Demmig-Adams & Adams, 1992, 1996). Because many stresses decrease a plant's capacity to use absorbed radiation for photosynthesis (photoinhibition), quantification of photodissipation processes, such as the xanthophyll cycle, have been shown to explain changes in RUE across a range of environmental conditions and stress types (Schöner & Krause, 1990; Demmig-Adams & Adams 1992; Verhoeven et al., 1997; Chaves et al., 2002). Thus, the PRI provides an opportunity to detect changes in RUE that occur due to a number of plant-environment interactions. However, the PRI has primarily been used to estimate changes in leaf level de-epoxidation state of the xanthophyll cycle and PSII photochemical efficiency (*e.g.*, Gamon et al. 1992; Penuelas et al. 1995; Gamon and Surfus 1999; Methy 2000; Guo and Trotter 2004) and canopy RUE efficiency (*e.g.*, Nichol et al. 2000; Penuelas and Inoue 2000) across relatively brief observational periods. Although long term observations of PRI from tower- (*e.g.*, Hilker et al., 2008a, 2008b) and satellite-based (Rahman et al., 2004; Drolet et al. 2005) platforms are possible, very few studies have attempted to use the PRI to monitor changes in canopy RUE across long-term (*i.e.*, weekly, seasonally, and interannually) observational periods. Furthermore, a few studies suggest that the PRI may be influenced by chlorophylls (Nakaji et al., 2006), carotenoids (Filella et al., 2009; Liu et al. 2009) and the carotenoid/chlorophyll ratio (*e.g.*, Sims and Gamon 2002; Stylinski et al. 2002). Because the PRI represents a potentially powerful tool for understanding variability in plant canopy photosynthesis across a wide range of temporal and spatial scales, studies that seek to understand the dynamics of canopy photosynthetic processes and their relationship to the PRI are of utmost importance.

In Chapter 1, *Temporal Assessment of PRI from a Deciduous Forest Canopy: The Role of Phenological Changes in Pigments, Canopy Structure and Photosynthetic Potential*, weekly and seasonal trends in canopy-level PRI were compared with seasonal changes in canopy photosynthesis and phenological changes in canopy structure. Biophysical measurements were combined with leaf optical and radiative

transfer modeling techniques to elucidate the mechanisms responsible for PRI variability across a phenological gradient. Simulation modeling results suggested that the PRI is significantly influenced by several factors, some of which are unrelated to xanthophyll pigment activity.

The results of Chapter 1 are followed up on in Chapter 2, *Influence of Leaf Chlorophyll and Carotenoid Content on the Photochemical Reflectance Index*, by investigating how total pools of leaf-level chlorophylls and carotenoids affect the PRI. Measurements of leaf pigments and spectral reflectance were obtained from several deciduous tree species. These data were used to test and validate a novel approach for remotely quantifying carotenoid content with PRI that was developed with a leaf optical properties simulation model.

Chapter 3, *A Simple Filtered Photodiode Instrument for Continuous Measurement of Narrowband NDVI and PRI over Vegetated Canopies*, describes the development and testing of a novel optical sensor system; the QuadPod. The QuadPod was developed to provide an inexpensive alternative to commercially available spectroradiometers and to facilitate unattended and automated ground-based measurement of narrowband spectral vegetation indices. Chapter 3 was published in the peer-reviewed journal *Agricultural and Forest Meteorology* (Garrity et al. 2010).

In Chapter 4, *Estimating the Influence of Changing Sky Diffuse Fraction on Gross and Net Carbon Assimilation*, the potential effects of past, current, and future global dimming and brightening trends on canopy photosynthesis and total growing season carbon assimilation were investigated. Diurnal relationships between sky diffuse fraction and forest carbon assimilation were integrated to predict how much carbon gain or loss may occur with global and local changes in the solar radiation regime.



## References

- Asner GP, Wessman CA, & Archer SA. (1998). Scale dependence of absorption of photosynthetically active radiation in terrestrial ecosystems. *Ecological Applications*, 8, 1003-1021.
- Asner GP, Nepstad D, Cardinot G, & Ray D. (2004). Drought stress and carbon uptake in an Amazon forest measured with spaceborne imaging spectroscopy. *Proceedings of the National Academy of Sciences*, 101, 6039-6044.
- Aubinet M, Grelle A, Ibrom A, Rannik U, Moncrieff J, Foken T, Kowalski AS, Martin PH, Berbigier P, Bernhofer C, Clement R, Elbers J, Granier A, Grunwald T, Morgenstern K, Pilegaard K, Rebmann C, Snijders W, Valentini R, & Vesala T. (2000). Estimates of the annual net carbon and water exchange of forests: The EUROFLUX methodology. *Advances in Ecological Research*, 30, 113-175.
- Baldocchi DD, Hicks BB, Meyers TP. (1988). Measuring biosphere-atmosphere exchanges of biologically related gases with micrometeorological methods. *Ecology*, 69, 1331-1340.
- Baldocchi DD. (2003). Assessing the eddy covariance technique for evaluating carbon dioxide exchange rates of ecosystems: past, present, and future. *Global Change Biology*, 9, 1-14.
- Bradford JB, Hicke JA, & Lauenroth WK. (2005). The relative importance of light-use efficiency modifications from environmental conditions and cultivation for estimation of large-scale net primary productivity. *Remote Sensing of Environment*, 96, 246-255.
- Campbell GS, & Norman JM. (1998). *An Introduction to Environmental Biophysics*. 2<sup>nd</sup> Edition, Springer, New York.

- Carlson TN, & Ripley DA. (1997). On the relation between NDVI, fractional vegetation cover, and leaf area index. *Remote Sensing of Environment*, 62, 241-252.
- Chaves MM, Pereira JS, Maroco J, Rodrigues ML, Ricardo CPP, Osorio ML, Carvalho I, Faria T, & Pinhero C. (2002). How plants cope with water stress in the field. Photosynthesis and growth. *Annals of Botany*, 89, 907-916.
- Clearwater MJ, & Gould KS. (1995). Leaf orientation and light interception by juvenile *Pseudopanax-crassifolius* (Cunn) C-Koch in a partially shaded forest environment. *Oecologia*, 104, 363-371.
- Coops NC, Waring RH, & Landsberg JJ. (1998). Assessing forest productivity in Australia and New Zealand using a physiologically-based model driven with averaged monthly weather data and satellite derived estimates of canopy photosynthetic capacity. *Forest Ecology and Management*, 104, 113-127.
- Demmig-Adams B, & Adams WW. (1992). Photoprotection and other responses of plants to high light stress. *Annual Review of Plant Physiology and Molecular Biology*, 43, 599-626.
- Demmig-Adams B, & Adams WW. (1996). The role of xanthophyll cycle carotenoids in the protection of photosynthesis. *Trends in Plant Science*, 1, 21-26.
- Drolet GG, Huemmrich KF, Hall FG, Middleton EM, Black TA, Barr AG, & Margolis HA. (2005). A MODIS-derived photochemical reflectance index to detect inter-annual variations in the photosynthetic light-use efficiency of a boreal deciduous forest. *Remote Sensing of Environment*, 98, 212-224.

- Dubayah R, & Vankatwijk V. (1992). The topographic distribution of annual incoming solar radiation in the Rio-Grande river basin. *Geophysical Research Letters*, 19, 2231-2234.
- Duursma RA, Kolari P, Peramaki M, Pulkkinen M, Makela A, Nikinmaa E, Hari P, Aurela M, Berbigier P, Bernhofer CH, Grunwald T, Loustau D, Molder M, Verbeeck H, & Vesala T. (2009). Contributions of climate, leaf area index and physiology to variation in gross primary production of six coniferous forests across Europe: a model-based analysis. *Tree Physiology*, 29, 621-639.
- Fan S, Gloor M, Mahlman J, Pacala S, Sarmiento J, Takahashi T, & Tans P. (1998). A large terrestrial carbon sink in North America implied by atmospheric and oceanic carbon dioxide data and models. *Science*, 282, 442-446.
- Fillela I, Porcar-Castell A, Munne-Bosch S, Back J, Garbulsky MF, & Penuelas J. (2009). PRI assessment of long-term changes in carotenoids/chlorophyll ratio and short-term changes in de-epoxidation state of the xanthophyll cycle. *International Journal of Remote Sensing*, 30, 4443-4455.
- Frank HA, Cogdell RJ. (1996). Carotenoids in photosynthesis. *Photochemistry and Photobiology*, 63, 257-264.
- Gamon JA, Field CB, Bilger W, Bjorkman O, Fredeen AL, & Penuelas J. (1990). Remote sensing of the xanthophyll cycle and chlorophyll fluorescence in sunflower leaves and canopies. *Oecologia*, 85, 1-7.
- Gamon JA, Penuelas J, & Field CB. (1992). A narrow-waveband spectral index that tracks diurnal changes in photosynthetic efficiency. *Remote Sensing of Environment*, 41, 35-44.

- Gamon JA, Field CB, Goulden ML, Griffin KL, Hartley AE, Joel G, Penuelas J, & Valentini R. (1995). Relationships between NDVI, canopy structure, and photosynthesis in three California vegetation types. *Ecological Applications*, 5, 28-41.
- Gamon JA, Serrano L, & Surus JS. (1997). The photochemical reflectance index: an optical indicator of photosynthetic radiation use efficiency across species, functional types, and nutrient levels. *Oecologia*, 112, 492-501.
- Gamon JA, & Surfus JS. (1999). Assessing leaf pigment content and activity with a reflectometer. *New Phytologist*, 143, 105-117.
- Gamon JA, Rahman AF, Dungan JL, Schildhauer M, & Huemmrich KF. (2006). Spectral Network (SpecNet) – what is it and why do we need it? *Remote Sensing of Environment*, 103, 227-235.
- Garrity SR, Vierling LA, & Bickford K. (2010). A simple filtered photodiode instrument for continuous measurement of narrowband NDVI and PRI over vegetated canopies. *Agricultural and Forest Meteorology*, 150, 489-496.
- Grant RH, Heisler GM, & Gao W. (1996). Photosynthetically-active radiation: Sky radiance under clear and overcast conditions. *Agricultural and Forest Meteorology*, 82, 267-292.
- Gu L, Baldocchi DD, Wofsy SC, Munger JW, Michalsky JJ, Urbanski SP, & Boden TA. (2003). Response of a deciduous forest to the Mount Pinatubo eruption: Enhanced photosynthesis. *Science*, 299, 2035-2038.
- Guo J, & Trotter CM. (2004). Estimating photosynthetic light-use efficiency using the photochemical reflectance index: variations among species. *Functional Plant Biology*, 31, 255-265.

- Hari P, & Makela A. (2003). Annual pattern of photosynthesis in Scots pine in the boreal zone. *Tree Physiology*, 23, 145-155.
- Hicke JA, Asner GP, Randerson JT, Tucker C, Los S, Birdsey R, Jenkins JC, & Field C. (2002). Trends in North American net primary productivity derived from satellite observations, 1982-1998. *Global Biogeochemical Cycles*, 16, 1018.
- Hilker T, Coops NC, Schwalm CR, Jassal RS, Black TA, Krishnan P. (2008a). Effects of mutual shading of tree crowns on prediction of photosynthetic light-use efficiency in a coastal Douglas-fir forest. *Tree Physiology*, 28, 825-834.
- Hilker T, Coops NC, Hall FG, Black TA, Wulder MA, Nesic Z, & Krishnan P. (2008b). Separating physiologically and directionally induced changes in PRI using BRDF models. *Remote Sensing of Environment*, 112, 2777-2788.
- Hollinger DY, Goltz SM, Davidson EA, Lee JT, Tu K, & Valentine HT. (1999). Seasonal patterns and environmental control of carbon dioxide and water vapour exchange in an ecotonal boreal forest. *Global Change Biology*, 5, 891-902.
- Houghton, RA. (2000). Interannual variability in the global carbon cycle. *Journal of Geophysical Research-Atmospheres*, 105, 20121-20130.
- Knapp AK, & Smith MD. (2001). Variation among biomes in temporal dynamics of aboveground primary productivity. *Science*, 291, 481-484.
- Law BE, Falge E, Gu L, Baldocchi DD, Bakwin P, Berbigier P, Davis K, Dolman AJ, Falk M, Fuentes JD, Goldstein A, Granier A, Grelle A, Hollinger D, Janssens IA, Jarvis P, Jensen NO, Katul NO, Mahli Y, Matteucci G, Meyers T, Monson R, Munger W, Oechel W, Olson R, Pilegaard K, Paw U KT, Thorgeirsson H, Valentini R, Verman S, Vesala T, Wilson K, & Wofsy S. (2002). Environmental

- controls over carbon dioxide and water vapor exchange of terrestrial vegetation. *Agricultural and Forest Meteorology*, 113, 97-120.
- Lindroth A, Lagergren F, Aurela M, Bjarnadottir B, Christensen T, Dellwik E, Grelle A, Ibrom A, Johansson T, Lankreijer H, Launiainen S, Laurila T, Molder M, Nikinmaa E, Pilegaard K, Sigurdsson BD, & Vesala T. (2008). Leaf area index is the principal scaling parameter for both gross photosynthesis and ecosystem respiration of Northern deciduous and coniferous forests. *Tellus B*, 60, 129-142.
- Liu N, Zhi-Fang L, Van Devender A, Lin G-Z, Peng C-L, Pan X-P, Chen S-W, Gu Q. (2009). Spectral reflectance indices and pigment functions during leaf ontogenesis in six subtropical landscape plants. *Journal of Plant Growth Regulation*, 58, 73-84.
- Methy M. (2000). Analysis of photosynthetic activity at the leaf and canopy levels from reflectance measurements: A case study. *Photosynthetica*, 38, 505-512.
- Moncreiff JB, Malhi Y, & Leuning R. (1996). The propagation of errors in long-term measurements of land-atmosphere fluxes of carbon and water. *Global Change Biology*, 2, 231-240.
- Monteith JL. (1972). Solar radiation and production in tropical ecosystems. *Journal of Applied Ecology*, 9, 747-766.
- Monteith JL. (1977). Climate and the efficiency of crop production in Britain. *Philosophical Transactions of the Royal Society of London. Series B, Biological Sciences*, 281, 277-294.
- Oliphant A, Susan C, Grimmond B, Schmid HP, & Wayson CA. (2006). Local-scale heterogeneity of photosynthetically active radiation (PAR), absorbed PAR and net

- radiation as a function of topography, sky conditions, and leaf area index. *Remote Sensing of Environment*, 103, 324-337.
- Penuelas J, Fillela I, & Gamon JA. (1995). Assessment of photosynthetic radiation-use efficiency with spectral reflectance. *New Phytologist*, 131, 291-296.
- Penuelas J, & Inoue Y. (2000). Reflectance assessment of canopy CO<sub>2</sub> uptake. *International Journal of Remote Sensing*, 21, 3353-3356.
- Polley HW, Emmerich W, Bradford JA, Sims PL, Johnson DA, Saliendra NZ, Svejcar T, Angell R, Frank AB, Phillips RL, Snyder KA, & Morgan JA. (2010). Physiological and environmental regulation of interannual variability in CO<sub>2</sub> exchange on rangelands in the western United States. *Global Change Biology*, 16, 990-1002.
- Potter CS, Randerson JT, Field CB, Matson PA, Vitousek PM, Mooney HA, & Klooster SA. (1993). Terrestrial ecosystem production: A process model based on global satellite and surface data. *Global Biogeochemical Cycles*, 7, 811-841.
- Rahman AF, Cordova VD, Gamon JA, Schmid HP, & Sims DA. (2004). Potential of MODIS ocean bands for estimating CO<sub>2</sub> flux from terrestrial vegetation: A novel approach. *Geophysical Research Letters*, 31, L10503.
- Randerson JT, Thompson MV, Conway TJ, Fung IY, & Field CB. (1997). The contribution of terrestrial sources and sinks to trends in the seasonal cycle of atmospheric carbon dioxide. *Global Biogeochemical Cycles*, 11, 535-560.
- Richardson AD, Hollinger DY, Aber JD, Ollinger SV, & Braswell BH. (2007). Environmental variation is directly responsible for short- but not long-term variation in forest-atmosphere carbon exchange. *Global Change Biology*, 13, 788-803.

- Running SW, Nemani RR, Heinsch FA, Zhao M, Reeves M, & Hashimoto M. (2004). A continuous satellite-derived measure of global terrestrial primary production. *BioScience*, 54, 547-560.
- Schöner S, & Krause GH. (1990). Protective systems against active oxygen species in spinach: response to cold acclimation in excess light. *Planta*, 180, 383-389.
- Sellers PJ. (1985). Canopy reflectance, photosynthesis and transpiration. *International Journal of Remote Sensing*, 6, 1335-1372.
- Sigurdsson BD, & Vesala T. (2008). Leaf area index is the principal scaling parameter for both gross photosynthesis and ecosystem respiration of Northern deciduous and coniferous forests. *Tellus Series B - Chemical and Physical Meteorology*, 60B, 129-142.
- Sims DA, & Gamon JA. (2002). Relationships between leaf pigment content and spectral reflectance across a wide range of species, leaf structures, and developmental stages. *Remote Sensing of Environment*, 81, 337-354.
- Sims DA, Luo H, Hastings S, Oechel WC, Rahman AF, & Gamon JA. (2006). Parallel adjustments in vegetation greenness and ecosystem CO<sub>2</sub> exchange in response to drought in a Southern California chaparral ecosystem. *Remote Sensing of Environment*, 103, 289-303.
- Stylinski CD, Gamon JA, & Oechel WC. (2002). Seasonal patterns of reflectance indices, carotenoid pigments and photosynthesis of evergreen chaparral species. *Oecologia*, 131, 366-374.
- Ustin SL, Gitelson AA, Jacquemoud S, Schaepman M, Asner GP, Gamon JA, & Zarco-Tejada P. (2009). Retrieval of foliar information about plant pigment



- systems from high resolution spectroscopy. *Remote Sensing of Environment*, 113, S67-S77.
- Verhoeven AS, Demmig-Adams B, & Adams WW. (1997). Enhanced employment of the xanthophyll cycle and thermal energy dissipation in spinach exposed to high light and N stress. *Plant Physiology*, 113, 817-824.
- White MA, Running SW, & Thornton PE. (1999). The impact of growing-season length variability on carbon assimilation and evapotranspiration over 88 years in the eastern US deciduous forest. *International Journal of Biometeorology*, 42, 139-145.
- Young AJ. (1991). The photoprotective role of carotenoids in higher plants. *Physiologia Plantarum*, 83, 702-708.
- Yuan W, Liu S, Zhou G, Zhou G, Tieszen LL, Baldocchi D, Bernhofer C, Gholz H, Goldstein AH, Goulden ML, Hollinger DY, Hu Y, Law BE, Stoy PC, Vesala T, & Wofsy SC. (2007). Deriving a light use efficiency model from eddy covariance flux data for predicting daily gross primary production across biomes. *Agricultural and Forest Meteorology*, 143, 189-207.

## CHAPTER 1

### TEMPORAL ASSESSMENT OF PRI FROM A DECIDUOUS FOREST CANOPY: THE ROLE OF PHENOLOGICAL CHANGES IN PIGMENTS, CANOPY STRUCTURE AND PHOTOSYNTHETIC POTENTIAL

#### **Abstract**

The photochemical reflectance index (PRI) is increasingly used to assess leaf and canopy photosynthetic radiation use efficiency (RUE). At the daily time scale the PRI has been shown to be highly correlated with photosynthetic downregulation mediated by the xanthophyll cycle. However, recent studies have observed that, in addition to xanthophylls, the PRI is influenced by other plant pigments. This may complicate the use of PRI for accurately describing seasonal changes in RUE, especially for plant canopies that undergo large shifts in the quantity of chlorophyll and carotenoids. To better understand these dynamic between phenological changes and the PRI, we measured canopy-level PRI of a deciduous forest in northern lower Michigan. Measurements were made beginning at the early stages of leaf expansion and continued beyond the peak of leaf development. We found that trends in PRI were significantly ( $p < 0.05$ ) related to changes in canopy quantum efficiency, photosynthetic potential, and leaf area index (LAI). Simulations from a coupled leaf radiative transfer model (PROSPECT-5) and canopy reflectance model (SAIL) were used to simulate field conditions, and demonstrated that seasonal changes in the chlorophyll/carotenoid ratio and LAI could account for much of the observed variation in PRI. Our findings show that seasonal variability in canopy chlorophyll, carotenoids, and LAI must be taken into account when using the PRI for understanding temporal patterns in vegetation-atmosphere gas exchange in deciduous forest canopies.

## 1. Introduction

Terrestrial photosynthesis is an important component of the global carbon cycle (Schimel, 1995; Schlesinger, 1997). Remote sensing has emerged as an important component of terrestrial carbon cycle research by providing information about the structure and function of plant canopies (Tucker & Sellers, 1986; Turner et al., 2004; Ustin et al., 2004; Kokaly et al., 2009), including the pigments and physiological processes associated with photosynthesis (Hilker et al., 2008a; Ustin et al., 2009). An important development in remote sensing of photosynthetic activity has been the Photochemical Reflectance Index (PRI), which was produced for estimating photosynthetic radiation use efficiency (RUE; Hilker et al., 2008a; Ustin et al., 2009).

The PRI has been shown to be highly correlated with the de-epoxidation state of the xanthophyll cycle (Gamon et al., 1990, 1992). Xanthophylls are pigments that are involved in photosystem II down-regulation, which helps prevent damage to photosynthetic apparatuses when more radiation is absorbed than can be utilized for photosynthesis (Demmig-Adams & Adams, 1996). Because many stresses decrease a plant's capacity to use absorbed radiation for photosynthesis (photoinhibition), quantification of photodissipation processes, such as the xanthophyll cycle, can be used to monitor changes in RUE that occur due to a number of stress types (Schöner and Krause, 1990; Demmig-Adams and Adams, 1992; Verhoeven et al., 1997; Chaves et al., 2002). Thus, the PRI has been used to estimate short-term (i.e., minutes to hourly) changes in leaf level de-epoxidation state of the xanthophyll cycle and PSII photochemical efficiency (*e.g.*, Gamon et al. 1992; Penuelas et al. 1995; Gamon & Surfus 1999; Methy 2000; Guo & Trotter 2004), and diurnal changes in leaf and canopy RUE (*e.g.*, Nichol et al. 2000; Penuelas & Inoue 2000; Rahman et al. 2004; Hilker et al. 2008b, 2008c).

Recent leaf-level studies suggest that over long observational periods, the PRI is influenced by chlorophylls (Nakaji et al. 2006), carotenoids (Filella et al. 2009; Liu et

al. 2009), and the chlorophyll/carotenoid ratio (Sims and Gamon 2002; Styliniski et al. 2002). Furthermore, simulation modeling has demonstrated the sensitivity of PRI to canopy structural variables, including leaf area index (LAI) and leaf angle distribution (Barton & North 2001). These studies suggest that confounding factors may make the PRI-based estimation of long-term patterns in canopy RUE difficult. Therefore, it may be necessary to account for the influence of factors other than the xanthophyll cycle if the PRI is to be used for understanding seasonal and spatial trends in RUE.

Our objective was to determine how seasonal changes in deciduous canopy photosynthetic efficiency, pigment pools, and LAI influence the PRI. We hypothesized that short-term changes (several days) in PRI would be related to canopy physiology, and that longer-term changes (weeks) would be influenced by LAI, chlorophyll content, and carotenoid content. To address our objective, we measured trace gas exchange, LAI, and spectral reflectance at a temperate deciduous forest and combined these observations with leaf optical and canopy radiative transfer simulation models.

## 2. Methods

### 2.1. Site description

This study was conducted at the University of Michigan Biological Station (UMBS) Ameriflux tower in the northern lower Michigan (45° 33' 35" N, 84° 42' 49" W). The study area consisted of a mixed hardwood forest dominated by *Populus grandidentata* (bigtooth aspen), *Populus tremuloides* (quaking aspen), *Quercus rubra* (red oak), *Acer rubrum* (red maple), *Betula papyrifera* (paper birch), and *Pinus strobes* (eastern white pine). Mean canopy height was ~ 20 m and mean LAI during the peak of the growing season in 2007 was 3.8 m<sup>2</sup> m<sup>-2</sup>. The seasonal pattern of canopy LAI was obtained by scaling periodic measurements of plant area index (measured with a PAI-2000; LICOR) with leaf litter trap data. Additional site details

were given by Gough et al. (2007). All measurements used in this study were obtained during days 140-153 in 2006 and days 198-219 in 2007.

## 2.2. *CO<sub>2</sub> fluxes and calculation of Radiation Use Efficiency*

Hourly averaged estimates of ecosystem gross primary productivity (GPP) were obtained from tower-based measurements of CO<sub>2</sub> concentrations, vertical wind velocities, and modeled estimates of respiration specifically developed for the UMBS study area (Curtis et al. 2005). Gap-filled estimates were used when environmental conditions did not meet the criteria developed by Schmid et al. (2003). A rectangular hyperbola was used to model the relationship between incident photosynthetic photon flux density (PPFD) and GPP,

$$GPP = \frac{\alpha\beta PPFD_t}{\beta + \alpha PPFD_t} \quad (1)$$

where  $\alpha$  is the canopy quantum efficiency and  $\beta$  is the canopy photosynthetic potential (Ruimy et al. 1993; Rocha et al. 2004). To understand seasonal changes in photosynthetic capacity, light response curves were modeled for three time periods: (1) days 140-145, (2) days 145-153, and (3) days 198-219. Canopy RUE (mol C mol quanta) was calculated as the ratio between GPP and absorbed photosynthetic photon flux density (APPFD). Hourly APPFD was calculated as:

$$APPFD = PPFD_t * (1 - \rho) * (1 - e^{(-K_b(\Psi)*LAI)}) \quad (2)$$

where  $PPFD_t$  was the hourly averaged total incident PPFD measured above the canopy,  $\rho$  was canopy reflected PPFD (%), and  $K_b$  was the hourly averaged canopy extinction coefficient, which was dependent on solar zenith angle ( $\Psi$ ) and canopy leaf angle distribution (Campbell & Norman, 1988).

### 2.3. Reflectance data

Two spectrometers were mounted on the UMBS Ameriflux tower at 46 m above ground level (26 m above the average canopy height). For measurements acquired in 2006, a UniSpec DC spectrometer was used (PP Systems, Haverhill, MA, USA), and for measurements acquired in 2007 an ASD V/NIR instrument was used (ASD, Boulder, CO, USA). Both spectrometers were dual channel and simultaneously measured radiance and irradiance. The uplooking fiber optic was attached to a cosine receptor and monitored irradiance, whereas the downlooking fiber optic was attached to a 3° (UniSpec DC) or 10° (ASD V/NIR) field of view foreoptic and monitored radiance from the canopy surrounding the flux tower. Differences between sensors were assumed to be negligible because the data from each instrument were used to calculate relative reflectances.

Diurnal reflectance data were collected at five minute intervals between 0600 and 1800 EST. Diurnal reflectance measurements were filtered to exclude data collected during periods when the foreoptics were wet. A despiking algorithm was applied to the remaining data to remove those observations where the difference between a running average and each individual observation was greater than 1.5 standard deviations. Filtered reflectance data were hourly averaged and used to calculate the PRI as:

$$PRI = \frac{\rho_{531} - \rho_{570}}{\rho_{531} + \rho_{570}} \quad (3)$$

where  $\rho$  is the reflectance at the specified wavelength (nm). Reflectance measurements were corrected using reflectance values periodically obtained from a Spectralon reference panel (Lapsphere Inc., Gamon et al. 2006).

#### 2.4 Leaf and canopy reflectance modeling

We used leaf- and canopy-level reflectance models to understand how PRI related to changes in canopy pigment pools, LAI, and physiology. A semi-empirical bidirectional reflectance distribution function (BRDF; Lucht et al., 2000; Los et al. 2005; Hilker et al. 2008b) was calculated for diurnal PRI measurements acquired during the green up period in 2006 using the LiSparse (Li & Strahler, 1986) and Ross-Thick (Roujean et al., 1992) kernels. The BRDF was formulated as:

$$\rho PRI(\theta_v, \theta_s, \Delta\phi) = k_i + k_g K_L\left(\theta_v, \theta_s, \Delta\phi, \frac{h}{b}, \frac{b}{r}\right) + k_v K_R(\theta_v, \theta_s, \Delta\phi) \quad (4)$$

where

$k_i$	isotropic scattering component
$k_g$	geometric scattering component
$K_L$	Li-Sparse kernel
$k_v$	volumetric scattering component
$K_R$	Ross-Thick kernel
$\theta_v$	view zenith angle
$\theta_s$	solar zenith angle
$\Delta\Phi$	azimuth angle
$\frac{h}{b}$	crown relative height
$\frac{b}{r}$	crown relative shape

The ratios  $h/b$  and  $b/r$  are fixed parameters that describe the geometry of the canopy (Wanner et al., 1995), where  $h$  is the height to the center of the crown,  $b$  is the crown vertical radius, and  $r$  is the horizontal radius (Lucht et al., 2000). For our study, ratios were assumed to be  $h/b = 2$ , and  $b/r = 1$ .

The semi-empirical BRDF model should only be fit to measurements acquired under similar illumination and physiological conditions (Hall et al., 2008). Therefore, observations were stratified according to sky diffuse fraction (SDF), RUE, and LAI. The BRDF model (Eq. 3) was independently fit to the observations in each stratum using robust linear least squares regression. The kernels derived from each inverse model fit were regressed against each class type to determine the influence of LAI, RUE, and sky diffuse fraction on the PRI (after Hilker et al. 2008b).

Because the BRDF model could not decouple the various influences of canopy developmental dynamics on the PRI, it was necessary to couple a leaf reflectance model with a canopy reflectance model to simulate the effects of both canopy structure and pigment pools. We used the PROSPECT leaf optical model (Jacquemoud & Baret, 1990) to test the influence of changing pigment pools on the PRI at the leaf level. We selected the PROSPECT-5 version of the model (Feret et al., 2008) because it had the capability to model the influence of chlorophyll (Chl) and carotenoid (Car) pigments on spectral reflectance of wavelengths used to calculate the PRI. Pigment contents were manipulated in order to model the expected response of PRI during deciduous canopy development. Because we did not have pigment samples for the UMBS forest, we used input values that were representative of those obtained from dicotyledonous plants (Guo & Trotter 2004, Liu et al. 2009) and deciduous trees from the Leaf Optical Properties EXperiment (LOPEX) database (Hosgood et al., 1995; Table 1). Pigment contents for juvenile, young, mature, and senescent leaves (Liu et al. 2009) provided an estimate of phenological changes in pigments that could be expected to occur at the UMBS forest canopy.

Modeled reflectance values derived from PROSPECT-5 simulations were used as inputs to the SAIL radiative transfer model (Verhoef, 1984). The combined model, commonly referred to as PROSAIL (Jacquemod et al., 2009), allowed us to investigate the combined influence of pigments and LAI on the PRI. A background reflectance spectrum was not available for the UMBS study site so the mean reflectance from the earliest day in our study was used instead. PROSAIL simulations



were conducted using the following input parameters: LAI ranging from 0 to 1.5 m<sup>2</sup> m<sup>-2</sup> (the range of LAI values occurring across our study period), the mesophyll structural parameter (N) was held constant at 2, leaf water content (Cw) and dry matter (Cm) were held constant at 0.01 g cm<sup>-2</sup>, solar zenith angle was 45°, and time of day was 1200.

### *2.5 Statistical analysis*

Monotonic trends in seasonal time series of measured variables were evaluated with Mann-Kendall rank correlations (Mann 1945) using the ‘Kendall’ package in the R software package (version 2.9.0, R Development Core Team). SigmaPlot (Systat Software, Inc.) was used to fit light response curves and for regression analysis. Regression coefficients were compared using 95% confidence intervals. Statistical tests were considered significant when  $p < 0.05$ .

## **3. Results**

### *3.1 Seasonal trends*

Across the entire observational period, significant positive trends were observed for hourly averaged PRI, RUE, and LAI (Figs. 1a,b). In 2006, the trend in PRI was stronger ( $\tau = 0.55$ ) than the PRI trend in 2007 ( $\tau = 0.20$ ; Fig. 1a). Canopy RUE (Fig. 1b) and LAI (Fig. 1c) also had strong trends during the 2006 period ( $\tau = 0.4$  and 1.0, respectively) and were comparatively more stable during the 2007 period ( $\tau = -0.11$  and 0.32, respectively). Daily averaged PRI was significantly correlated with RUE (Fig. 2). The range of LAI values represents between 44% and 78% of the maximum canopy PAI in 2006 and 99.5% and 100% of maximum canopy PAI in 2007. Subsequently, we will refer to the 2006 observations as the “greenup” period and the 2007 observations as the “full leafout” period.

We found that LAI explained 55% of the variation in hourly averaged PRI during greenup. Residuals from the greenup LAI-PRI regression were significantly correlated with APPFD (Fig. 3). The slope of the relationship between the residuals and APPFD was significantly steeper than the slope of the regression between APPFD and PRI during the full leafout period. Similar results were obtained from the BRDF analysis, where the isotropic kernel weights were significantly correlated with LAI and RUE (Figs. 4a,b) during the greenup period. However, no significant relationship was observed between the isotropic kernel weights and SDF (Fig. 4c).

We found significant differences in the regression coefficients for the relationship between PPF and PRI across time periods 1-3 (Table 2). In general, the intercept increased whereas the slope decreased. For the same time periods there were significant increases in canopy quantum efficiency and photosynthetic potential.

### *3.3 Leaf and canopy level simulations*

PROPSSET-5 simulations demonstrated the influence of isolated Chl or Car content on the PRI across a pigment contents ranging from 1-120  $\mu\text{g cm}^{-2}$  (Fig. 5a). There was a positive trend in PRI as Chl content increased from 0 to 85  $\mu\text{g cm}^{-2}$ . For Chl content exceeding 85  $\mu\text{g cm}^{-2}$ , there was a negative trend in PRI. Carotenoid contents between 0 and 105  $\mu\text{g cm}^{-2}$  caused a negative trend in PRI. There was no significant trend in PRI when Car content exceeded 105  $\mu\text{g cm}^{-2}$ .

For simulations where both Chl and Car exceeded 0  $\mu\text{g cm}^{-2}$ , the direction and magnitude of the PRI response was dependent on the Chl/Car ratio (Fig. 5b). For Chl/Car ratios less than 4:1, PRI decreased with increasing Chl content when Chl content was between 0 and 55  $\mu\text{g cm}^{-2}$ , and increased with Chl contents greater than 55  $\mu\text{g cm}^{-2}$ . For Chl/Car ratios greater than or equal to 4:1, PRI increased with increasing Chl content. Figure 4c shows the range of PRI values that resulted from a simulated developmental sequence where Chl/Car ratios ranged from 1:1 to 7:1.

Simulations with PROSAIL showed that the range of simulated PRI values increased with increasing LAI for Chl/Car ratios greater than or equal to 2:1 and decreased when Chl/Car ratios were less than 2:1 (Figs. 6a). There was a positive trend in the mean simulated PRI with increasing Chl/Car ratio, regardless of both LAI and the total amount of Chl present in canopy leaves (Fig. 6b).

#### **4. Discussion**

The PRI is most commonly used to estimate leaf-level de-epoxidation state of the xanthophyll cycle (e.g., Gamon et al. 1992; Penuelas et al. 1995; Gamon & Surfus 1999; Methy 2000; Guo & Trotter 2004), and therefore, should be correlated with canopy RUE when radiation levels exceed what is used for photosynthesis. Our results corroborated these previous studies, showing that daily averaged PRI was significantly correlated with canopy RUE. However, our results also demonstrated that the sensitivity of PRI to changes in RUE was inconsistent across the phenological gradient covered in our study. The sensitivity of hourly PRI measurement to incident PPFD declined as seasonal development of the canopy progressed from green up to fully leafed out (see Fig. 3). Similarly, Nakaji et al. (2006) demonstrated that the slope of the PRI-RUE relationship was correlated with seasonal changes in leaf pigments, nitrogen content, and air temperature. It has been suggested that leaves with high values of saturating irradiance and high photosynthetic capacity (e.g., fully developed or sun-acclimated) have a lower requirement for photoprotection compared to young or shade-adapted leaves with low values of saturating irradiance and low photosynthetic capacity (Guo & Trotter, 2004). This may result in a narrower range of variability in PRI for fully developed or sun-adapted leaves than that for young or shade-adapted leaves because the absolute content of xanthophylls in the de-epoxidized form would be smaller. Our field-based observations support this hypothesis.

Simulations with PROSPECT-5 showed a relatively large range of expected PRI values for low Chl/Car ratios, which are expected to occur in the early stages of leaf development and during senescence (e.g., Jiang et al., 2005; Liu et al., 2009; see Figs. 5b). However, the broad range of expected PRI values in the modeled results was attributable to variations in Chl content and not to leaf-level physiological changes. As the Chl/Car ratio increased, the expected range of PRI decreased even though the range of pigment contents in the model was constant. Simulations with PROSAIL provided similar results, showing that as LAI increased the range of expected values of PRI generally decreased regardless of the Chl/Car ratio and absolute pigment content (Fig. 7). Because measurements of xanthophyll pigments were not available and because the PROSPECT-5 model was not capable of isolating the influence of xanthophyll pigment interconversion on the PRI, it is still uncertain why there was a broader range of variability in PRI measurements during green up compared to measurements from the fully leafed out canopy.

The results from the three modeling approaches showed that the PRI is significantly influenced by changes in leaf physiology, pigments, and canopy structure, all of which occur during deciduous canopy phenological development. The BRDF response of the PRI was dependent on several variables in this deciduous-dominated canopy. Analysis of BRDF isotropic kernel weights indicated that PRI was significantly related to LAI and RUE, which is consistent with the idea that the isotropy of the canopy is dependent on leaf pigments (Hilker et al., 2008b), which are expected to change in predictable patterns with tree phenology (Jiang et al., 2005; Liu et al., 2009). Furthermore, modeled results of the influence of canopy structure on the PRI have suggested that LAI may confound the PRI-RUE relationship (Barton & North, 2001). Although BRDF modeling confirmed correlative relationships between PRI and the two of the three biophysical variables tested in our study, there was significant co-linearity among the tested variables. Therefore, the analysis of isotropic kernel weights did not allow us to determine the relative contribution of each biophysical variable to the variability in PRI observations.

The simulation modeling results proved to be more useful for understanding the contributions of leaf pigments and canopy structure to the observed trends in the PRI. At the leaf level, Chl and Car content had nearly opposite effects on the PRI when evaluated in isolation from each other. When combined, the effect of the pigments on the PRI was dependent on the Chl/Car ratio. These results are consistent with studies that have found significant correlation between pigment ratios and PRI measurements across time scales longer than a few days (Stylinski et al., 2002; Fillela et al., 2009), when evaluating the PRI response across different species (Sims & Gamon, 2002; Guo & Trotter, 2004; Chapter 3), or across leaves with large variation in pigment contents (Chapter 3).

Although canopy pigment contents measurements were not available for our study, pigment contents used in the simulation models were based on values reported in other studies for similar vegetation and, therefore, were assumed to be within the range of values expected to occur at the UMBS forest. Using these pigment content values and LAI as inputs for PROSAIL simulations allowed us to approximately reconstruct the pattern of the overall observed PRI trend. Although we are uncertain what the actual content of Chl and Car were during the study period, envelopes of expected values that were simulated with PROSAIL (see Fig. 7) suggest that the Chl/Car ratio was somewhere between 2:1 and 4:1. Overall, our results demonstrate that the PRI is most sensitive to changes in Chl/Car ratio (see Figs 5b,c). Leaf area index also had an influence on the PRI, but it appears to primarily be responsible for determining the magnitude of the PRI response to the Chl/Car ratio (see Fig. 6b).

Because the PRI responds to rapid changes in xanthophylls and slower changes in photosynthetic pigments, LAI, and photosynthetic potential, long-term measurements may be useful for tracking the photosynthetic phenology of deciduous canopies, while still providing information about diurnal changes in RUE that occur due to changes in xanthophyll pigments. Although traditional measurements of plant canopy phenology (e.g., budbreak, leaf expansion, and senescence) are relatively well established, photosynthetic development, capacity, and total carbon assimilation may be difficult

to predict from traditional phenologically-based estimates (Morecroft et al. 2003). For example, a significant difference in the time between budbreak and maximum light-saturated assimilation rate for *Quercus robur* showed that by assuming full photosynthetic acclimation upon budbreak an estimation of the annual carbon gain would exceed the actual carbon gain by approximately 28% (Morecroft et al. 2003). Similarly, carbon assimilation in deciduous forests can be overestimated if mid-season, age related declines in canopy photosynthetic capacity are not accounted for. For example modeled estimates of carbon exchange over-estimated eddy covariance measured carbon exchange by 25%, because available predictor variables (e.g., LAI and leaf nitrogen) were relatively constant during the study period and failed to account for declines in photosynthetic capacity (Wilson et al. 2001). If the PRI is indicative of photosynthetic capacity as the results of our study suggest, then it may provide a non-invasive method for remotely determining changes in photosynthetic capacity and total forest carbon assimilation due to phenological changes in leaf area and pigments as well as physiological adjustments (e.g., due to stresses and age-related decline in photosynthetic capacity and pigment content) that occur throughout a growing season. When combined with its use for estimating short-term changes in xanthophyll pigments, and thus RUE, the PRI may be considered a multi-temporal scale index that is capable of detecting both short and long term changes in several factors that are important for understanding canopy-atmosphere CO<sub>2</sub> exchange (Fig. 8).

Our simulations were limited to modeling the influence of Chl and Car pigments on the PRI. However, many pigments that are classified as carotenoids are important for light harvesting and photoprotection (Young, 1991). The pools of each carotenoid pigment are likely to vary over differing time scales in response to environmental change. For example, the total pool size of the xanthophyll pigments, violaxanthin, antheraxanthin, and zeaxanthin, are known to fluctuate ontogenetically and in response to stress (Young, 1991; Demmig-Adams & Adams, 1996). Our understanding of the PRI would benefit from investigations into how the different pools of carotenoids influence the PRI. For example, it may be of interest to

understand if some carotenoids are more influential on the PRI than others, especially if they contribute to seasonal photosynthetic acclimation or response to stress. Furthermore, while we focused on relationships among canopy-level PRI and phenology in a deciduous forest, the seasonal dynamics of evergreen canopies are likely to differ in both pattern and magnitude and thus may influence PRI to a different degree.

## Acknowledgements

This study was funded by an NSF IGERT fellowship (NSF grant DGE-0504552) awarded by the University of Michigan Biosphere-Atmosphere Research Training (BART) program to S. Garrity, NSF grant DBI-0537040 (L. Vierling, PI), an NSF-ESPCoR grant to the State of Idaho, and US Department of Energy Cooperative Agreement No. DE-FC03-90ER610100. We would like to thank Thomas Hilker for providing assistance with the BRDF modeling, Peter Curtis and Christoph Vogel for providing flux data, and Ron Robberecht for providing helpful comments on earlier versions of this manuscript.

## References

- Campbell, J.S., & Norman J.M. (1998). *An Introduction to Environmental Biophysics*. Springer, New York.
- Chaves, M.M., Pereira, J.S., Maroco, J., Rodrigues, M.L., Ricardo, C.P.P., Osorio, M.L., Carvalho, I., Faria, T., & Pinhero, C. (2002). How plants cope with water stress in the field. Photosynthesis and growth. *Annals of Botany*, **89**, 907-916.
- Curtis, P.S., Vogel, C.S., Gough, C.M., Schmid, H.P., Su, H.-B., & Bovard, B.D. (2005). Respiratory carbon losses and the carbon-use efficiency of a northern hardwood forest, 1999-2003. *New Phytologist*, **167**, 437-456.

- Demmig-Adams, B., & Adams, W.W. (1992). Photoprotection and other responses of plants to high light stress. *Annual Review of Plant Physiology and Plant Molecular Biology*, 43, 599-626.
- Demmig-Adams, B., & Adams, W.W. (1996). The role of xanthophyll cycle carotenoids in the protection of photosynthesis. *Trends in Plant Science*, 1, 21-26.
- Faret, J-B., Francois, C., Asner, G.P., Gitelson, A.A., Martin, R.E., Bidel, L.P.R., Ustin, S.L., le Marie, G., & Jacquemoud, S. (2008). PROSPECT-4 and 5: Advances in the leaf optical properties model separating photosynthetic pigments. *Remote Sensing of Environment*, 112, 3030-3043.
- Fillella, I., Porcar-Castell, A., Munne-Bosch, S., Back, J., Garbulsky, M.F., & Penuelas, J. (2009). PRI assessment of long-term changes in carotenoids/chlorophyll ratio and short-term changes in de-epoxidation state of the xanthophyll cycle. *International Journal of Remote Sensing*, 30, 4443-4455.
- Gamon, J.A., C.B. Field, W. Bilger, O. Bjorkman, A.L. Fredeen, & Penuelas, J. (1990). Remote sensing of the xanthophyll cycle and chlorophyll fluorescence in sunflower leaves and canopies. *Oecologia*, 85, 1-7.
- Gamon, J.A., Penuelas, J., & Field, C.B. (1992). A narrow-waveband spectral index that tracks diurnal changes in photosynthetic efficiency. *Remote Sensing of Environment*, 41, 35-44.
- Gamon, J.A., & Surfus, J.S. (1999). Assessing leaf pigment content and activity with a reflectometer. *New Phytologist*, 143, 105-117.



- Gamon, J.A., Rahman, A.F., Dungan, J.L., Schildhauer, M., & Huemmrich, K.F., (2006). Spectral Network (SpecNet) – what is it and why do we need it? *Remote Sensing of Environment*, 103, 227-235.
- Gough, C.M., C.S. Vogel, K.H. Harrold, K. George, & Curtis, P.S. (2007). The legacy of harvest and fire on ecosystem carbon storage in a northern temperate forest. *Global Change Biology*, 13, 1935-1949.
- Hall, F.G., Hilker, T., Coops, N.C., Lyapustin, A., Huemmrich, K.F., Middleton, E., Margolis, H., Drolet, G., & Black, T.A. (2008). Multi-angle remote sensing of forest light use efficiency by observing PRI variation with canopy shadow fraction. *Remote Sensing of Environment*, 112, 3201-3211.
- Hilker, T., Coops, N.C., Wulder, M.A., Black, T.A., & Guy, R.D. (2008a). The use of remote sensing in light use efficiency based models of gross primary production: A review of current status and future requirements. *Science of the Total Environment*, 404, 411-423.
- Hilker, T., Coops, N.C., Hall, F.G., Black, T.A., Wulder, M.A., Nestic, Z., & Krishan, P. (2008b). Separating physiologically and directionally induced changes in PRI using BRDF models. *Remote Sensing of Environment*, 112, 2777-2788.
- Hilker, T., Coops, N.C., Schwalm, C.R., Jassal, R.S., Black, T.A., & Krishnan, P. (2008c). Effects of mutual shading of tree crowns on prediction of photosynthetic light-use efficiency in a coastal Douglas-fir forest. *Tree Physiology*, 28, 825-834.
- Hosgood, B., Jacquemoud, S., Andreoli, G., Verdebout, J., Pedrini, G., & Schmuck, G. (1995). *Leaf Optical Properties Experiment 93 (LOPEX93)*. Joint Research Center, Institute for Remote Sensing Applications, Ispra (Italy), Report EUR-16095-EN, European Commission, Luxembourg.

- Jacquemoud, S., & Baret, F. (1990). PROSPECT: A model of leaf optical properties spectra. *Remote Sensing of Environment*, 34, 75-91.
- Jacquemoud, S., Verhoef, W., Baret, F., Bacour, C., Zarco-Tejada, P.J., Asner, G.P., Francois, C., & Ustin, S.L. (2009). PROSPECT + SAIL models: A review of use for vegetation characterization. *Remote Sensing of Environment*, 113, S56-S66.
- Jiang, C.-D., Li, P.-M., Gao, H.-Y., Zou, Q., Jiang, G.-M., & Li, L.-H. (2005). Enhanced photoprotection at the early stages of leaf expansion in field-grown soybean plants. *Plant Science*, 168, 911-919.
- Kokaly, R.F., Asner, G.P., Ollinger, S.V., Martin, S.E., & Wessman, C.A. (2009). Characterizing canopy biochemistry from imaging spectroscopy and its application to ecosystem studies. *Remote Sensing of Environment*, 113, S78-S91.
- Li, X., & Strahler, A.H. (1986). Geometric-optical bidirectional reflectance modeling of a conifer forest canopy. *IEEE Transactions on Geoscience and Remote Sensing*, 24, 906-919.
- Los, S.O., North, P.R.J., Grey, W.M.F., & Barnsley, M.J. (2005). A method to convert AVHRR normalized difference vegetation index time series to a standard viewing and illumination geometry. *Remote Sensing of Environment*, 99, 400-411.
- Lucht, W., Schaaf, C.B., & Strahler, A.H. (2000). An algorithm for the retrieval of albedo from space using semiempirical BRDF models. *IEEE Transactions on Geoscience and Remote Sensing*, 38, 977-998.
- Mann, H.B. (1945). Nonparametric tests against trend. *Econometrica*, 13, 245-259.
- Methy, M. (2000). Analysis of photosynthetic activity at the leaf and canopy levels from reflectance measurements: a case study. *Photosynthetica*, 38, 505-512.

- Morecroft, M.D., Stokes, V.J., & Morison, J.I.L. (2003) Seasonal changes in the photosynthetic capacity of canopy oak (*Quercus robur*) leaves: the impact of slow development on annual carbon uptake. *International Journal of Biometeorology*, 47, 221-226.
- Nakaji, T., Oguma, H., & Fujinuma, Y. (2006). Seasonal changes in the relationship between photochemical reflectance index and photosynthetic light use efficiency of Japanese larch needles. *International Journal of Remote Sensing*, 27, 493-509.
- Nichol, C.J., Huemmrich, K.F., Black, T.A., Jarvis, P.G., Walthall, C.L., Grace, J., & Hall, F.G. (2000). Remote sensing of photosynthetic-light-use efficiency of boreal forest. *Agricultural and Forest Meteorology*, 101, 131-142.
- Penuelas, J., Filella, I., & Gamon, J.A. (1995). Assessment of photosynthetic radiation-use efficiency with spectral reflectance. *New Phytologist*, 131, 291-296.
- Penuelas, J., & Inoue, Y. (2000). Reflectance assessment of canopy CO<sub>2</sub> uptake. *International Journal of Remote Sensing*, 21, 3353-3356.
- Rahman, A.F., Cordova, V.D., Gamon, J.A., Schmid, H.P., & Sims, D.A. (2004). Potential of MODIS ocean bands for estimating CO<sub>2</sub> flux from terrestrial vegetation: a novel approach. *Geophysical Research Letters*, 31, L10503, doi:10.1029/2004GL019778.
- Rocha A.V., Su H.-B., Vogel, C.S., Schmid, H.P., & Curtis, P.S. (2004). Photosynthetic and water use efficiency responses to diffuse radiation by an aspen-dominated northern hardwood forest. *Forest Science*, 50, 793-801.

- Roujean, J.L., Leroy, M., & Deschamps, P.Y. (1992). A bidirectional reflectance model of the earth's surface for the correction of remote-sensing data. *Journal of Geophysical Research-Atmospheres*, 97, 20455-20468.
- Schimel, D.S. (1995). Terrestrial ecosystems and the carbon cycle. *Global Change Biology*, 1, 77-91.
- Schlesinger, W.H. (1997). *Biogeochemistry. An Analysis of Global Change*. Academic Press, San Diego.
- Schmid, H.P., Su, H.-B., Vogel, C.S., & Curtis, P.S. (2003). Ecosystem-atmosphere exchange of carbon dioxide over a mixed hardwood forest in northern lower Michigan. *Journal of Geophysical Research-Atmospheres*, 108, 4417, doi:10.1029/2002JD003011.
- Schöner, S., & Krause, G.H. (1990). Protective systems against active oxygen species in spinach: response to cold acclimation in excess light. *Planta*, 180, 383-389.
- Sims, D.A., & Gamon, J.A. (2002). Relationships between leaf pigment content and spectral reflectance across a wide range of species, leaf structures and developmental stages. *Remote Sensing of Environment*, 81, 337-354.
- Stylinski, C.D., Gamon, J.A., & Oechel, W.C. (2002). Seasonal patterns of reflectance indices, carotenoid pigments and photosynthesis of evergreen chaparral species. *Oecologia*, 131, 366-374.
- Tucker, C.J., & Sellers, P.J. (1986). Satellite remote sensing of primary production. *International Journal of Remote Sensing*, 7, 1395-1416.

- Turner, D.P., Ollinger, S.V., & Kimball, J.S. (2004). Integrating remote sensing and ecosystem process models for landscape- to regional-scale analysis of the carbon cycle. *Bioscience*, 54, 573-584.
- Ustin, S.L., Roberts, D.A., Gamon, J.A., Asner, G.P., & Green, R.O. (2004). Using imaging spectroscopy to study ecosystem processes and properties. *Bioscience*, 54, 523-534.
- Ustin, S.L., Gitelson, A.A., Jacquemoud, S., Schaepman, M., Asner, G.P., Gamon, J.A., & Zarco-Tejada, P. (2009). Retrieval of foliar information about plant pigment systems from high resolution spectroscopy. *Remote Sensing of Environment*, 113, S67-S77.
- Verhoef, W. (1984). Light scattering by leaf layers with application to canopy reflectance modeling: the SAIL model. *Remote Sensing of Environment*, 16, 125-141.
- Verhoeven, A.S., Demmig-Adams, B., & Adams, W.W. (1997). Enhanced employment of the xanthophyll cycle and thermal energy dissipation in spinach exposed to high light and N stress. *Plant Physiology*, 113, 817-824.
- Wanner, W., Li, X., & Strahler, A.H. (1995). On the derivation of kernels for kernel-driven models of bidirectional reflectance. *Journal of Geophysical Research*, 100, 21077-21089.
- Wilson, K.B., Baldocchi, D.D., & Hanson, P.J. (2001). Leaf age affects the seasonal pattern of photosynthetic capacity and net ecosystem exchange of carbon in a deciduous forest. *Plant, Cell and Environment*, 24, 571-583.

Young, A., & Britton, G. (1990). Carotenoids and stress. In 'Stress responses in plants: adaptation and acclimation mechanisms'. (Eds R.G. Alscher and J.R. Cumming) pp. 87-112. (Wiley-Liss: New York).

Young, A.J. (1991). The photoprotective role of carotenoids in higher plants. *Physiologia Plantarum*, 83, 702-708.

**Table 1.** Leaf chlorophyll and carotenoid content for deciduous tree species from the LOPEX database, Guo and Trotter (2004), and Liu et al. (2009). Pigment values reported by Liu et al. (2009) were obtained across a developmental gradient: juvenile (J), young (Y), mature (M) and senescent (S).

	LOPEX	Guo & Trotter	Liu et al. (Juvenile)	Liu et al. (Young)	Liu et al. (Mature)	Liu et al. (Senescent)
<i>Chl (mg/cm<sup>2</sup>)</i>						
Min	42.0	24.1	-	-	-	-
Max	72.8	88.2	-	-	-	-
Mean	54.9	58.6	-	-	-	-
<i>Car (mg/cm<sup>2</sup>)</i>						
Min	7.5	9.0	-	-	-	-
Max	16.1	16.6	-	-	-	-
Mean	11.3	13.6	-	-	-	-
<i>Chl/Car</i>						
Min	4.1	2.4	2.5	2.9	3.1	2.6
Max	5.7	5.7	5.0	6.3	7.1	6.3
Mean	4.9	4.2	3.4	3.9	4.5	3.9

**Table 2.** Slope and intercept of the linear least squares relationship between incident PPFD and the PRI and changes in canopy quantum efficiency ( $\alpha$ ) and canopy photosynthetic potential ( $\beta$ ) derived from fitted light response curves for three time periods, where 1 = days 140-145, 2 = days 146-153, and 3 = days 198-219. Numbers in parentheses are the 95% confidence intervals of the regression coefficients.

Time period	PPFD vs. PRI			PPFD vs. GPP		
	Intercept	Slope	$r^2$	$\alpha$	$\beta$	$r^2$
1	-0.085 (0.009)	$-5 \times 10^{-6}$ ( $8 \times 10^{-6}$ )	0.60	0.008 (0.002)	15.9 (6.1)	0.89
2	-0.016 (0.009)	$-4 \times 10^{-6}$ ( $8 \times 10^{-6}$ )	0.52	0.020 (0.011)	19.0 (7.0)	0.56
3	-0.022 (0.002)	$-9 \times 10^{-6}$ ( $2 \times 10^{-6}$ )	0.36	0.029 (0.004)	37.6 (4.7)	0.86



## Figures

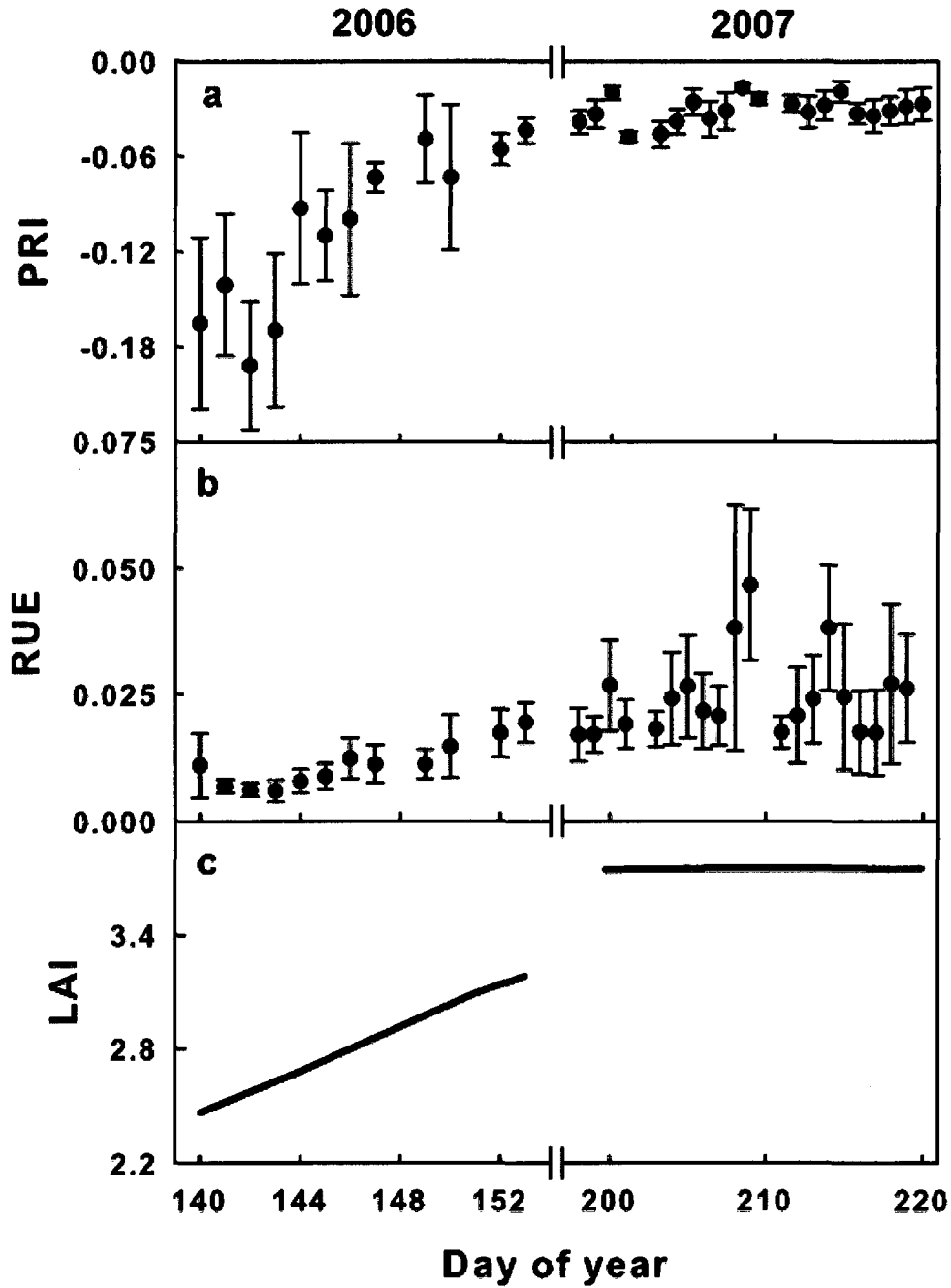


**Figure 1.** Mean daily values of (a) PRI, (b) RUE, and (c) LAI. Error bars represent the  $\pm 1$  SD each daily mean. The break in the x-axes signifies the difference between data collected in 2006 (left) and 2007 (right).

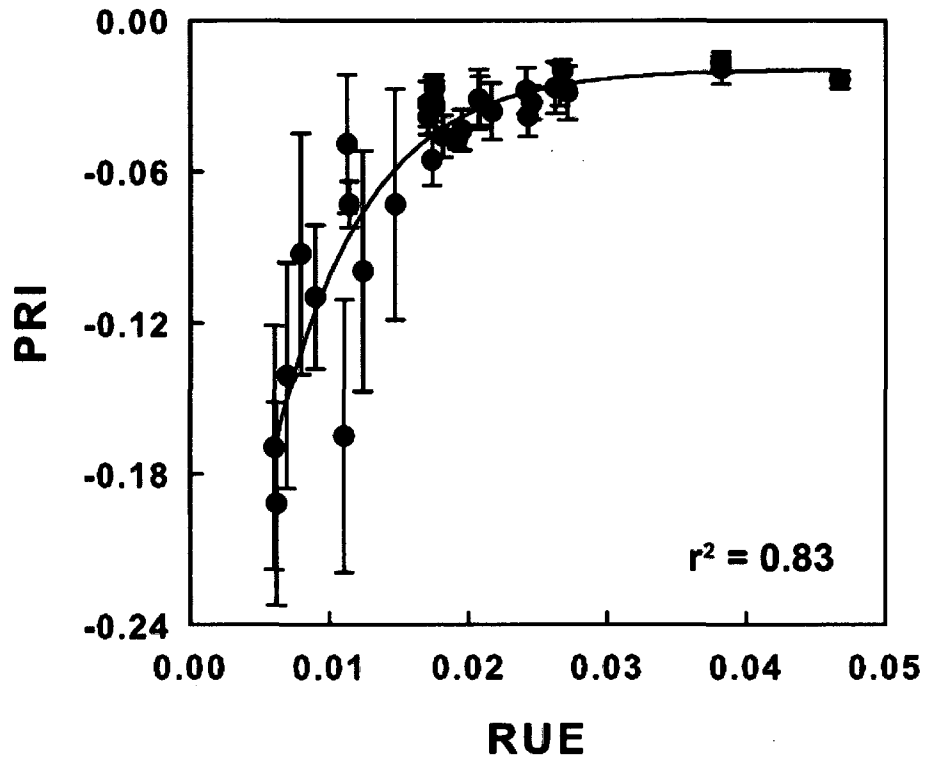


**Figure 2.** Regression results for the relationship between daily averaged RUE and PRI. Error bars represent the  $\pm 1$  SD for mean daily PRI.

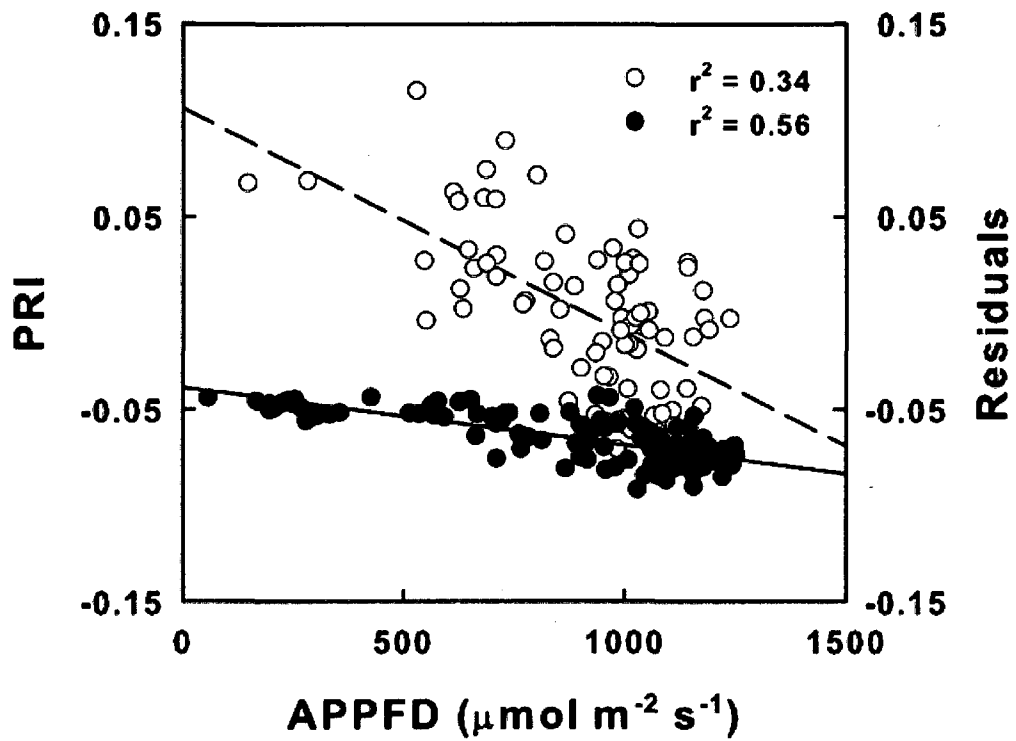


**Figure 3.** Regression results for the relationship between PRI and APPFD during the fully leafed out period (closed circles), and between the residuals from the PRI-LAI regression and APPFD during the green up period (open circles).

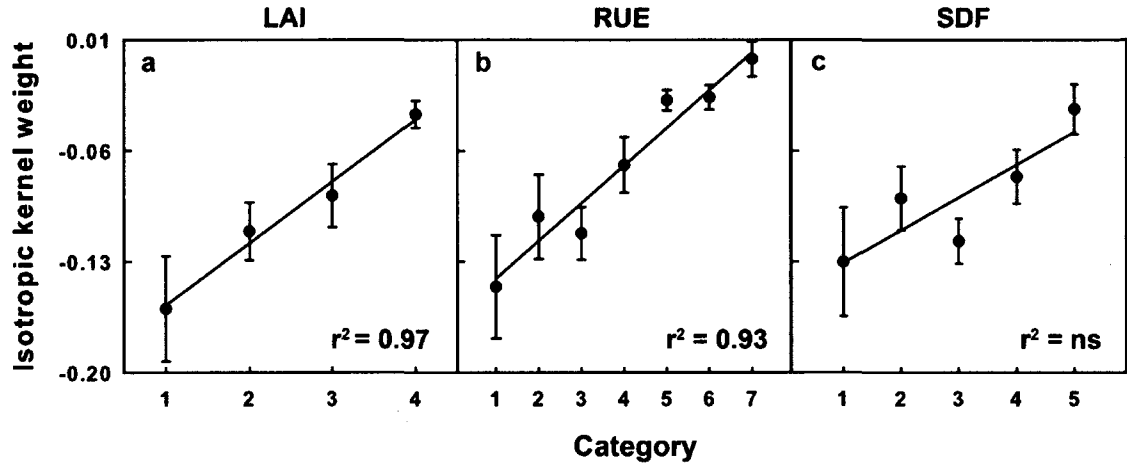


**Figure 4.** Regression between the BRDF isotropic kernel weight and the strata for (a) LAI, (b) RUE, and (c) SDF. The coefficient of determination was significant for LAI and RUE, but not significant for SDF. Error bars represent  $\pm 1$  SD for the mean of each category.

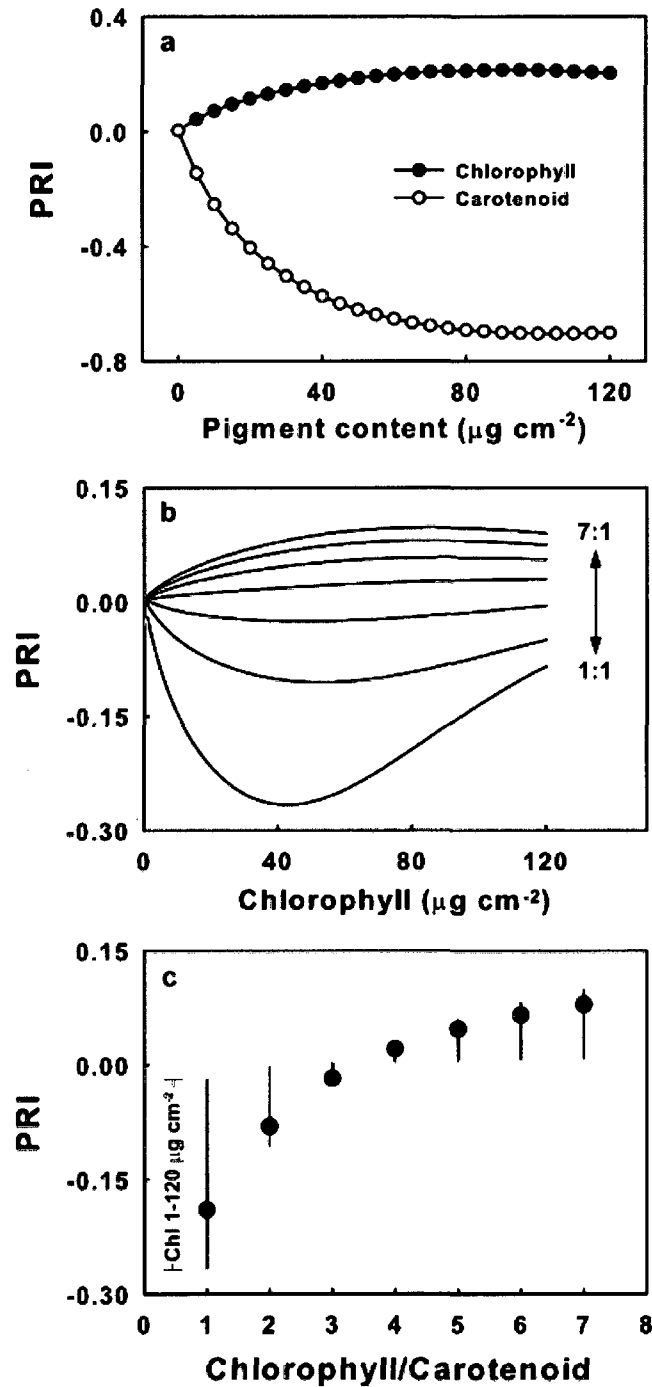


**Figure 5.** Results from PROSPECT simulations, where (a) is the response of simulated PRI to carotenoid content (closed circles) or chlorophyll content (open circles). In each case one pigment was increased from 0 to  $100 \mu\text{g cm}^{-2}$  at  $5 \mu\text{g cm}^{-2}$  increments while the other was held constant at  $0 \mu\text{g cm}^{-2}$ . (b) The response of simulated PRI to increasing Chl

content, where Car content was varied as a constant fraction Chl content. (c) The response of simulated PRI to increasing Chl/Car ratios, where the vertical lines represent the range of resulting values for each ratio that occurred due to variability in Chl content, and closed circles represent the mean for each ratio. Chlorophyll content was varied between 1 and 120  $\mu\text{g cm}^{-2}$  for each ratio simulation.

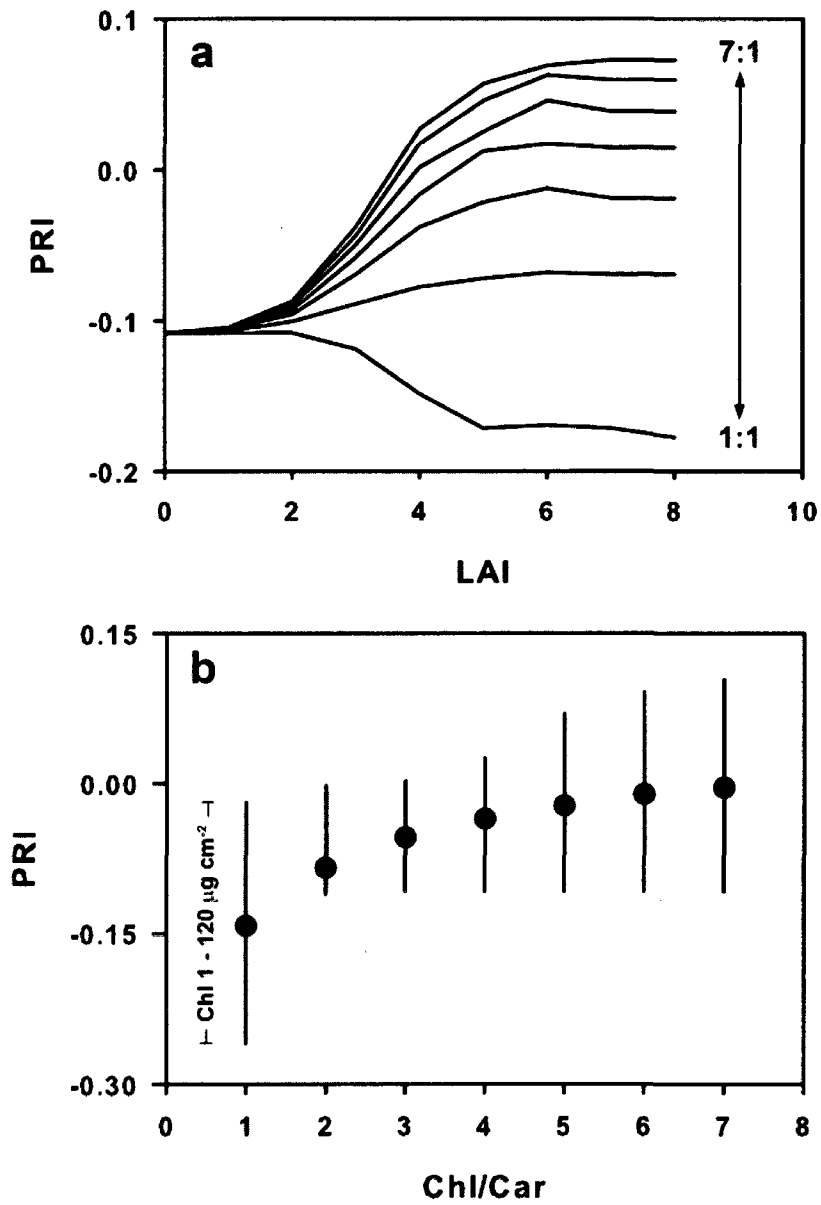


**Figure 6.** PROSAIL simulated canopy level PRI values with increasing (a) LAI or (b) Chl/Car ratio, where the vertical lines represent the range of resulting values for each ratio that occurred due to variability in Chl content, and closed circles represent the mean for each ratio. Chlorophyll content was varied between 1 and 120  $\mu\text{g cm}^{-2}$  for each ratio simulation.

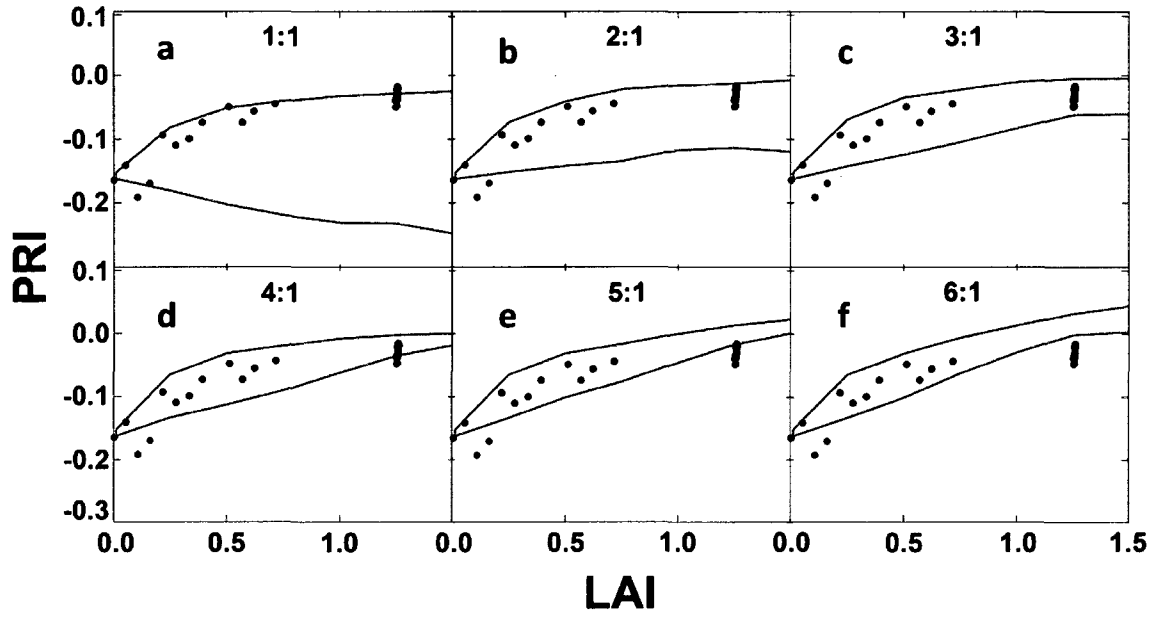
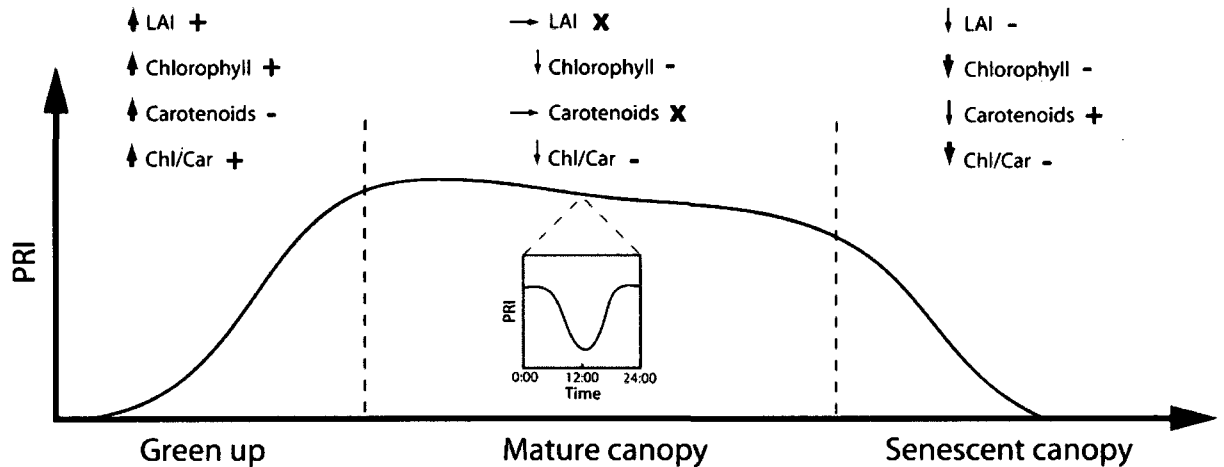


Figure 7. Results from PROSAIL simulations where envelopes represent the range of PRI values expected as LAI increased for a range of Chl/Car ratios (a-f).





**Figure 8.** Conceptual diagram of the expected seasonal PRI trend for a deciduous forest canopy based on the results of our study. The size of the arrow next to the variable (LAI, Chl, Car, or Chl/Car ratio) indicates the magnitude of change in that variable during the time period in which it occurs (green up, mature, or senescence). The symbols to the right of the variable names indicate the influence that each will have on the PRI, where (+) indicates an increase, (-) indicates a decrease, and (x) indicates no effect. The subset figure represents a typical diurnal trend, where the PRI response is primarily a function of changes in xanthophyll pigments.

## CHAPTER 2

### INFLUENCE OF LEAF CHLOROPHYLL AND CAROTENOID CONTENT ON THE PHOTOCHEMICAL REFLECTANCE INDEX

#### Summary

- The Photochemical Reflectance Index (PRI) is used as an indicator of leaf and plant canopy photosynthetic radiation use efficiency. However, the RUE-PRI relationship has been shown to be inconsistent over time, likely due to changes in leaf chlorophyll, carotenoids and the carotenoid/chlorophyll ratio.
- We measured reflectance spectra and physical and biochemical properties from 24 leaves of two deciduous tree species and acquired pigment and reflectance data from the Leaf Optical Properties EXperiment database for an additional nine species. Measurements were used as inputs for the PROSPECT-5 leaf optical model.
- We found measurements of PRI to be significantly ( $p < 0.05$ ) correlated with chlorophyll content, carotenoid content, and the carotenoid/chlorophyll ratio. However, only the PRI-carotenoid/chlorophyll ratio was consistent across all analyses. Two predictive equations were derived from PROSPECT-5 simulations: PRI(c<sub>lm</sub>) predicted the carotenoid/chlorophyll ratio ( $r^2 = 0.99$ ), and CI(c<sub>lm</sub>) predicted chlorophyll content ( $r^2 = 0.98$ ). Multiplying PRI(c<sub>lm</sub>) with CI(c<sub>lm</sub>) mathematically canceled ( $\text{car chl}^{-1} \text{ chl} = \text{car}$ ) the influence of chlorophyll content on PRI(c<sub>lm</sub>) and thus allowed for the prediction of carotenoid content ( $r^2 = 0.83$ ).
- Our results confirm that the PRI is significantly influenced by variations in chlorophyll and carotenoid pools and demonstrate a new approach for non-destructive estimation of leaf carotenoid content using the PRI.

## Introduction

The photochemical reflectance index (PRI) is a spectral vegetation index used in physiological and biogeochemical research as a means for estimating leaf and plant canopy photosynthetic radiation use efficiency (RUE). Gamon et al. (1990, 1992) first demonstrated that changes in the PRI were significantly correlated with the de-epoxidation state of the xanthophyll cycle. The xanthophyll cycle, consisting of the rapid and reversible conversion of the xanthophyll pigment violaxanthin to zeaxanthin, is an important mechanism that allows leaves to harmlessly dissipate excess light energy (Young, 1991; Demmig-Adams and Adams, 1996). The de-epoxidation state of the xanthophyll cycle has been shown to be an indicator of RUE across a wide range of stress levels and types (Schöner and Krause, 1990; Demmig-Adams and Adams, 1992; Verhoeven et al., 1997; Chaves et al., 2002). Several studies have used the PRI for estimating leaf-level RUE (e.g., Gamon et al., 1997; Penuelas et al., 1995; Methy, 2000; Guo & Trotter, 2004). Increasingly, the PRI is being used at the plant canopy scale (e.g., Nichol et al. 2000; Rahman et al., 2004; Hilker et al., 2008) to understand diurnal and seasonal dynamics of RUE because of its importance for understanding plant photosynthesis (Monteith, 1972, 1977; Gamon et al., 2001).

Although the PRI is used as an indicator of photosynthetic efficiency, a growing number of studies are finding that, when measured across time periods longer than a few days, the PRI is apparently influenced by leaf pigments other than xanthophylls. For example, several studies have found a correlation between the carotenoid/chlorophyll ratio and the PRI (Sims & Gamon, 2002; Stylinski et al., 2002; Nakaji et al., 2006; Filella et al. 2009). Nakaji et al. (2006) reported a high correlation between PRI measurements and Japanese larch (*Larix kaempferi*) leaf chlorophyll content when measured across a growing season. Nakaji et al. (2006) also found that the relationship between PRI and RUE was significantly correlated with leaf nitrogen content, carotenoids, xanthophylls, and the carotenoid/chlorophyll ratio. The influence of different pigments on the PRI needs to be accounted for if it is to be used for multi-temporal assessments of xanthophyll activity.

Furthermore, a better understanding of how the PRI responds to leaf biochemical properties may reveal new approaches for remotely quantifying photosynthetic pigments.

One potential use of the PRI may be non-destructive, *in-situ* quantification of carotenoids. Carotenoids play an important role in photosynthetic function, including accessory light harvesting and energy transfer (Frank & Cogdell, 1996; Ritz et al. 2000), as well as photoprotection (Siefermann-Harms, 1987; Young, 1991; Demmig-Adams, 1998). The ability to remotely quantify carotenoid pigment content may enhance our understanding of light absorption and photosynthetic performance, allowing us to better understand photosynthetic acclimation and response to stress.

We used a combined observation- and modeling-based approach to quantify the influence of different pigment types on the PRI at the leaf level. Our objectives were to 1) describe the influence of carotenoid and chlorophyll pigments on the PRI, and 2) develop and test an approach for estimating leaf carotenoid content using the PRI. We hypothesized that if the PRI was significantly related to the carotenoid/chlorophyll ratio, then it could be combined with a chlorophyll vegetation index that had no sensitivity to carotenoids, which would cancel the effect of chlorophyll on the PRI and allow for prediction of carotenoid content. This hypothesis was formulated as:

$$Carotenoid = \frac{Carotenoid}{Chlorophyll} \times Chlorophyll \quad (1)$$

and reformulated as:

$$Carotenoid = PRI \times Chlorophyll Index \quad (2)$$

where PRI (Eq. 2) serves as a proxy for the carotenoid/chlorophyll ratio (Eq. 1).

## Materials and Methods

### Leaf measurements

Ten bur oak (*Quercus macrocarpa*) and 10 sugar maple (*Acer saccharum*) saplings were grown in individual 3.79 L pots. The growing substrate was a mixture of equal parts of vermiculite and forestry grade peat moss (Sun Gro Horticulture Distribution Inc., Bellevue, WA, USA). Each seedling was initially fertilized with 12.5 kg m<sup>-3</sup> of controlled release fertilizer. Leaf pigment content of the saplings was manipulated by randomly applying different water treatments to each sapling, with soil water content ranging between 50 - 100 % of field capacity. Increasing water stress is known to result in decreasing photosynthetic rate, which in turn affects a plant's ability to synthesize plant pigments (Marschner, 1995).

A randomly selected leaf of each sapling was removed with a razor blade and the reflectance of the adaxial side of a 1.56 cm<sup>2</sup> subarea of the leaf was measured with an ASD FieldSpec Pro spectroradiometer (Analytical Spectral Devices, Boulder, CO). Each spectral measurement was preceded by a dark current measurement and a white reference measurement using a white Spectralon® (Labsphere Inc.) reference panel. To reduce the errors associated with illumination effects a fiber optic contact probe was pressed to the leaf surface, ensuring that the leaf subarea was illuminated by a constant light source inside the contact probe (Contact Probe, Analytical Spectral Devices, Boulder, CO). The PRI and red edge Chlorophyll Index (CI) vegetation indices were derived from the measured spectra. These indices were calculated as:

$$PRI = \frac{\rho_{531} - \rho_{570}}{\rho_{531} + \rho_{570}} \quad (3)$$

and

$$CI = \frac{\rho_{760}}{\rho_{700}} - 1 \quad (4)$$

where  $\rho$  was the percent reflectance at the specified wavelength. The CI was selected because preliminary tests confirmed previous studies that showed this index to be significantly ( $p < 0.05$ ) and linearly related to chlorophyll content (Gitelson et al. 2003). We compared measurements of PRI with chlorophyll content, carotenoid content, and the carotenoid/chlorophyll ratio.

Chlorophyll and carotenoid content of the spectrally measured leaf subarea was determined by immersing small pieces ( $< 0.25 \text{ mm}^2$ ) in 10 ml of aqueous 80% acetone (Lichtenthaler and Wellburn, 1983). The solution was stored in a dark room for 24 hours. Pigment extracts were filtered and the absorbancy was measured at 470 nm, 644 nm, and 663 nm with a Thermo scientific GENESYS 20<sup>TM</sup> visible spectrophotometer (Thermo Fisher Scientific Inc., MA, USA). Chlorophyll and carotenoid content of the pigment extract solution was calculated with coefficients determined by Lichtenthaler and Wellburn (1983) in units of  $\mu\text{g cm}^{-2}$  of projected (one-sided) leaf area.

A  $3.5 \text{ cm}^2$  disc was removed from each leaf to determine the dry matter (Cm) and water content (Cw). The fresh weight of each leaf sample was measured and re-weighed after 48 hours in a drying oven at  $80^\circ\text{C}$  to obtain the dry weight. Cw was calculated as the difference between the fresh and dry weight and Cm was the dry weight. Both Cm and Cw were expressed in  $\text{mg cm}^{-2}$  of projected leaf area. A parameter describing the structure of leaf mesophyll (N) cannot be directly measured (Feret et al., 2008) and had to be estimated. Specific leaf area (SLA) was used to estimate N using the hyperbolic relationship described by Jacquemoud and Baret (1990):

$$N = \frac{0.9SLA + 0.025}{SLA - 1} \quad (5)$$

where SLA was calculated as the leaf area per unit leaf dry weight.

In addition to the 24 leaf samples collected in this study, leaf-level pigment and spectral reflectance data from nine deciduous tree species were obtained from the Leaf Optical Properties EXperiment (LOPEX) database (Hosgood et al. 1995) and used in our analysis.

## Model simulations

We used the PROSPECT leaf optical model (Jacquemoud & Baret, 1990) to test the effects of changing leaf pigment pools on the PRI. The PROSPECT-5 version of the model (Ferret et al., 2008) was used because it has the capability to independently model the influence of chlorophyll and carotenoid pigments on spectral reflectance between 400 to 2500 nm at 1 nm increments. Measurements of leaf carotenoid content, chlorophyll content,  $C_w$ ,  $C_m$ , and  $N$  were used as inputs into the model to simulate PRI and CI. Simulated PRI values were compared with measured values of chlorophyll content, carotenoid content, and the carotenoid/chlorophyll ratio.

To evaluate the isolated influence of chlorophyll or carotenoid content on the PRI, model runs were conducted where each pigment type was allowed to increase from 0 to 100  $\mu\text{g cm}^{-2}$  at 5  $\mu\text{g cm}^{-2}$  increments while the other pigment type was held constant at 0  $\mu\text{g cm}^{-2}$ . For these simulations  $C_w$ ,  $C_m$ , and  $N$  were held constant at their respective mean value, which was derived from the leaf measurements.

An additional eight model runs were conducted to develop algorithms for predicting leaf pigment contents with the vegetation indices. Four runs were conducted with chlorophyll content values identical to the leaf-measured values while carotenoid content was assigned to one of four constant values: 0  $\mu\text{g cm}^{-2}$ , 7  $\mu\text{g cm}^{-2}$ , 14  $\mu\text{g cm}^{-2}$ , and 21  $\mu\text{g cm}^{-2}$ . The other four model runs were similar, except that carotenoid content values were identical to leaf-measured values while chlorophyll content was assigned one of four constant values: 10  $\mu\text{g cm}^{-2}$ , 20  $\mu\text{g cm}^{-2}$ , 40  $\mu\text{g cm}^{-2}$ , and 60  $\mu\text{g cm}^{-2}$ . The results from all eight model simulations were used to build regression models describing the relationship

between chlorophyll content and CI and between the carotenoid/chlorophyll ratio and PRI.

### Leaf pigment content prediction

Leaf-measured PRI and CI were input into the regression models that were developed using data generated from PROSPECT-5 simulations. The fitted vegetation indices, PRI(c<sub>lm</sub>) and CI(l<sub>m</sub>), where (c<sub>lm</sub>) indicates curvilinear model and (l<sub>m</sub>) indicates linear model, were used to predict the observed carotenoid/chlorophyll ratio and chlorophyll content from leaf samples, respectively. In a conceptual manner similar to that presented by Eitel et al. (2008), PRI(c<sub>lm</sub>) was multiplied by CI(l<sub>m</sub>) to cancel the effects of chlorophyll on the PRI. This allowed for prediction of carotenoid content following Equations 1 and 2.

### Statistical analysis

Regression analysis was used to model and evaluate the relationship between both measured and simulated spectral vegetation indices and leaf pigments. Linear and non-linear regression tests and modeling were performed using SigmaPlot 9.0 (SPSS Inc.). Student's *t*-tests were used for all pairwise comparisons. Coefficients of determination and pairwise comparisons were considered significant when  $p < 0.1$ . A two-one-sided regression-based bootstrap ( $n = 1000$ ) equivalence test (Robinson et al., 2005; Eitel et al. 2007) was performed using the 'equivalence' package in R to evaluate the equivalency between vegetation index-based predictions and *in situ* measurements of leaf carotenoid content. The null hypothesis of dissimilarity between the means of predicted and measured carotenoid content was rejected ( $\alpha = 0.05$ ) if the mean of the differences (mean (predicted – measured)) was contained within a  $\pm 25\%$  region of similarity. The equivalence test also allowed us to determine if the slope of the least squares fit between predicted and measured carotenoid content was significantly equivalent to unity at the 25% equivalence level.



## Results

### Leaf pigments

For the combined sampled and LOPEX-derived pigment data, chlorophyll content ranged from 10.40 to 72.79  $\mu\text{g cm}^{-2}$  (mean  $\pm$  1 SD: 24.10  $\pm$  16.47  $\mu\text{g cm}^{-2}$ ) and carotenoid content ranged from 2.38 to 16.11  $\mu\text{g cm}^{-2}$  (mean  $\pm$  1 SD: 7.29  $\pm$  3.30  $\mu\text{g cm}^{-2}$ ). The carotenoid/chlorophyll ratio ranged from 0.175 to 0.275 (mean  $\pm$  1 SD: 0.219  $\pm$  0.023). Chlorophyll and carotenoid content were significantly correlated ( $r^2 = 0.94$ ; Fig. 1). For leaves sampled as part of this study chlorophyll content was negatively related to the carotenoid/chlorophyll ratio ( $r^2 = 0.23$ ; Fig. 2a). For LOPEX leaves, carotenoid content was positively related to the carotenoid/chlorophyll ratio ( $r^2 = 0.24$ ; Fig. 2b).

### Influence of pigments on PRI

For leaves sampled as part of this study, measured and simulated PRI were positively related to chlorophyll content ( $r^2 = 0.63$  and  $0.57$  respectively; Figs. 3a and 3d) and carotenoid content ( $r^2 = 0.54$  and  $0.37$  respectively; Figs. 3b and 3e). For LOPEX leaves, measured and simulated PRI were negatively related to chlorophyll content ( $r^2 = 0.34$  for both; Figs. 3a and 3d) and carotenoid content ( $r^2 = 0.35$  and  $0.56$  respectively; Figs. 3b and 3e). For all leaves, measured and simulated PRI was negatively related to the carotenoid/chlorophyll ratio ( $r^2 = 0.22$  and  $0.83$  respectively; Figs. 2c and 2f). When evaluated in isolation, increasing carotenoid content caused simulated PRI to decrease whereas increasing chlorophyll content caused simulated PRI to increase (Fig. 4).

### Combined index carotenoid prediction

A curvilinear, exponential decay regression model (Eq. 6) was fit to the relationship between simulated PRI and the carotenoid/chlorophyll ratio ( $r^2 = 0.98$ ; Fig. 5):

$$\frac{\text{Carotenoid}}{\text{Chlorophyll}} = y_0 + a \times \exp(-b \times PRI) \quad (6)$$

where  $y_0$ ,  $a$ , and  $b$  were empirically derived parameters ( $y_0 = -0.51$ ,  $a = 0.84$ ,  $b = 3.62$ ). Similarly, a linear regression model (Eq. 7) was fit to the relationship between simulated CI and chlorophyll content ( $r^2 = 0.98$ ; Fig. 6):

$$\text{Chlorophyll } (\mu\text{g cm}^{-2}) = y_0 + a \times CI \quad (7)$$

where  $y_0$ ,  $a$ ,  $b$ , and  $c$  were empirically derived parameters ( $y_0 = 0.30$ ,  $a = 17.52$ ). Within PROSPECT-simulations, prediction of chlorophyll content by fitted values of CI (CI(lm)) were not significantly ( $\alpha = 0.05$ ) influenced by carotenoid content (Fig. 7).

The combined index, PRI(cIm)xCI(lm), obtained by fitting measured and LOPEX-derived vegetation indices to Equations 6 and 7, was highly correlated to *in situ* measurements of carotenoid content ( $r^2 = 0.83$ ; Fig. 8). The relationship between the combined index and carotenoid content was not significantly ( $\alpha = 0.05$ ) influenced by chlorophyll content (Fig. 9). Bootstrapped equivalence testing demonstrated that the means of predicted and measured carotenoid content were statistically equivalent ( $\alpha = 0.05$ ). However, the slope was not statistically equivalent to 1 ( $\alpha = 0.05$ ). Results from 1000 bootstrap repetitions estimated the slope to be less than 0.75 approximately 6% of the time, and within the 0.75 to 1.25 region approximately 94 % of the time.

## Discussion

Several studies have shown that changes in PRI are correlated with short-term (i.e., hourly to daily) changes in photosynthetic efficiency (e.g., Gamon et al., 1992, 1997; Penuelas et al., 1995; Methy, 2000; Guo & Trotter, 2004). Our results show that the PRI is also significantly influenced by changes in leaf pigment pools, but the nature of the relationship is inconsistent. Results from both measurements and simulations showed that

the sign of the relationship between both chlorophyll content and PRI, and carotenoid content and PRI was positive for samples obtained for this study and negative for those obtained from the LOPEX database (see Figs. 3a, 3b, 3d, 3e). Simulations where either carotenoid or chlorophyll content were held constant at  $0 \mu\text{g cm}^{-2}$  (see Fig. 4) demonstrate that chlorophyll causes PRI to increase whereas carotenoid causes PRI to decrease, with carotenoids exerting the greatest influence. Because the simulated PRI-chlorophyll relationship and the PRI-carotenoid relationship are both opposite and nonlinear, we would expect the PRI to be most strongly associated with the carotenoid/chlorophyll ratio. Indeed, we found that although the relationship between PRI, carotenoids, and chlorophyll was inconsistent, the relationship between PRI and the carotenoid/chlorophyll ratio was consistently negative for all leaf-measured, LOPEX-derived, and simulated data (see Figs. 3c and 3f). Therefore, assuming that chlorophyll and carotenoid content are positively correlated (as they were in the present study (see Fig. 1)), whenever there is a positive relationship between carotenoid/chlorophyll and chlorophyll or carotenoid content then PRI will have a negative relationship with each pigment type (see Fig. 5). Conversely, whenever there is a negative relationship between the carotenoid/chlorophyll ratio and chlorophyll or carotenoid content then PRI will have a positive relationship with each pigment type (see Fig. 5). In support of this conclusion we found that PRI was positively related to leaf-sampled chlorophyll (see Fig. 3a) and carotenoid content (see Fig. 3b) while leaf-sampled chlorophyll content was negatively correlated with the carotenoid/chlorophyll ratio (see Fig. 2a). Similarly, PRI was negatively correlated with LOPEX-derived chlorophyll (see Fig. 3a) and carotenoid content (see Fig. 3b), and there was a positive correlation between carotenoid content and the carotenoid/chlorophyll ratio (see Fig. 2b). This conclusion is further supported by data from a previous study that reported a positive PRI-chlorophyll and PRI-carotenoid correlation (Nakaji et al. 2006). We found that the chlorophyll and carotenoid contents reported by Nakaji et al. (2006) were negatively related to the carotenoid/chlorophyll ratio (see Fig. 10). These results provide strong evidence that any relationship between PRI and either chlorophyll or carotenoid content is primarily a function of how each pigment is related to the carotenoid/chlorophyll ratio.

Although there were differences in the strength of the PRI-carotenoid/chlorophyll relationship between the observed and modeled data (see Figs. 3c and 3f respectively), in either case the results were consistent with several studies that have reported a negative relationship between the carotenoid/chlorophyll ratio and the PRI when sampled across long time periods (Stylinski et al., 2002; Nakaji et al., 2006; Fillela et al., 2009) or across different species (Sims & Gamon, 2002; Guo & Trotter, 2004). Because this relationship has often been cited, we expected a higher correlation between leaf-measured PRI or LOPEX-derived PRI and the carotenoid/chlorophyll ratio. It is possible that the relationship was lower than expected because of variability in the de-epoxidation state of the xanthophyll cycle between leaf samples. This may especially be the case because in the present study the plants from which leaf samples were collected were presumably under a wide range of drought stress, which would have caused variability in xanthophyll pigments (Demmig-Adams and Adams, 1992; Chaves et al., 2002). A limitation of this study was that there were no measurements of the de-epoxidation state of the xanthophyll cycle for the leaf samples so it is impossible to know what effect this may have had on PRI measurements. Furthermore, PROSPECT-5 did not have the ability to isolate the influence of xanthophylls on spectral reflectance. Further investigation into the drivers of PRI variability would benefit from simultaneous measurements of chlorophylls, carotenoids, and the de-epoxidation state of the xanthophyll cycle. The ability to model xanthophyll contribution to spectral reflectance and transmittance may also be beneficial.

Because the PRI was highly correlated to the carotenoid/chlorophyll ratio, we hypothesized that multiplying it by a chlorophyll vegetation index would allow for prediction of carotenoid content. We found that simulated CI was strongly related to chlorophyll content (see Fig. 6), but was not significantly influenced by carotenoid content (see Fig. 7). Therefore, it provided a suitable index for combining with PRI. The combined index,  $PRI(c_{lm}) \times CI(l_m)$ , was not significantly influenced by variations in chlorophyll content (see Fig. 9) and performed reasonably well for predicting carotenoid content in leaf samples from this study and from the LOPEX database (see Fig. 8). Although the mean, and therefore intercept, of predicted carotenoid content and actual carotenoid content was statistically equivalent, the slope of the relationship was not

equivalent to unity. The results indicate that  $PRI(cIm) \times CI(lm)$  underestimates carotenoid content when it is less than  $6.5 \mu\text{g cm}^{-2}$  and overestimates carotenoid content when it is greater than or equal to  $6.5 \mu\text{g cm}^{-2}$ . The possibility that variation in xanthophyll pigments had an impact on the relationship between measured PRI and the carotenoid/chlorophyll ratio cannot be disregarded. Because the 531 nm xanthophyll detection wavelength was originally selected to optimize detection of changes in the de-epoxidation state of the xanthophyll cycle (Gamon et al. 1990), our predictions of total carotenoid content may have been overly influenced by the activity of this single class of carotenoids. Improved predictions of total carotenoid content may be possible by selecting a broader (e.g.,  $> 10$  nm) carotenoid detection band centered at 531 nm for the PRI rather than the traditional use of a narrow band width detection region.

Our results show that 1) PRI is significantly influenced by chlorophyll content, carotenoid content, and the carotenoid/chlorophyll ratio, irrespective of the de-epoxidation state of the xanthophyll cycle, and 2) the PRI can be used in conjunction with other spectral vegetation indices to predict foliar carotenoid content in broadleaf tree species. These results suggest that caution should be applied when using the PRI to estimate leaf or plant canopy photosynthetic efficiency, especially across spatial or temporal scales where pigment contents vary significantly (e.g., multi-temporal satellite imagery). Although changes in plant pigments may confound PRI-based estimates of RUE, new opportunities for using the PRI for purposes beyond its original design for detecting the de-epoxidation state of the xanthophyll cycle may arise. For example, the combination of PRI and CI successfully canceled the effects of chlorophyll on the PRI, which allowed for prediction of carotenoid content. Therefore, the PRI may be considered to be more broadly useful for understanding photosynthetic efficiency and photoprotection than previously assumed.

## **Acknowledgements**

This work was supported by the Harold Heady Professorship at the University of Idaho, and by an NSF-ESPCoR grant to the State of Idaho. We would like to thank Anthony

Davis for providing plant material and Ronald Robberecht for providing helpful comments that improved the quality of this manuscript.

## References

- Chaves MM, Pereira JS, Maroco J, Rodrigues ML, Ricardo CPP, Osorio ML, Carvalho I, Faria T, Pinheiro C. 2002. How plants cope with water stress in the field. Photosynthesis and growth. *Annals of Botany* 89: 907-916.
- Daughtry CS, Walthall CL, Kim MS, Brown de Colstoun E, McMurtrey JE. 2000. Estimating corn leaf chlorophyll concentration from leaf and canopy reflectance. *Remote Sensing of Environment* 74: 229-239.
- Demmig-Adams B, Adams WW. 1992. Photoprotection and other responses of plants to high light stress. *Annual Review of Plant Physiology and Plant Molecular Biology* 43: 599-626.
- Demmig-Adams B, Adams WW. 1996. The role of xanthophyll cycle carotenoids in the protection of photosynthesis. *Trends in Plant Science* 1: 21-26.
- Eitel JUH, Long D, Gessler PE, Smith AMS. 2007. Using in-situ measurements to evaluate new RapidEye satellite series for prediction of wheat nitrogen status. *International Journal of Remote Sensing* 18: 4183-4190.
- Eitel JUH, Long DS, Gessler PE, Hunt ER. 2008. Combined Spectral Index to Improve Ground-Based Estimates of Nitrogen Status in Dryland Wheat. *Agronomy Journal* 100: 1694-1702.
- Faret J-B, Francois C, Asner GP, Gitelson AA, Martin RE, Bidet LPR, Ustin SL, le Marie G, Jacquemoud S. 2008. PROSPECT-4 and 5: Advances in the leaf optical properties model separating photosynthetic pigments. *Remote Sensing of Environment* 112: 3030-3043.

- Fillela I, Porcar-Castell A, Munne-Bosch S, Back J, Garbulsky MF, Penuelas J. 2009. PRI assessment of long-term changes in carotenoids/chlorophyll ratio and short-term changes in de-epoxidation state of the xanthophyll cycle. *International Journal of Remote Sensing* 30: 4443-4455.
- Frank HA, Cogdell RJ. 1996. Carotenoids in photosynthesis. *Photochemistry and Photobiology* 63: 257-264.
- Gamon JA, Field CB, Bilger W, Bjorkman O, Fredeen AL, Penuelas J. 1990. Remote sensing of the xanthophyll cycle and chlorophyll fluorescence in sunflower leaves and canopies. *Oecologia* 85: 1-7.
- Gamon JA, Penuelas J, Field CB. 1992. A narrow-waveband spectral index that tracks diurnal changes in photosynthetic efficiency. *Remote Sensing of Environment* 41: 35-44.
- Gamon JA, Serrano L, Surfus JS. 1997. The photochemical reflectance index: an optical indicator of photosynthetic radiation use efficiency across species, functional types, and nutrient levels. *Oecologia* 112: 492-501.
- Gamon JA, Field CB, Fredeen AL, Thayer S. 2001. Assessing photosynthetic downregulation in sunflower stands with an optically-based model. *Photosynthesis Research* 67: 113-125.
- Gitelson AA, Gritz Y, Merzlyak, MN. 2003. Relationships between leaf chlorophyll content and spectral reflectance and algorithms for non-destructive chlorophyll assessment in higher plant leaves. *Journal of Plant Physiology* 160: 271-282.

- Guo J, Trotter CM. 2004. Estimating photosynthetic light-use efficiency using the photochemical reflectance index: variations among species. *Functional Plant Biology* 31: 255-265.
- Hilker T, Coops NC, Schwalm CR, Jassal RS, Black TA, Krishnan P. 2008. Effects of mutual shading of tree crowns on prediction of photosynthetic light-use efficiency in a coastal Douglas-fir forest. *Tree Physiology* 28: 825-834.
- Hosgood B, Jacquemoud S, Andreoli G, Verdebout J, Pedrini G, Schmuck G. 1995. *Leaf Optical Properties Experiment 93 (LOPEX93)*. Joint Research Center, Institute for Remote Sensing Applications, Ispra (Italy), Report EUR-16095-EN, European Commission, Luxembourg.
- Jacquemoud S, Baret F. 1990. PROSPECT: A model of leaf optical properties spectra. *Remote Sensing of Environment* 34: 75-91.
- Lichtenthaler HK, Wellburn AR. 1983. Determination of total carotenoids and chlorophylls a and b of leaf extracts in different solvents. *Biochemical Society Transactions* 11: 591-592.
- Marschner H. 1995. *Mineral nutrition of higher plants*. London: Academic Press, London.
- Methy M. 2000. Analysis of photosynthetic activity at the leaf and canopy levels from reflectance measurements: a case study. *Photosynthetica* 38: 505-512.
- Monteith JL. 1972. Solar radiation and production in tropical ecosystems. *Journal of Applied Ecology* 9: 747-766.



- Monteith JL. 1977. Climate and the efficiency of crop production in Britain. *Philosophical Transactions of the Royal Society of London. Series B, Biological Sciences* 281: 277-294.
- Nakaji T, Oguma H, Fujinuma Y. 2006. Seasonal changes in the relationship between photochemical reflectance index and photosynthetic light use efficiency of Japanese larch needles. *International Journal of Remote Sensing* 27: 493-509.
- Nichol CJ, Huemmrich KF, Black TA, Jarvis PG, Walthall CL, Grace J, Hall FG. 2000. Remote sensing of photosynthetic light-use-efficiency of boreal forest. *Agricultural and Forest Meteorology* 101: 131-142.
- Penuelas J, Filella I, Gamon JA. 1995. Assessment of photosynthetic radiation-use efficiency with spectral reflectance. *New Phytologist* 131: 291-296.
- Rahman AF, Cordova VD, Gamon JA, Schmid HP, Sims DA. 2004. Potential of MODIS ocean bands for estimating CO<sub>2</sub> flux from terrestrial vegetation: a novel approach. *Geophysical Research Letters*, 31: L10503, doi:10.1029/2004GL019778.
- Robinson AP, Duursma RA, Marshall JD. 2005. A regression-based equivalence test for model validation: shifting the burden of proof. *Tree Physiology* 7: 903-913.
- Schöner S, Krause GH. 1990. Protective systems against active oxygen species in spinach: response to cold acclimation in excess light. *Planta* 180: 383-389.
- Siefermann-Harms D. 1987. The light-harvesting and protective functions of carotenoids in photosynthetic membranes. *Physiologia Plantarum* 69: 561-568.
- Sims DA, Gamon JA. 2002. Relationships between leaf pigment content and spectral reflectance across a wide range of species, leaf structures and developmental stages. *Remote Sensing of Environment* 81: 337-354.

Stylinski CD, Gamon JA, Oechel WC. 2002. Seasonal patterns of reflectance indices, carotenoid pigments and photosynthesis of evergreen chaparral species. *Oecologia* 131: 366-374.

Verhoeven AS, Demmig-Adams B, Adams WW. 1997. Enhanced employment of the xanthophyll cycle and thermal energy dissipation in spinach exposed to high light and N stress. *Plant Physiology* 113: 817-824.

Young AJ. 1991. The photoprotective role of carotenoids in higher plants. *Physiologia Plantarum* 83: 702-708.

## Figures

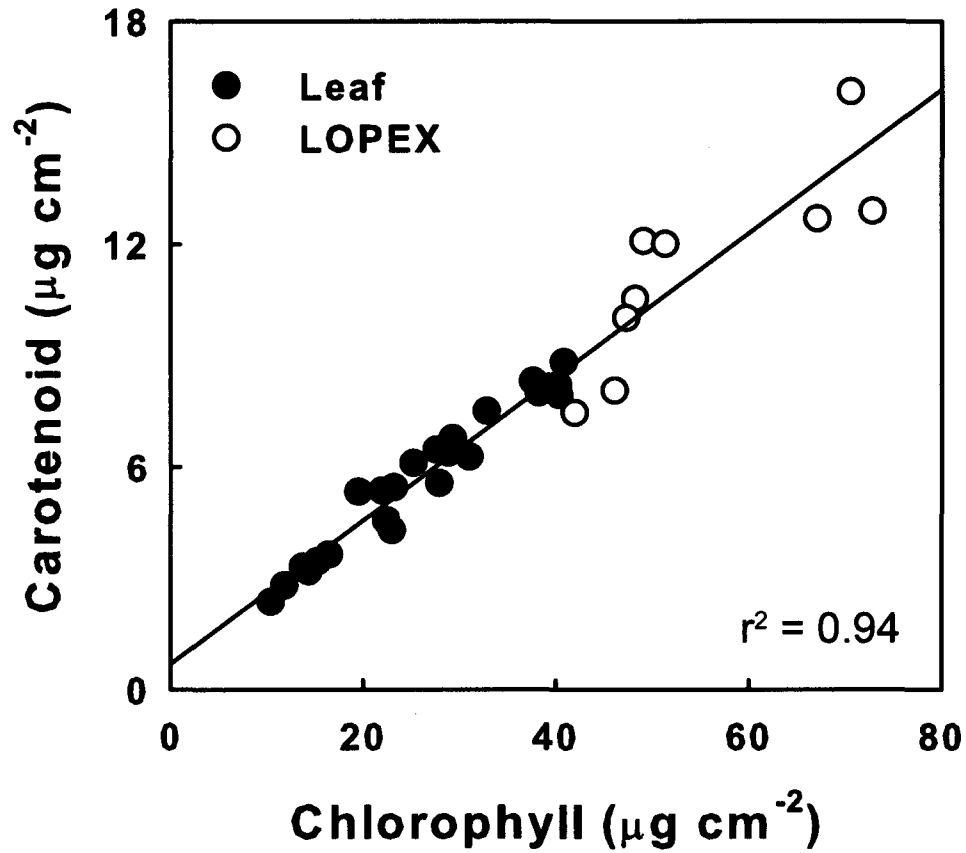


**Figure 1.** Least square regression between chlorophyll and carotenoid content from leaves sampled in this study (closed circles) and from the LOPEX database (open circles).

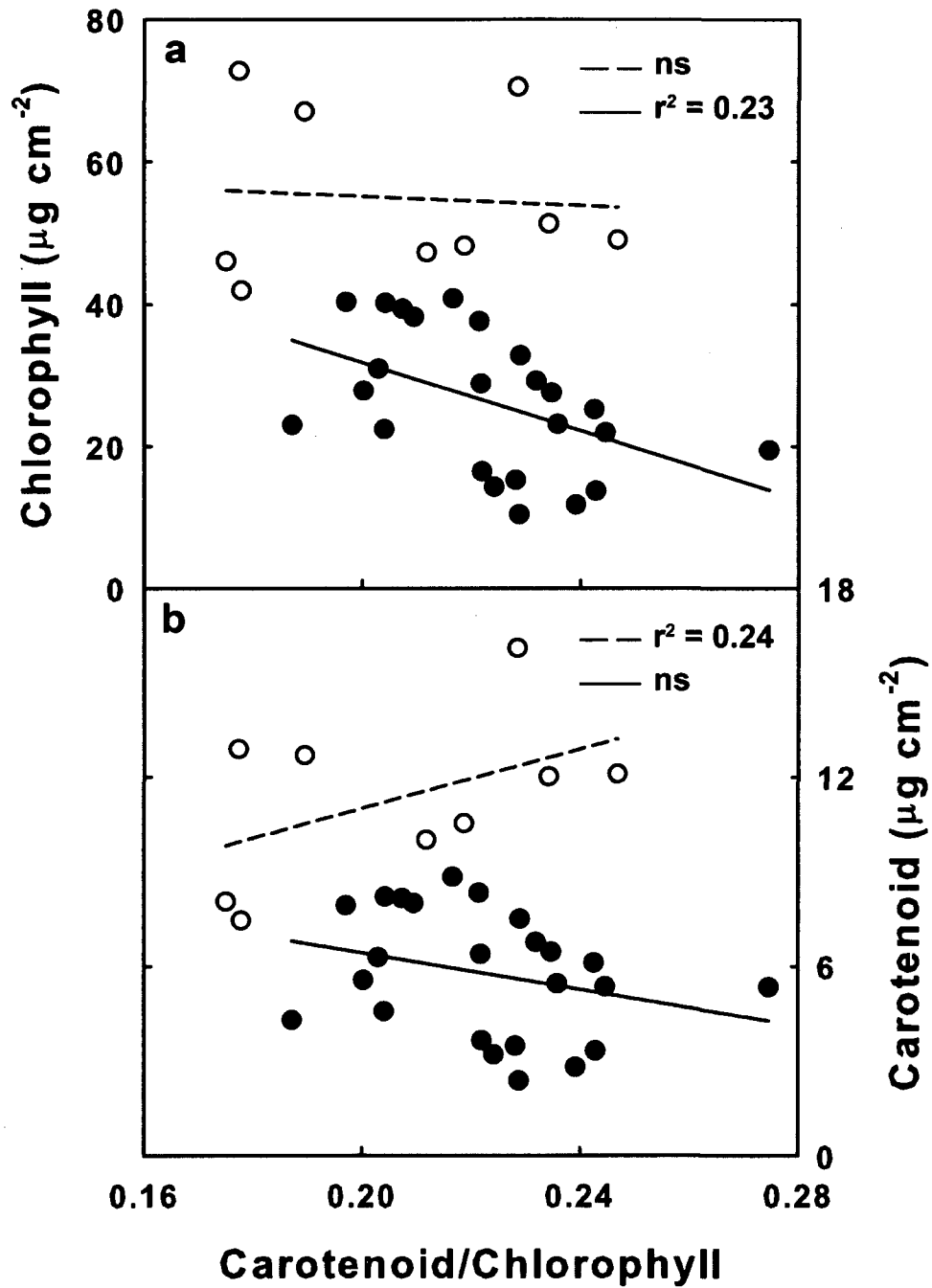


**Figure 2.** Least squares regression between the carotenoid/chlorophyll ratio and chlorophyll content (a) and carotenoid content (b) for leaves sampled in this study (closed circles) and from the LOPEX database (open circles). Solid lines are the least squares fit for the leaf data and dashed lines are the least squares fit for the LOPEX data.

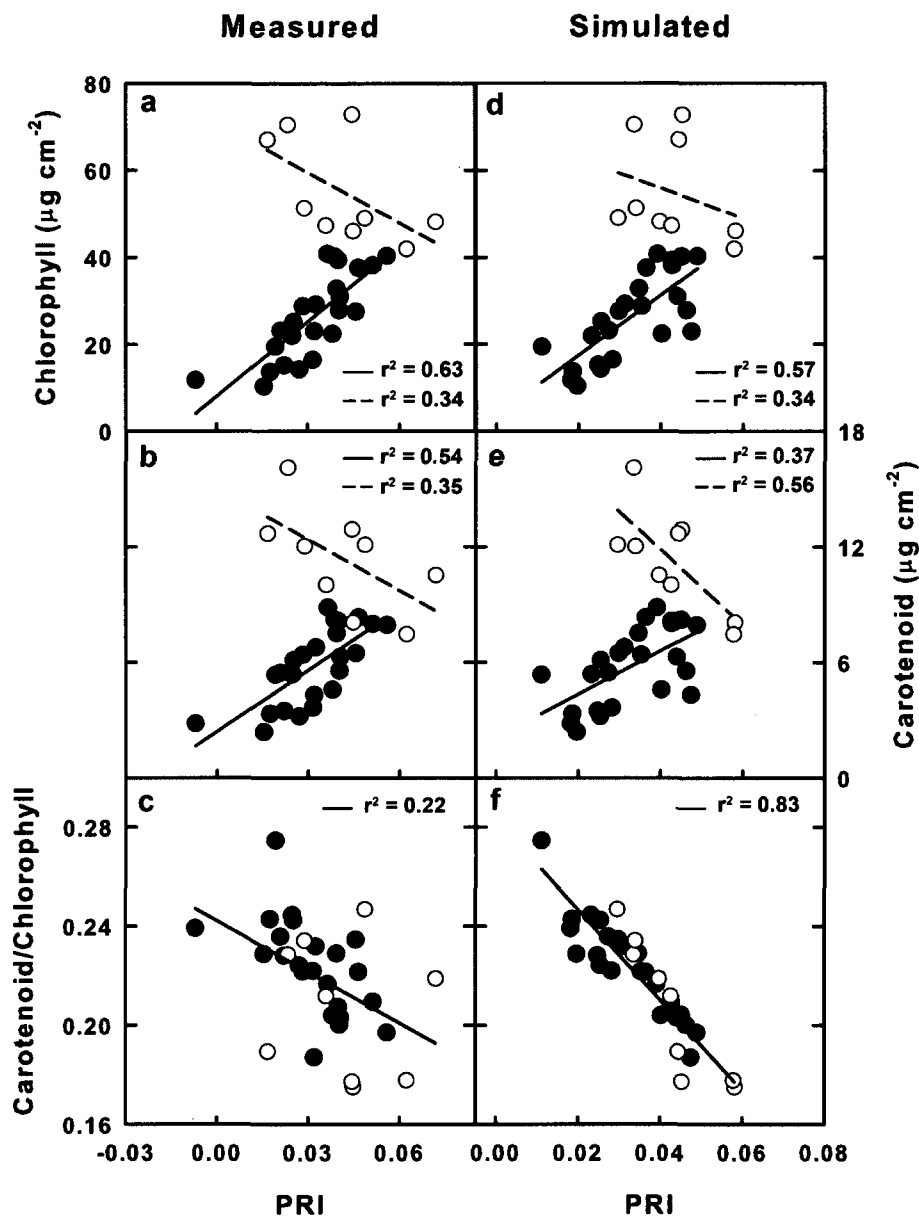


**Figure 3.** Least squares regression of leaf-derived (measured) PRI and PROSPECT-simulated (simulated) PRI versus chlorophyll content (a, d), carotenoid content (b, e), and the carotenoid/chlorophyll ratio (c, f). Closed circles represent leaves sampled for this study and closed circles represent data from the LOPEX database. In panels (a), (b), (d), and (e) solid lines are the least squares fit for the leaf data and dashed lines are the least squares fit for the LOPEX data. In panels (c) and (f) a single least squares line was fit to all data.

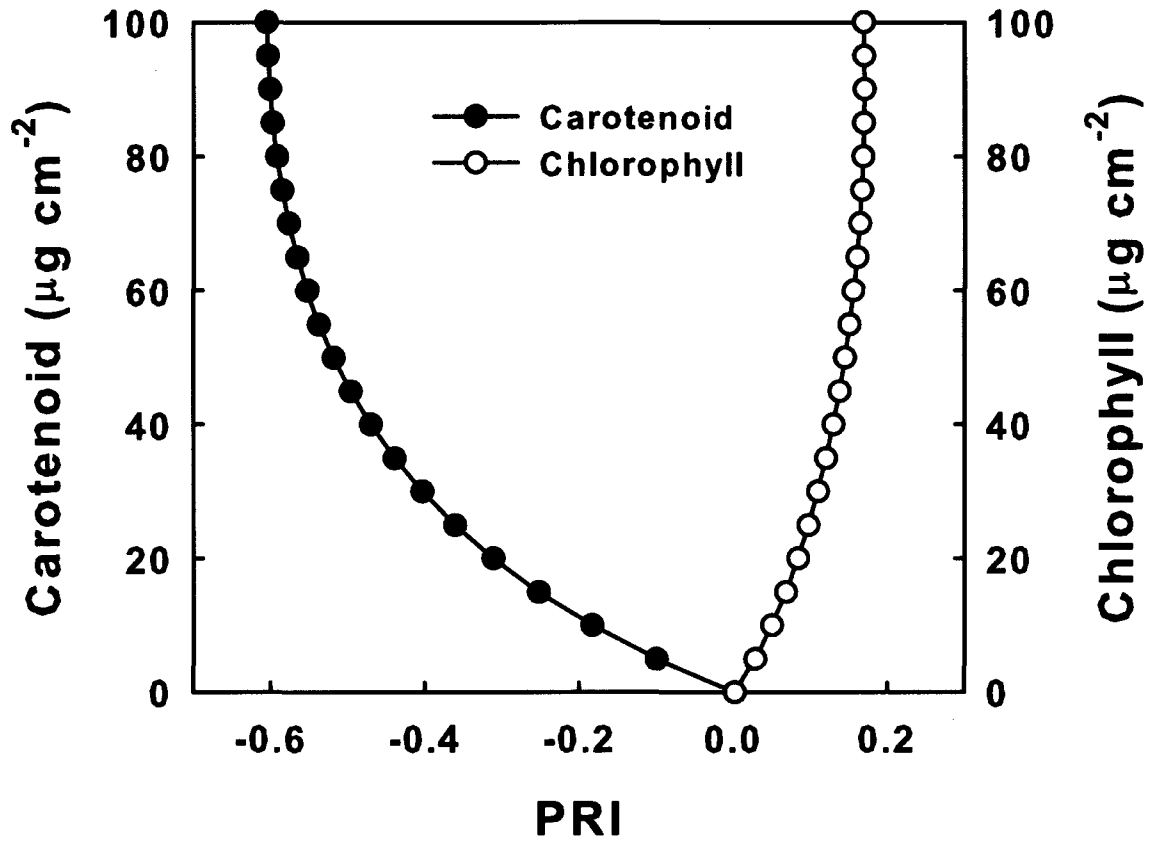


**Figure 4.** Response of PROSPECT-simulated PRI to carotenoid content (closed circles) or chlorophyll content (open circles). In each case one pigment was increased from 0 to 100  $\mu\text{g cm}^{-2}$  at 5  $\mu\text{g cm}^{-2}$  increments while the other was held constant at 0  $\mu\text{g cm}^{-2}$ .

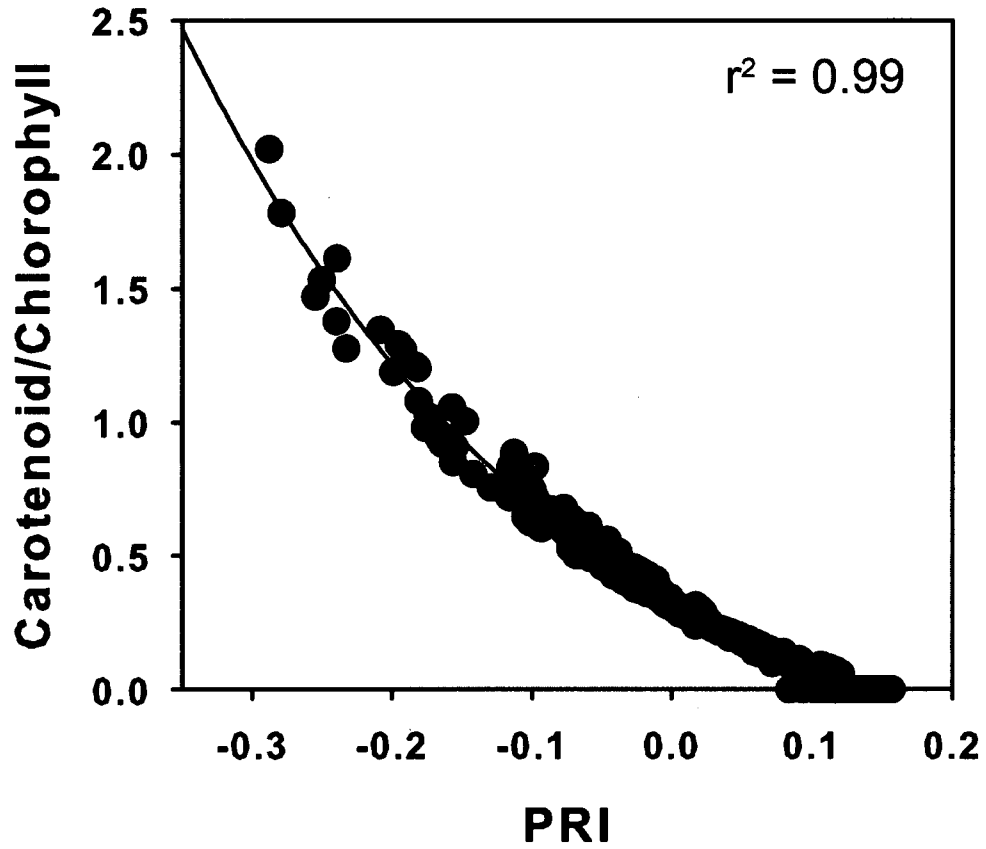


**Figure 5.** PROSPECT-simulated PRI versus the carotenoid/chlorophyll ratio. The curvilinear model fitted to these data was used to predict the leaf carotenoid/chlorophyll ratio using leaf measurements of PRI.

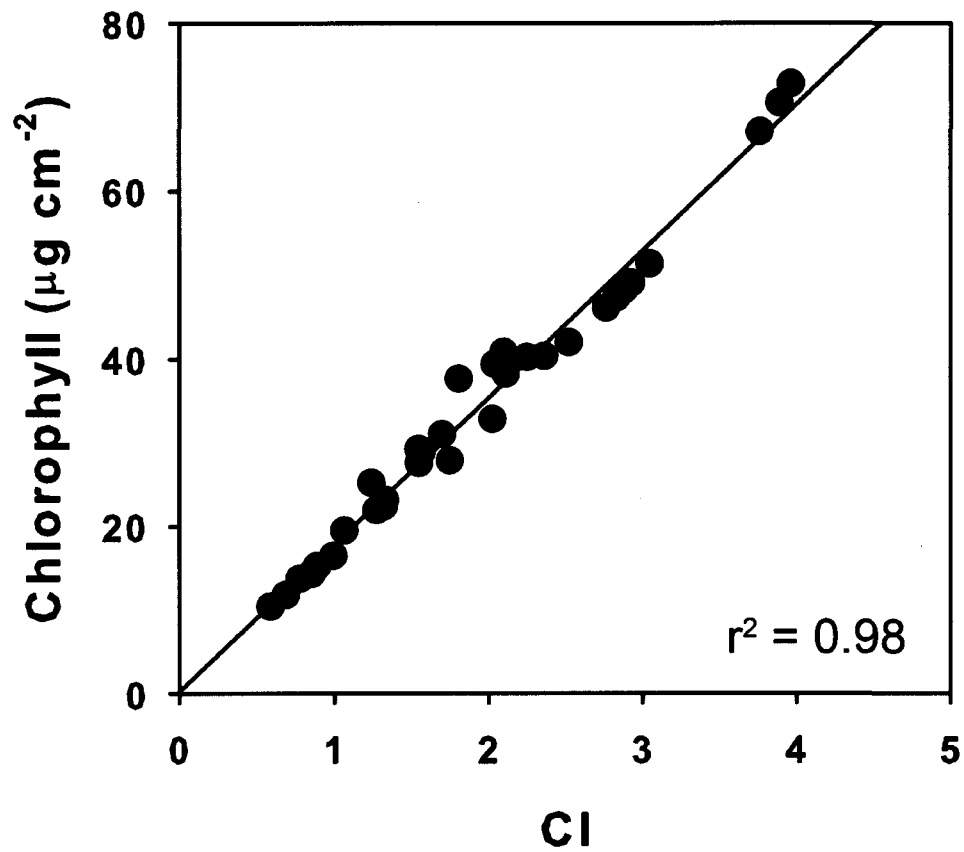


**Figure 6.** PROSPECT-simulated CI versus chlorophyll content. The linear model fitted to these data was used to predict leaf chlorophyll content using leaf measurements of CI.



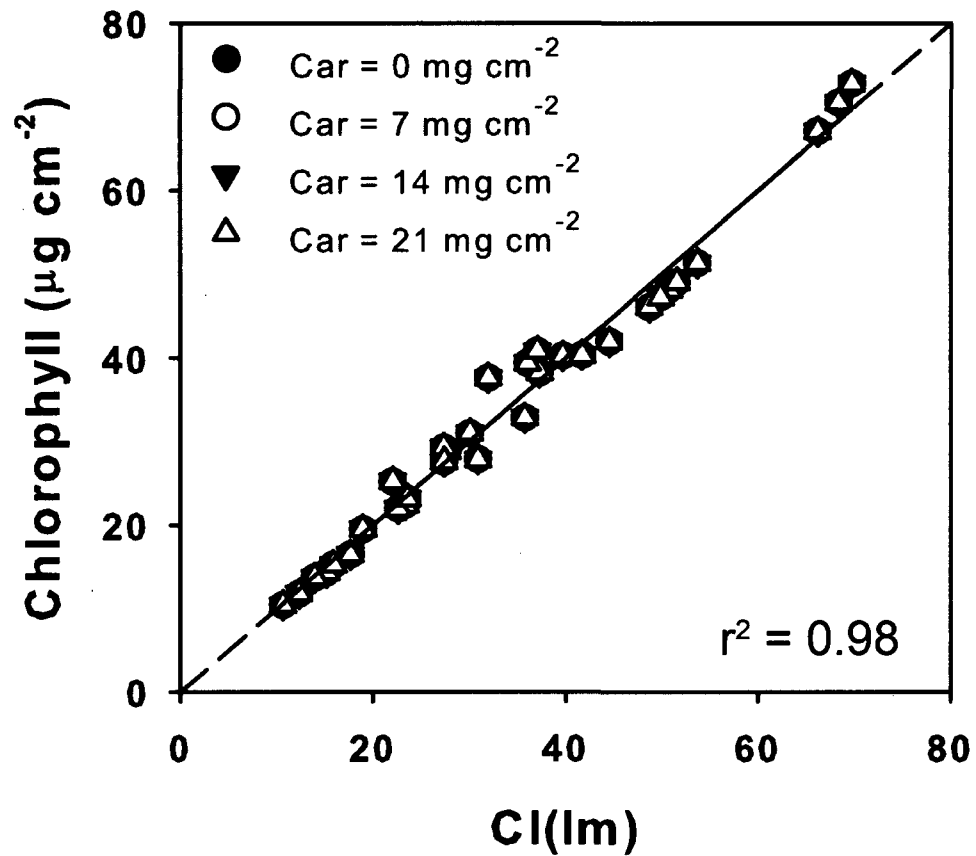


**Figure 7.** Fitted values of PROSPECT-simulated CI versus chlorophyll content across a range of carotenoid contents. Carotenoid content did not significantly influence the CI-chlorophyll relationship.

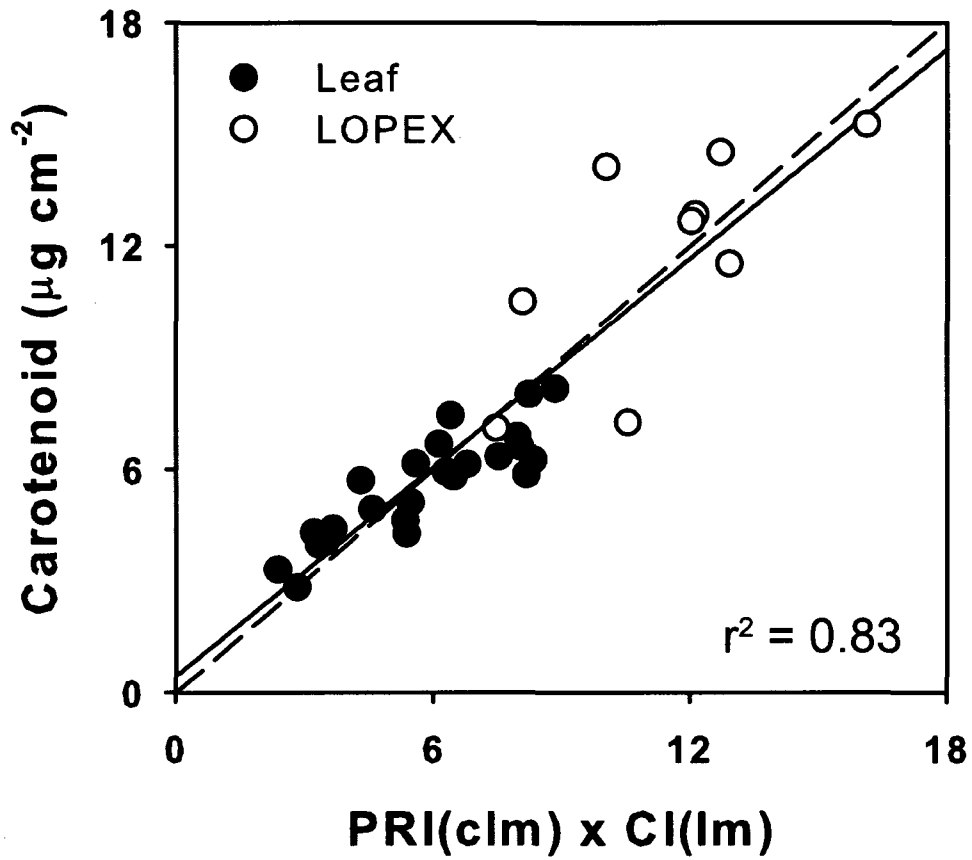


**Figure 8.** Predicted carotenoid content ( $\text{PRI}(\text{clm}) \times \text{CI}(\text{lm})$ ) versus measured carotenoid content. Closed circles represent data measured for this study and open circles represent data obtained from the LOPEX database. The dashed line represents the 1:1 relationship. Slope = 0.93, intercept =  $0.46 \mu\text{g cm}^{-2}$ , RMSE =  $1.43 \mu\text{g cm}^{-2}$ .

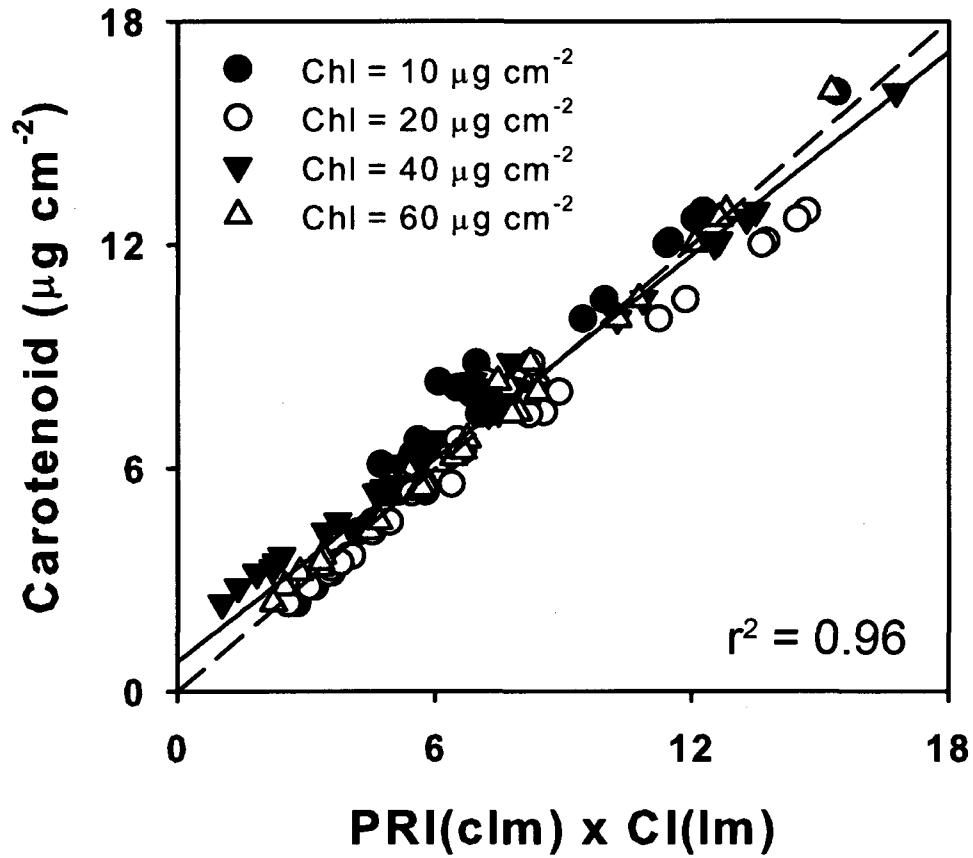


**Figure 9.** The carotenoid prediction equation (PRI(cIm) x CI(lm)) versus carotenoid content across a range of chlorophyll contents. Chlorophyll content did not significantly influence the predicted versus measured relationship. The dashed line represents the 1:1 relationship.

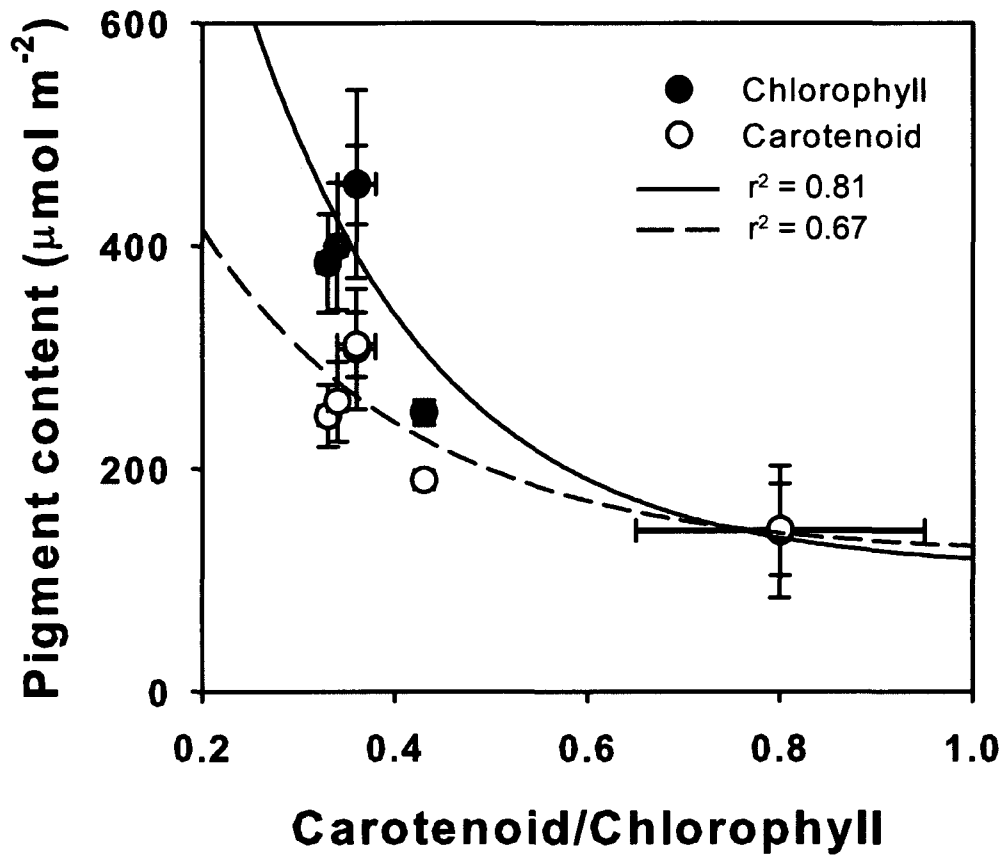


**Figure 10.** The carotenoid/chlorophyll ratio versus either chlorophyll content (closed circles) or carotenoid content (open circles). The solid line represents the least squares fit for chlorophyll content and the dashed line represents the least squares fit for carotenoid content. Data from Nakaji et al. (2006).

## CHAPTER 3

### A SIMPLE FILTERED PHOTODIODE INSTRUMENT FOR CONTINUOUS MEASUREMENT OF NARROWBAND NDVI AND PRI OVER VEGETATED CANOPIES

#### **Abstract**

Recent advances in understanding relationships between spectral reflectance of vegetation canopies and the structural and physiological drivers of canopy-atmosphere carbon dioxide exchange highlight the potential for using narrowband spectral vegetation indices to spatially scale CO<sub>2</sub> fluxes beyond the area of a tower footprint. However, ground reference observations of narrowband spectral reflectance in support of satellite observations can be challenging to obtain because 1) automated sampling of both upwelling and downwelling radiation is required over extended time periods to characterize diurnal and seasonal variability, 2) hyperspectral spectroradiometer data and hardware can be sensitive to environmental factors such as temperature and moisture, and 3) hyperspectral spectroradiometers are expensive, greatly limiting prospects for widespread automated sampling. We have therefore developed the QuadPod: a simple, lightweight, relatively low cost and low power sensor capable of continuously measuring upwelling and downwelling radiation in 10 nm wavebands centered at 532 nm, 568 nm, 676 nm, and 800 nm. QuadPod measurements can be combined to calculate spectral reflectance indices (*e.g.*, the photochemical reflectance index, PRI; and the normalized difference vegetation index, NDVI) useful for modeling canopy-atmosphere carbon exchange. The basic QuadPod instrument design described here can be implemented using any combination of optical filters in order to calculate other spectral vegetation indices.

## 1. Introduction

Networks of environmental instruments are increasingly used to provide critical information about biosphere-atmosphere interactions, with a major research focus on uncovering mechanisms influencing exchanges of mass and energy between plant canopies and the atmosphere (*e.g.*, Running et al., 1999). Networks of micro-meteorological flux towers, such as those represented globally by Fluxnet, are vital for understanding the processes controlling these exchanges of mass and energy (Baldocchi et al., 2001), and provide data necessary for calibrating and validating models designed to scale CO<sub>2</sub> fluxes from the footprint of these towers to the global extent (Cohen and Justice, 1999). Central to these scaling efforts are spectral remote sensing measurements collected from satellites (*e.g.* Running et al., 2004; Hill et al., 2006; Drolet et al. 2008; Sims et al., 2008), aircraft (*e.g.* Nichol et al., 2000; Fuentes et al., 2006), and increasingly, tower-based instruments (*e.g.* Leuning et al., 2006; Sims et al., 2006; Hall et al. 2008; Hilker et al., 2007, 2008a, 2008b). While tower-based spectral measurements show great potential for understanding links between canopy-level ecophysiological processes and global-level spectral observations (Gamon et al., 2006a), the number of towers that currently support spectral reflectance measurements is few, in part due to the high cost and complicated long-term operation of hyperspectral spectroradiometers.

### 1.1 Background theory

The primary use of spectral reflectance data in studies of vegetation productivity and CO<sub>2</sub> exchange involves the incorporation of spectrally derived vegetation indices into some form of vegetation productivity model. Monteith (1972) proposed a simple model of gross primary productivity (GPP) for crops, which has provided the basis for many models using remote sensing driven estimates of ecosystem productivity (Sims et al., 2006). This model relies on inputs of incident photosynthetically active radiation (PAR), the fraction of incident radiation absorbed by photosynthetic tissue (fPAR), and the efficiency with which absorbed radiation is used to fix carbon by the plant (mol C fixed per mol quanta absorbed), hereafter referred to as light use efficiency (LUE; Equation 1).

$$GPP = (PAR * fPAR) * LUE \quad \text{Eq. 1}$$

A growing body of work has demonstrated the utility of narrowband ( $\leq 10$  nm full width half maximum (FWHM) spectral resolution) optical remote sensing to derive both fPAR and LUE estimates that can in turn be used to estimate GPP based on Equation 1 (Rahman et al., 2001, 2004; Sims et al., 2005, 2006). The specific vegetation indices typically used in these and other studies for estimating fPAR and LUE are the Normalized Difference Vegetation Index (NDVI; Equation 2) and the Photochemical Reflectance Index (PRI; Equation 3), respectively. Sellers (1987) demonstrated the functional relationship between NDVI and fPAR, while Gamon et al. (1990, 1992) showed that changes in reflectance near 531 nm corresponded with xanthophyll pigment interconversion, which in many plants correlates highly with LUE. These narrowband vegetation indices are calculated as:

$$NDVI = (\rho_{800} - \rho_{675}) / (\rho_{800} + \rho_{675}) \quad \text{Eq. 2}$$

and

$$PRI = (\rho_{531} - \rho_{570}) / (\rho_{531} + \rho_{570}) \quad \text{Eq. 3}$$

where  $\rho$  is the reflectance at the specified wavelength.

To acquire such narrowband optical data, field- and satellite-based hyperspectral instruments that collect tens to hundreds of spectral bands are used. However, it is often a major challenge to adequately match temporal and spatial resolutions between flux source area as measured via tower-based micrometeorological instrumentation and optical signals measured by earth orbiting spectrometers. For example, the MODIS GPP product is produced as an 8 day composite (Running et al., 2004), whereas eddy covariance flux estimates are generally calculated on the half hourly to hourly time scale. To better understand the mechanisms driving the relationships between biosphere-atmosphere fluxes of CO<sub>2</sub> and canopy reflectance a growing number of researchers now use dual-channel spectroradiometers mounted on or around flux towers (Gamon et al., 2006a). These ‘dual-channel’ instruments provide both sky irradiance and canopy

radiance measurements to allow continuous calculation of canopy reflectance at spatial and temporal scales much finer than those available via aircraft- or satellite-based instruments and that more closely match the source footprint of flux towers (*e.g.*, Leuning et al., 2006; Sims et al., 2006; Hilker et al., 2007). The potential for using such high frequency diurnal canopy reflectance data was demonstrated by Hilker et al. (2008a, 2008b), who reported the effects of canopy shading on the relationship between the PRI and canopy LUE. Results from these studies have begun to provide significant insight relating to the mechanistic linkages between the spectral and physiological behavior of various vegetative communities, and underscore the need to expand such optical sampling to a larger number of tower locations.

As findings from the aforementioned studies indicate, for many vegetation canopies it may only be necessary to measure a limited number of narrow wavebands to accurately model canopy GPP under a variety of environmental conditions. Consequently, the instruments used to record narrowband reflectance from flux towers can be simplified. For example, it may be more desirable to deploy low-cost and low-maintenance instruments that detect a few narrow wavebands (*e.g.* the PRI and NDVI bands listed in Equations 2 and 3) rather than use dual-channel hyperspectral spectroradiometers capable of collecting hundreds of contiguous spectral channels. Indeed, photovoltaic semi-conductors (photodiodes) have a well established history in ecophysiological research and represent a potential alternative to spectroradiometers for measuring narrowband radiation required to model canopy-atmosphere CO<sub>2</sub> exchange. One of the earliest ecological applications of photodiodes was the use of filtered selenium and silicon photodiodes to measure photosynthetic photon flux density (PPFD) within plant canopies (Federer and Tanner, 1966; Biggs et al., 1971). Unfiltered Gallium Arsenide Phosphide photodiodes have a spectral response function similar to the PAR wavelengths in the range 400-700 nm and therefore have more recently become standard instrumentation for PPFD measurement across a wide range of environments, including crop canopies (*e.g.*, Gutschick et al., 1985), temperate and tropical forest canopies (*e.g.*, Pfitsch and Pearcy, 1992; Vierling and Wessman, 2000), and streambeds (*e.g.*, Melbourne and Daniel, 2003). Currently, photodiodes represent the core sensing apparatus in most commercially



available PPFD instruments. While typically used to quantify radiant energy across wide wavebands (*e.g.*, across the full PAR spectrum), these same photodiodes can be used to measure narrowband radiation when used with narrow bandpass filters (after Pontailier and Genty, 1996). Such a filtered narrowband instrument could be configured to continuously collect data to aid in understanding the diurnal and seasonal variability in these wavelengths and their corresponding canopy characteristics (see Gutschick et al., 1985, and Vierling et al., 1997 for further discussion). Recent developments in our understanding of canopy physiology, combined with current sensor technology and low cost, low power data logging options now make it practical to develop a sensor system to acquire temporally continuous spectral information above and within vegetation canopies.

Here, we describe a simple 4 band filtered photodiode-based sensor system (hereafter referred to as the QuadPod) for measuring downwelling and upwelling radiation in the NDVI and PRI wavelengths. These sensor systems represent an application of basic ‘off-the-shelf’ optics, circuit design, and miniaturized data logging technology to address questions that require high spatio-temporal resolution spectral data of vegetation canopies. The design of these sensors and component choices were based on the following criteria:

- 1) lightweight (~ 1 kg) to facilitate deployment above and within vegetation canopies and on micrometeorological towers;
- 2) relatively low cost and low maintenance operation to facilitate simultaneous deployment at many locations to quantify temporal and spatial variability in canopy radiative properties;
- 3) self-contained, low power, weather resistant, and capable of unattended, automated data collection; and

4) having a spectral resolution  $\leq 10$  nm FWHM to allow for the calculation of narrowband spectral vegetation indices, such as the PRI.

## 2. Instrument design and technical specifications

We assembled two types of QuadPod instruments using standard electronics and commercially available parts. One type of QuadPod was designed to measure upwelling radiation (radiance), while the other was designed to measure downwelling radiation (irradiance). The technical details of the components included in each sensor are described below, and a materials list is provided in Appendix A.

### 2.1 *Photodiodes*

We used silicon photodiodes as the primary light detecting component within the QuadPods (S2386-18K; Hamamatsu Corp., Bridgewater, NJ). These photodiodes had a spectral response range from 320 to 1100 nm, with peak sensitivity occurring at 960 nm (Fig. 1). This particular photodiode was chosen for three primary reasons: 1) it was sensitive to all wavelengths of interest (531 nm, 570 nm, 680 nm, and 800 nm), 2) it was insensitive to changes in temperature across the wavelength range from 450 nm to 900 nm, and 3) its radiometric response was linear.

### 2.2 *Narrow bandpass filters*

Because the photodiodes had too broad a spectral response range for calculating narrowband vegetation indices, it was necessary to spectrally filter the radiation reaching each sensor. We used narrow bandpass filters (Edmund Optics, Barrington, NJ, USA) that selectively transmitted narrow wavebands of radiation to strike the active sensing surface of each photodiode. These filters exhibit a 10 nm full width half maximum (FWHM) response curve with a central wavelength tolerance of  $\pm 2$  nm, as reported by the manufacturer and confirmed through our own ellipsometer tests (Fig. 2). Because the

filters were acquired from a commercial company that manufactured each filter for predetermined wavelengths, we chose those wavelengths that were advertised to be closest to the wavelengths needed for calculating the NDVI and PRI vegetation indices.

Ellipsometer tests confirmed that the center wavelengths of all bandpass filters were within  $\pm 2$  nm of those required for calculating these indices (532 nm, 568 nm, 676 nm, and 800 nm; Fig. 2).

A bandpass of less than or equal to 10 nm FWHM was selected primarily to facilitate measurements of the PRI. Most ground-based studies comparing PRI to LUE use spectrometers with fine spectral resolution ( $\leq 10$  nm). This level of spectral resolution is required because the xanthophyll spectral response has been shown to be specific to the 525 to 534 nm region (Gamon et al. 1990). Several recent studies have used MODIS bands to calculate PRI which compare reasonably well with canopy-level LUE (*e.g.* Rahman et al. 2004; Drolet et al. 2005, 2008). The MODIS bands used in these studies have a 10 nm bandwidth and are centered at 531 nm for xanthophyll detection and either 551 nm (Rahman et al. 2004; Drolet et al. 2008) or 667 nm (Drolet et al. 2005) for the reference band. Thus, the QuadPod instrument may aid interpretation of satellite-derived vegetation indices such as MODIS-based PRI as reported in previous studies (*e.g.* Rahman et al., 2004; Drolet et al., 2008). NDVI is often calculated from broadband reflectance data, however, several studies using hyperspectral instruments have demonstrated that narrow band data are suitable for calculating NDVI (*e.g.* Gamon and Surfus 1999; Sims and Gamon 2002). Although the exact wavelengths for use in calculating narrowband NDVI do vary, the wavelengths that we describe here (676 and 800 nm) fall within the regions of peak chlorophyll absorption and NIR reflectance, and are therefore suitable for NDVI calculation. However, should other (*i.e.* broader) wavebands be desired to calculate NDVI, wider FWHM bandpass filters can be substituted for those described here.

### 2.3 *Data logging*

Although a variety of data logging options currently exist to record data from environmental sensors, we chose small, lightweight, commercially manufactured data loggers to record the electrical output from the filtered photodiodes. We used a 4-channel, U-series Hobo data logger (U12-006, Onset Corp., Bourne, MA, USA) housed in a small plastic container to shield it from the environment. This data logger was powered by a CR-2032 lithium battery and was capable of recording voltage readings between 0-2.5 V at time intervals ranging from 1 second to 18 hours. These data loggers had a memory storage capacity of 64K bytes or 43,000 individual events. Hoboware software (Onset, Bourne, MA, USA) was used to program and communicate with the data logger via a laptop computer.

### 2.4 *Circuit design*

When exposed to photons within the spectral response range, photodiodes produce a current proportional to the amount of incoming energy. Although the Hobo data loggers were capable of recording electrical current measurements, the range of acceptable output current values was too narrow for our application (4-20 mA for a Hobo data logger). Following Phillips and Bond (1999) we used a surface mount operational amplifier (AD8668; Analog Devices, MA) as a current to voltage converter (Fig. 3). This amplifier was used to convert the photodiode current to a proportional voltage and scaled this output voltage to a range suitable for the data logger (0 to 2.5V).

The required amplifier gain, which is controlled by the resistance value of the feedback resistor, is dependent upon: 1) the output range of the photodiode, which is a function of the optical filter losses, and 2) radiation intensity. Therefore, the gain must be calculated for each application and the resistors sized according using Ohm's Law ( $V = I/R$ ). Adjustable resistors (potentiometers) could be substituted for the fixed resistors to allow for a greater range of application. The operational amplifier used here required a DC power source in the 5 to 16V range, which we have achieved using a 9V alkaline battery

(for autonomous deployment where an external power source is not available) or using a DC power supply (often available on micrometeorological flux towers). At a maximum output of 2.5V in all detectors, the current draw was observed to be 0.9 mA resulting in a power requirement of 0.0225 W. Although we used a current-to-voltage circuit to facilitate the use of Hobo data loggers, other data loggers that are capable of recording smaller voltages/currents (*e.g.* Campbell data loggers; Campbell Scientific Inc.; Logan, UT) may negate the need for signal amplification circuitry.

## 2.5 Housing

The QuadPod instrument housing was constructed to maximize durability, minimize size, and provide self-containment. The optical components were fitted into a cut and machined Acetal sheet measuring 3"x 3" x 0.625" (Professional Plastics, SDEL.625B, Fullerton, CA). Sensor mounts were cut and machined at the University of Idaho machine shop. The sensor mounts were secured to a plastic case (Polycase, LP41FXXT01, Avon, OH) that housed the amplifier circuit board (Fig. 4). Data loggers and 9V batteries were housed in a weather tight case (Polycase, DC-58F-G). Signal was routed from the sensor housing to the data logger housing through a ten-conductor cable (L-Com, CSTP5-500, North Andover, MA). Terminations were sealed using nylon waterproof cable glands.

## 2.6 Irradiance vs. Radiance Instrumentation

To calculate reflectance during remote, unattended operation, we designed upward-pointing QuadPods to quantify irradiance and downward-pointing QuadPods to quantify radiance in the wavebands of interest. Reflectance was calculated by dividing radiance by irradiance and multiplying by a cross-instrument calibration factor (CICF) derived from measurements of a spectralon panel (after Gamon et al., 2006b; Equation 4).

$$R_{corrected} = \left( \frac{rad_{target}}{irr_{sky}} \right) * \left( \frac{irr_{sky}}{rad_{panel}} \right) \quad \text{Eq. 4}$$

Where  $R_{corrected}$  is the corrected reflectance,  $rad_{target}$  is radiance from the target,  $rad_{panel}$  is radiance from the white reference panel, and  $irr_{sky}$  is downwelling irradiance. The configuration of the QuadPod is designed to quantify the hemispherical-conical reflectance factor defined by Schaepman-Strub et al. (2006). Anderson et al. (2006) demonstrated that the CICF is dependent on illumination conditions. Therefore, CICFs should be characterized across a range of illumination conditions so that they may be appropriately applied as sun angle or diffuse sky condition varies.

Both radiance and irradiance QuadPod instruments used a diffuser material as part of their foreoptic design. Based on results from Biggs et al. (1971) and Mimms (personal communication), we used 1.3 mm thick virgin grade Teflon® (DuPont, Wilmington, DE, USA) material to improve the cosine response for the irradiance instrument. To test the cosine response, simultaneous field-based irradiance measurements were made with an NDVI-only irradiance QuadPod instrument equipped with a Teflon® diffuser and a LI-COR quantum sensor (LI-COR, Lincoln, NE; LI-190). We used the quantum sensor data solely as a field-based control. These measurements were normalized and compared to a normalized ideal cosine response (Fig. 6a). Except where clouds obscured the sun, the deviation from the ideal response was similar for the two instruments up to a solar zenith angle of approximately 60° ( $\pm 20\%$ ; Fig. 6b). At solar zenith angles greater than 60° the NDVI instrument response was consistently closer to the ideal response than was the LI-COR quantum sensor. The irradiance instrument's Teflon® diffuser foreoptic was designed to quantify hemispherical irradiance whereas the radiance instrument's foreoptic combined a Teflon® diffuser with a field stop to allow for conical measurements of radiance.

Bare bandpass filters are subject to shifts in transmission wavelengths as the angle of incidence increases. Using a UniSpec DC spectrometer (PP Systems, Haverhill, MA), we compared transmission through a bare filter and a Teflon diffused filter from 300 to 1100 nm. We found that the use of Teflon prevented significant shifts in the central wavelength of the bandpass through the filters in the QuadPod instruments (Fig. 7). These tests

demonstrate that there is no need for out of band blocking when using this combination of filter and photodiode.

### 2.7 *Spectrometer comparison*

We compared our QuadPod to a UniSpec DC (dual-channel) spectrometer, an instrument commonly mounted on flux towers to quantify canopy NDVI and PRI (*e.g.* Hall et al., 2008; Hilker et al., 2007, 2008a,b). QuadPod and UniSpec measurements were simultaneously collected under natural sky conditions. The UniSpec instrument was programmed with a fixed integration time to allow consistent comparisons with the QuadPod. Comparisons of analogous bands between the QuadPod and UniSpec were evaluated using regression analysis. For each band comparison, the coefficient of determination was greater than 0.98 (Fig. 8).

### 2.8 *Instrument performance*

We tested the QuadPod instrument to assess temperature sensitivity and repeatability. To determine the repeatability of the instrument, data were collected under clear sky conditions at 1 second intervals for 120 seconds. The dataset was detrended using a least-squares fit to account for changing radiation intensity due to solar zenith angle changes. Detrended data were divided into four contiguous 30 second groups. The mean standard deviation of the four 30 second groups was 0.4 mV. In our application we designed each sensor to produce approximately 2.5 V output at periods during peak incoming solar radiation (*e.g.* solar noon, clear sky, mid-growing season). At this maximum output level an error of 0.4 mV represents 0.0016 % of the total signal. Because these instruments are relatively new, a valid assessment of their long term stability has not been made. In-house calibrations of QuadPod sensors conducted over the past year indicate that the sensors are highly stable; however, we suggest that calibrations be conducted annually to ensure that data quality does not suffer from potential instrument degradation.

To assess temperature effects, light was blocked from the detectors while temperature within the sensor head was allowed to increase 33° C. Voltage output from the current-to-voltage circuit was measured at ambient room temperature and again following the temperature increase using a multimeter. The mean change in voltage output was 0.009 mV/° C, meaning that under a maximum output level the error introduced by temperature effects would be  $0.009\text{mV}/2500\text{mV}=0.00036\%$  per degree C. In addition, because the QuadPod is a dual channel instrument, both irradiance and radiance sensors are exposed to the same temperature. Therefore, temperature-induced noise would be further minimized due to the fact that to calculate reflectance values, a ratio is performed using the outputs of the up- and down-facing sensors.

The QuadPod was field-tested for several days at a desert grassland flux tower site in New Mexico. At the start of the testing period the ecosystem was a net source of CO<sub>2</sub> to the atmosphere (Fig. 9). Immediately following a precipitation event a green up period occurred that resulted in a shift from a net C source to a net sink. The QuadPod captured the vegetation green up response with an increase in both mean midday NDVI and PRI.

### **3. Discussion and Conclusions**

We have deployed several QuadPods as described here at various field locations to quantify incident radiation, reflected radiation, and transmitted radiation above and within vegetation canopies. Field-based testing locations include a northern mixed hardwood forest in Michigan, a shrub-steppe ecosystem in Idaho, a semi-arid ponderosa pine forest in Colorado, a temperate rain forest in British Columbia, a tropical forest in French Guiana, and a continuum of vegetation types occurring across a topographic and climatic gradient in New Mexico. The instruments have been exposed to a wide range of environmental conditions including rain, wind, and temperature fluctuations ranging from approximately -3 to 38° C. Data collection is continuing and results from these various experiments are forthcoming.



For our specific objective of monitoring high frequency temporal changes in canopy reflectance as they relate to canopy-atmosphere CO<sub>2</sub> exchange, we chose a photodiode and bandpass filters that, when used in combination, would allow for the calculation of the NDVI and PRI spectral vegetation indices. However, other wavelengths could be used for different applications. The silicon photodiode used in this study was sensitive to wavelengths ranging from 320 nm to 1100 nm and, given the appropriate bandpass filter, could be used to calculate other commonly used vegetation indices such as the enhanced vegetation index, green index, water band index, and many other indices found to be of use in vegetation monitoring (e.g. Penuelas et al. 1997; Huete et al. 2002; Gitelson et al. 2003). Simple modifications to the present housing system to add more sensor ports would allow for more than four bands to be measured simultaneously; thereby expanding the instrument's utility for calculating additional vegetation indices.

Although the QuadPod instruments described here are not intended to fully replace narrowband spectroradiometers, they possess several qualities that make them quite useful for a wide variety of research relating to vegetation canopy structure and function. The instruments are relatively inexpensive to build (~ \$720 in parts for a complete pair of uplooking/downlooking NDVI/PRI sensors), have low power consumption (0.0225 W max), are lightweight (~1.4 kg) and are relatively simple to construct and operate. We have demonstrated that these instruments have a low temperature response, good repeatability, and a highly linear relationship with measurements derived from a UniSpec spectroradiometer. Therefore, we believe that these or similar instruments could be built for deployment at many flux tower locations simultaneously for better understanding vegetation properties that contribute to biosphere-atmosphere exchanges of mass and energy. For example, these or similar sensor systems can be cross-calibrated and adopted as a standard addition to the FLUXNET network of towers or to other similar networks that study vegetation properties such as phenology (Schwartz, 1994; Huemmerich et al. 1999; Richardson et al. 2009). Such networks of narrowband optical sensors could assist our understanding of ecosystem specific, temporal and/or spatial changes in canopy reflectance that may indicate how vegetation function and trace gas exchange respond to various types of environmental change around the globe.

## Acknowledgements

This study was funded by an NSF IGERT fellowship to S. Garrity (BART) and NSF grant DBI-0537040 (L. Vierling, PI). We would like to thank David McIlroy for providing access to the University of Idaho Physics Lab ellipsometer, Forrest Mimms for his helpful suggestions regarding diffuser material and thickness, Javier Naupari, Alex Guenther, Nicholas Coops, Thomas Hilker, Martin van Leeuwen, Marcy Litvak, Andrew Fox, and Benoit Burban for allowing us to test these sensor systems at their research locations, and the SpecNet working group for their continued efforts to link canopy spectral reflectance properties with biosphere-atmosphere exchanges of trace gases. Four anonymous reviewers provided comments to improve earlier versions of this manuscript.

## References

- Anderson, K., Milton, E.J., and Rollin, E.M. 2006. Calibration of dual-beam spectroradiometric data. *International Journal of Remote Sensing* 27, 975-986.
- Baldocchi, D., Falge, E., Gu, L., Olson, R., Hollinger, D., Running, S., Anthoni, P., Bernhofer, Ch., Davis, K., Evans, R., Fuentes, J., Goldstein, A., Katul, G., Law, B., Lee, X., Malhi, Y., Meyers, T., Munger, W., Oechel, W., Paw U, K.T., Pilegaard, K., Schmid, H.P., Valentini, R., Verma, S., Vesala, T., Wilson, K., and Wofsy, S. 2001. FLUXNET: A new tool to study the temporal and spatial variability of ecosystem-scale carbon dioxide, water vapor, and energy flux densities. *Bulletin of the American Meteorological Society* 82, 2415-2434.
- Biggs W.W., Edison, A.R., Eastin, J.D, Brown, K.W., Maranville, J.W., and Clegg, M.D. 1971. Photosynthesis light sensor and meter. *Ecology* 52, 125-131.
- Cohen, W.B., and Justice, C.O. 1999. Validating MODIS terrestrial ecology products: linking *in situ* and satellite measurements. *Remote Sensing of Environment* 70, 1-3.

- Drolet, G.G., Huemmerich, K.F., Hall, F.G., Middleton, E.M., Black, T.A., Barr, A.G., and Margolis, H.A. 2005. A MODIS-derived photochemical reflectance index to detect inter-annual variations in the photosynthetic light-use efficiency of a boreal deciduous forest. *Remote Sensing of Environment* 98, 212-224.
- Drolet, G.G., Middleton, E.M., Huemmerich, K.F., Hall, F.G., Amiro, B.D., Barr, A.G., Black, T.A., McCaughey, J.H., and Margolis, H.A. 2008. Regional mapping of gross light-use efficiency using MODIS spectral indices. *Remote Sensing of Environment* 112, 3064-3078.
- Federer, C.A., and Tanner, C.B. 1966. Sensors for measuring light available for photosynthesis. *Ecology* 47, 654-657.
- Filella, I., Amaro, T., Araus, J.L., and Penuelas, J. 1996. Relationship between photosynthetic radiation-use efficiency of Barley canopies and the photochemical reflectance index (PRI). *Physiologia Plantarum* 96, 211-216.
- Fuentes, D.A., Gamon, J.A., Cheng, Y., Claudio, H.C., Qiu, H., Mao, Z., Sims, D.A., Rahman, A.F., Oechel, W., and Luo, H. 2006. Mapping carbon and water vapor fluxes in a chaparral ecosystem using vegetation indices derived from AVIRIS. *Remote Sensing of Environment* 103, 312-323.
- Gamon, J.A., Field, C.B., Bilger, W., Bjorkman, O., Fredeen, A.L., and Penuelas, J. 1990. Remote sensing of the xanthophylls cycle and chlorophyll fluorescence in sunflower leaves and canopies. *Oecologia* 85, 1-7.
- Gamon, J.A., Peñuelas, J., and Field, C.B. 1992. A narrow-waveband spectral index that tracks diurnal changes in photosynthetic efficiency. *Remote Sensing of Environment* 41, 35-44.

- Gamon, J.A., Surfus, J.S. 1999. Assessing leaf pigment content and activity with a reflectometer. *New Phytologist* 143, 105-117.
- Gamon, J.A., Rahman, A.F., Dungan, J.L., Schildhauer, M., and Huemmrich, K.F. 2006a. Spectral Network (SpecNet) – What is it and why do we need it? *Remote Sensing of Environment* 103, 227-235.
- Gamon JA, Cheng YF, Claudio H, MacKinney L, Sims DA. 2006b. A mobile tram system for systematic sampling of ecosystem optical properties. *Remote Sensing of Environment* 103, 246-254.
- Gitelson, A.A., Vina, A., Arkebauer, T.J., Rundquist, D.C., Keydan, G., and Leavitt, B. 2003. Remote estimation of leaf area index and green biomass in maize canopies. *Geophysical Research Letters* 30, 1248, doi:10.1029/2002GL016450.
- Gutschick, V.P., Barron, M.H., Waechter, D.A., and Wolf, M.A. 1985. Portable monitor for solar radiation that accumulates irradiance histograms for 32 leaf-mounted sensors. *Agricultural and Forest Meteorology* 33, 281-290.
- Hall, F.G., Hilker, T., Coops, N.C., Lyapustin, A., Huemmerich, K.F., Middleton, E., Margolis, H., Drolet, G., and Black, T.A. 2008. Multi-angle remote sensing of forest light use efficiency of forest light use efficiency by observing PRI variation with canopy shadow fraction. *Remote Sensing of Environment* 112, 3201-3211.
- Hilker, T., Coops, N.C., Nestic, Z., Wulder, M.A., and Black, A.T. 2007. Instrumentation and approach for unattended year round tower based measurements of spectral reflectance. *Computers and Electronics in Agriculture* 56, 72-84.
- Hilker, T., Coops, N.C., Schwalm, C.R., Jassal, R.S., Black, A.T., and Krishnan, P. 2008a. Effects of mutual shading of tree crowns on prediction of photosynthetic light-use efficiency in a coastal Douglas-fir forest. *Tree Physiology* 28, 825-834.

- Hilker, T., Coops, N.C., Hall, F.G., Black, T.A., Wulder, M.A., Nesic, Z., and Krishnan, P. 2008b. Separating physiologically and directionally induced changes in PRI using BRDF models. *Remote Sensing of Environment* 112, 2777-2788.
- Hill, M.J., Held, A.A., Leuning, R., Coops, N.C., Hughes, D., and Cleugh, H.A. 2006. MODIS spectral signals at a flux tower site: Relationships with high-resolution data, and CO<sub>2</sub> flux and light use efficiency measurements. *Remote Sensing of Environment* 103, 351-368.
- Huemmerich, K.F., Black, T.A., Jarvis, P.G., McCaughey, J.H., and Hall F.G. 1999. High temporal resolution NDVI phenology from micrometeorological radiation sensors. *Journal of Geophysical Research* 104, 27935-27944.
- Huete, A., Didan, K, Miura, T., Rodriguez, E.P., Gao, X., and Ferreira, L.G. 2002. Overview of the radiometric and biophysical performance of the MODIS vegetation indices. *Remote Sensing of Environment* 83, 195-213.
- Leuning, R., Hughes, D., Daniel, P., Coops, N.C., and Newnham, G. A multi-angle spectrometer for automatic measurement of plant canopy reflectance spectra. *Remote Sensing of Environment* 103, 236-245.
- Melbourne, B.A., Daniel, P.J. 2003. A low-cost sensor for measuring spatiotemporal variation of light intensity on the streambed. *Journal of the North American Benthological Society* 22, 143-151.
- Mimms, F. Personal communication.
- Monteith, J.L. 1972. Solar radiation and productivity in tropical ecosystems. *Journal of Applied Ecology* 9, 747-766.

- Nichol, C.J., Huemmrich, K.F., Black, T.A., Jarvis, P.G., Walthall, C.L., Grace, J., and Hall, F.G. 2000. Remote sensing of photosynthetic-light-use efficiency of boreal forest. *Agricultural and Forest Meteorology* 101, 131-142.
- Penuelas, J., Pinol, J., Ogaya, R., and Filella, I. 1997. Estimation of plant water concentration by the reflectance water index WI (R900/R970). *International Journal of Remote Sensing* 18, 2869-2875.
- Pfitsch, W.A., and Pearcy, R.W., 1992. Growth and reproductive allocation of *Adenocaulon bicolor* following experimental removal of sunflecks. *Ecology* 73, 2109-2117.
- Phillips, N., and Bond, B.J. 1999. A micro-power precision amplifier for converting the output of light sensors to a voltage readable by miniature data loggers. *Tree Physiology* 19, 547-549.
- Pontailleur, J.Y., and Genty, B. 1996. A simple red: far-red sensor using Gallium Arsenide Phosphide detectors. *Functional Ecology* 10, 535-540.
- Rahman, A.F., Gamon, J.A., Fuentes, D.A., Roberts, D.A., and Prentiss, D. 2001. Modeling spatially distributed ecosystem flux of boreal forest using hyperspectral indices from AVIRIS imagery. *Journal of Geophysical Research* 106, 33,579-33,591.
- Rahman, A.F., Cordova, V.D., Gamon, J.A., Schmid, H.P., and Sims, D.A. 2004. Potential of MODIS ocean bands for estimating CO<sub>2</sub> flux from terrestrial vegetation: A novel approach. *Geophysical Research Letters* 31, L10503, doi:10.1029/2004GL019778.
- Richardson, A.D., Braswell, B.H., Hollinger, D.Y., Jenkins, J.P., and Ollinger, S.V. 2009. Near-surface remote sensing of spatial and temporal variation in canopy phenology. *Ecological Applications* 19, 1417-1428.

- Rouse, J.W., Haas, R.H., Schell, J.A., and Deering, D.W. 1973. Monitoring vegetation systems in the Great Plains with ERTS. Third ERTS Symposium, NASA SP-351 I, 309-317.
- Running, S.W., Baldocchi, D.D., Turner, D.P., Gower, S.T., Bakwin, P.S., and Hibbard, K.A. 1999. A global terrestrial monitoring network integrating tower fluxes, flask sampling, ecosystem modeling and EOS satellite data. *Remote Sensing of Environment* 70, 108-127.
- Running, S.W., Nemani, R.R., Heinsch, F.A., Zhao, M., Reeves, M., and Hashimoto, H. 2004. A continuous satellite-derived measure of global terrestrial primary production. *BioScience* 54, 547-560.
- Schaepman-Strub, G., Schaepman, M.E., Painter, T.H., Dangel, S., and Martonchik, J.V. 2006. Reflectance quantities in optical remote sensing—definitions and case studies. *Remote Sensing of Environment* 103, 27-42.
- Schwartz, M.D. 1994. Monitoring global change with phenology: the case of the spring green wave. *International Journal of Biometeorology* 38, 18-22.
- Sellers, P.J. 1987. Canopy reflectance, photosynthesis, and transpiration, pt. II: The role of biophysics in the linearity of their interdependence. *Remote Sensing of Environment* 21, 143–183.
- Sims, D.A., Gamon, J.A. 2002. Relationships between leaf pigment content and spectral reflectance across a wide range of species, leaf structures and developmental stages. *Remote Sensing of Environment* 81, 337-354.
- Sims, D.A., Rahman, A.F., Cordova, V.D., Baldocchi, D.D., Flanagan, L.B., Goldstein, A.H., Hollinger, D.Y., Misson, L., Monson, R.K., Schmid, H.P., Wofsy, S.C., and

- Xu, L. 2005. Midday values of gross CO<sub>2</sub> flux and light use efficiency during satellite overpass can be used to directly estimate eight-day mean flux. *Agricultural and Forest Meteorology* 131, 1-12.
- Sims, D.A., Luo, H., Hastings, S., Oechel, W.C., Rahman, A.F., and Gamon, J.A. 2006. Parallel adjustments in vegetation greenness and ecosystem CO<sub>2</sub> exchange in response to drought in a Southern California chaparral ecosystem. *Remote Sensing of Environment* 103, 289-303.
- Sims, D.A., Rahman, A.F., Cordova, V.D., El-Masri, B.Z., Baldocchi, D.D., Bolstad, P.V., Flanagan, L.B., Goldstein, A.H., Hollinger, D.Y., Misson, L., Monson, R.K., Oechel, W.C., Schmid, H.P., Wofsy, S.C., and Xu, L. 2008. A new model of gross primary productivity for North American ecosystems based solely on the enhanced vegetation index and land surface temperature from MODIS. *Remote Sensing of Environment* 112, 1633-1646.
- Vierling, L.A., Deering, D.W., and Eck, T.F. 1997. Differences in arctic tundra vegetation type and phenology as seen using bidirectional radiometry in the early growing season. *Remote Sensing of Environment* 60, 71-82.
- Vierling, L.A., and Wessman, C.A. 2000. Photosynthetically active radiation heterogeneity within a monodominant Congolese rain forest canopy. *Agricultural and Forest Meteorology* 103, 265-278.



## Figures

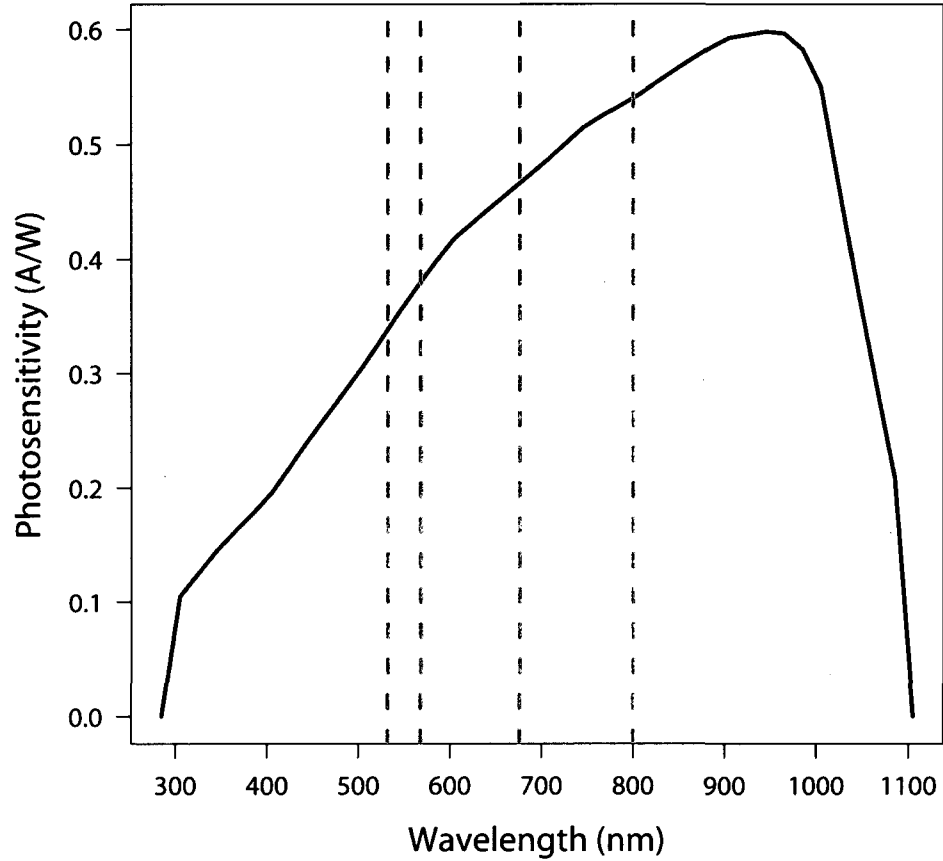


**Figure 1.** Photosensitivity of the silicon photodiode used in the QuadPod instruments (data from Hamamatsu Corporation). The wavelengths used to calculate vegetation indices from the photodiode sensors in this study are denoted by vertical gray lines at 532, 568, 676 and 800 nm.

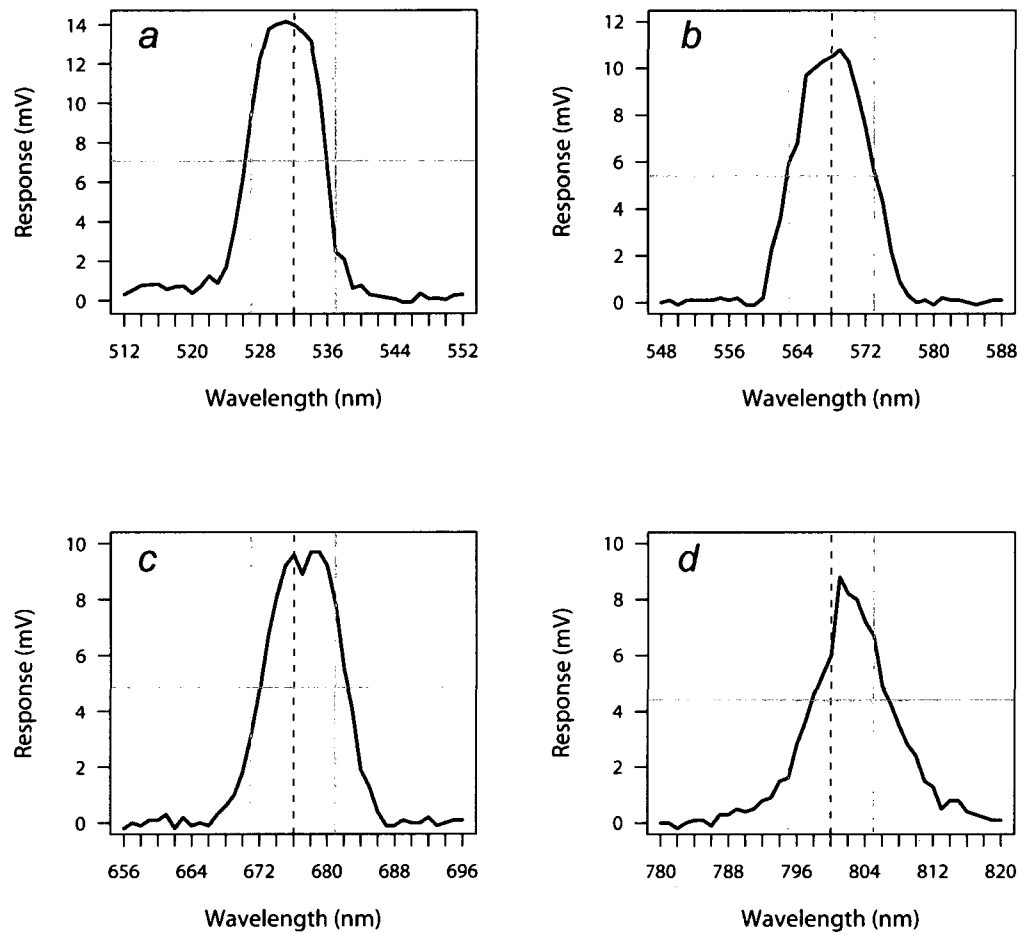


**Figure 2.** Photodiode voltage response using four different narrow bandpass filters. These data were generated using an ellipsometer set at a 1 nm wavelength sampling interval as a light source. The full width half maximum and peak transmissivity values of the bandpass filters (as specified by the manufacturer) are denoted by gray and dashed lines, respectively.

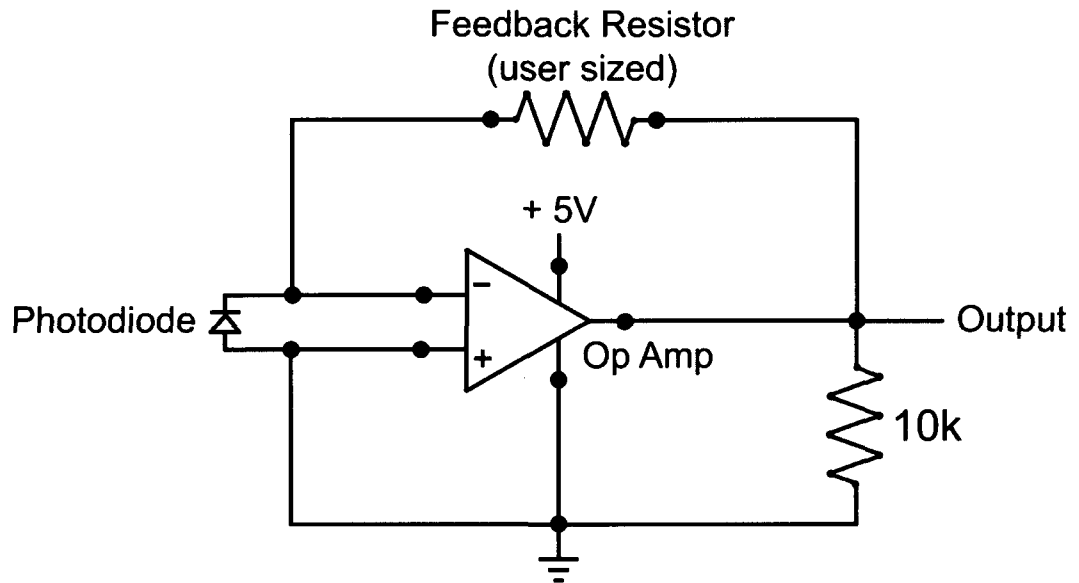


**Figure 3.** Electrical schematic of the current to voltage converter, including amplification circuit necessary for use with Hobo data loggers.

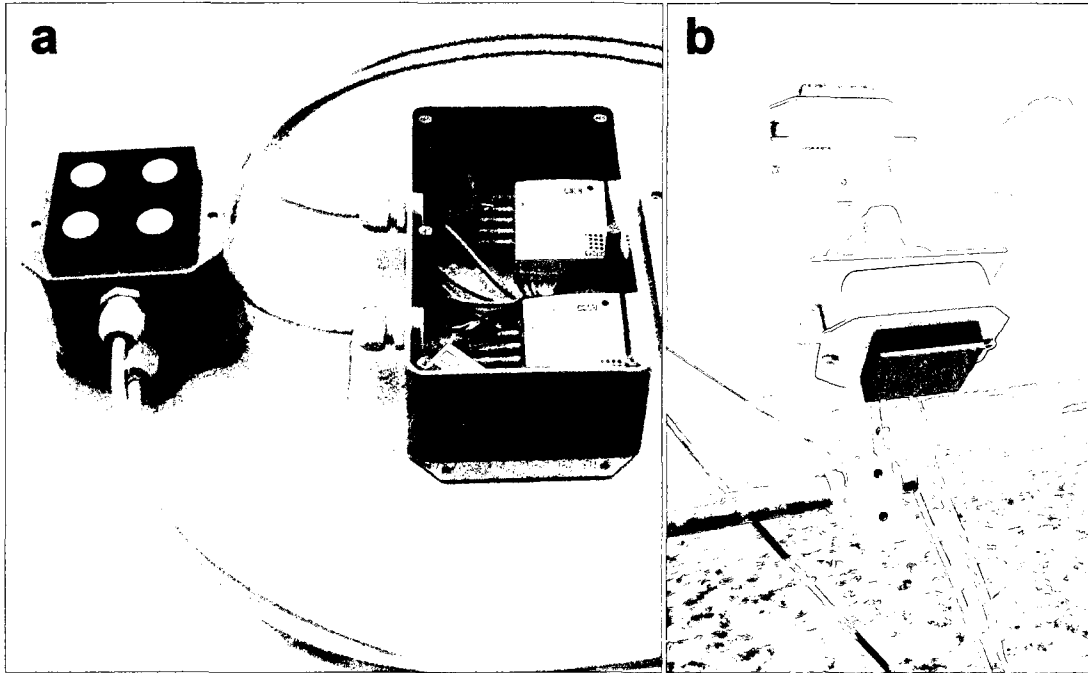


**Figure 4.** (A) Image of QuadPod instrument complete with irradiance and radiance sensor heads and data logger housing. (B) Image of QuadPod radiance and irradiance sensor heads mounted at a field-based study location.

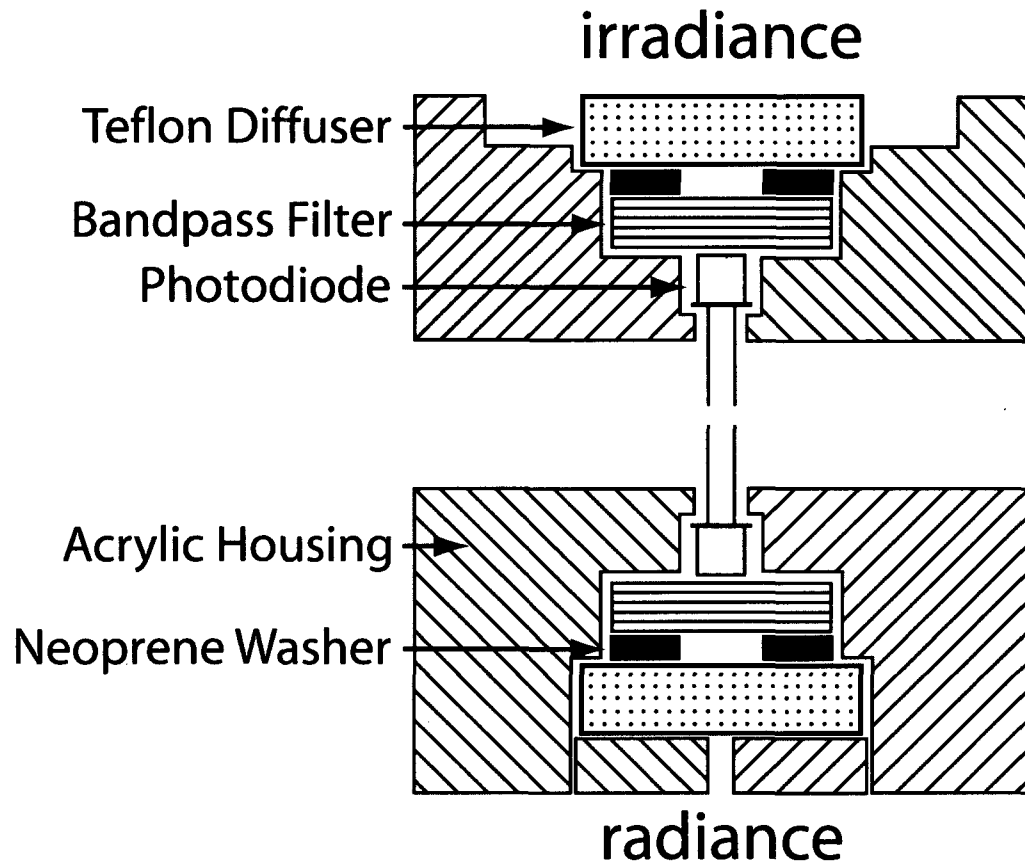


**Figure 5.** Housing and parts schematic of QuadPod irradiance and radiance sensor heads.

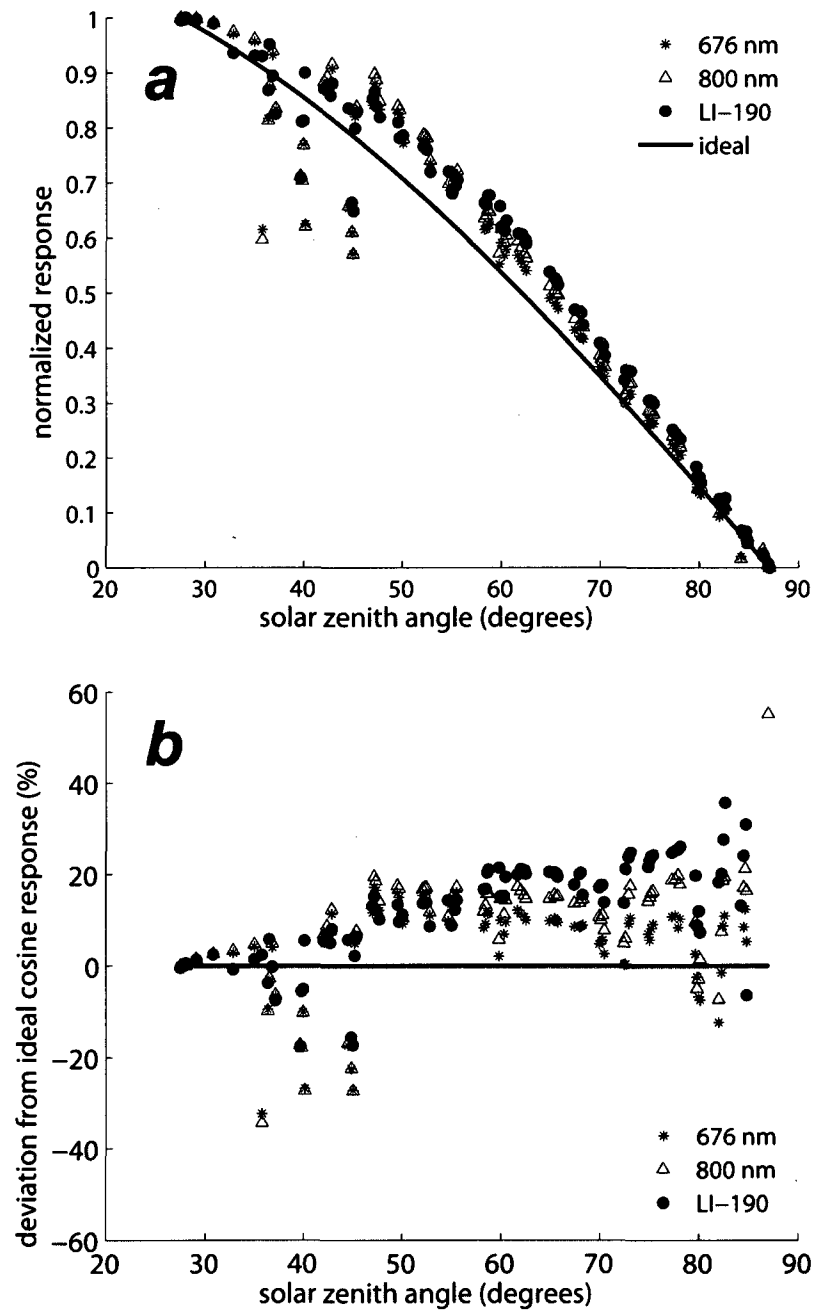


**Figure 6.** (A) Comparison of the normalized ideal cosine response and the normalized response between a LI-COR quantum sensor (LI-190) and a 676 nm and 800 nm filtered photodiode from the QuadPod fitted with a Teflon<sup>®</sup> diffusing disc. (B) The percent deviation of each detector's response from the ideal cosine response.

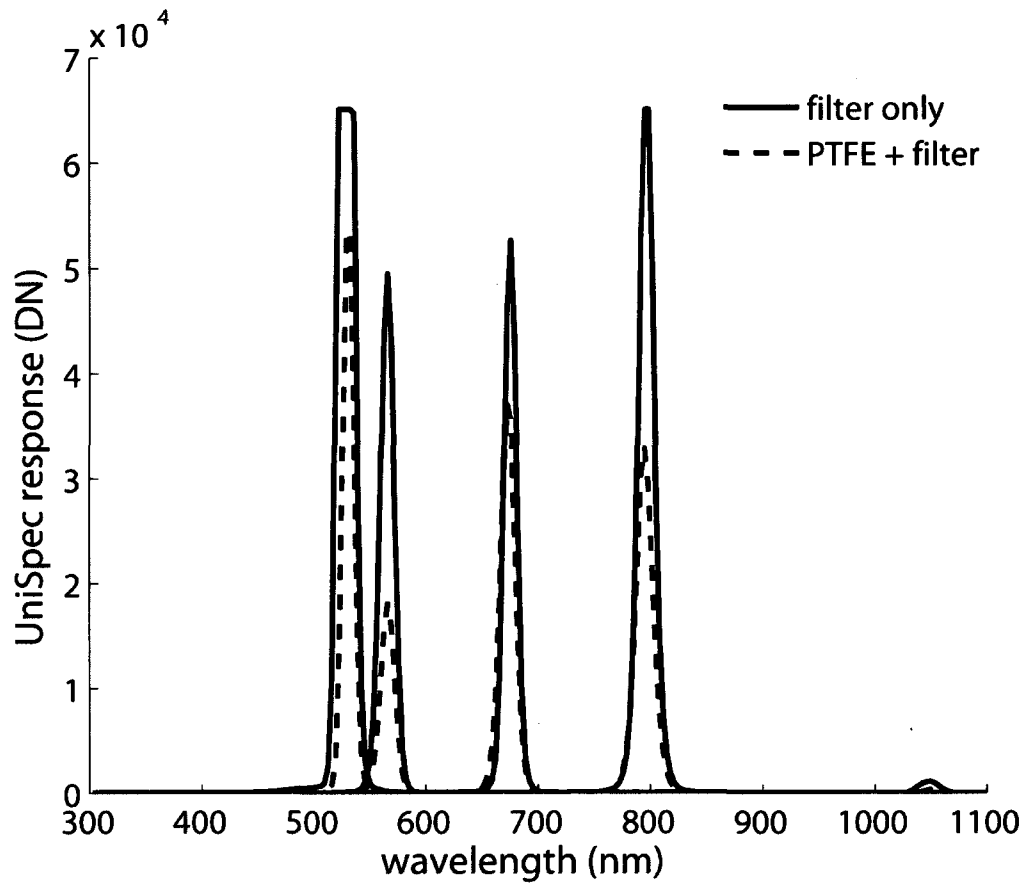


**Figure 7.** Comparison of transmitted radiation through bare bandpass filters and bandpass filters with a Teflon diffuser.

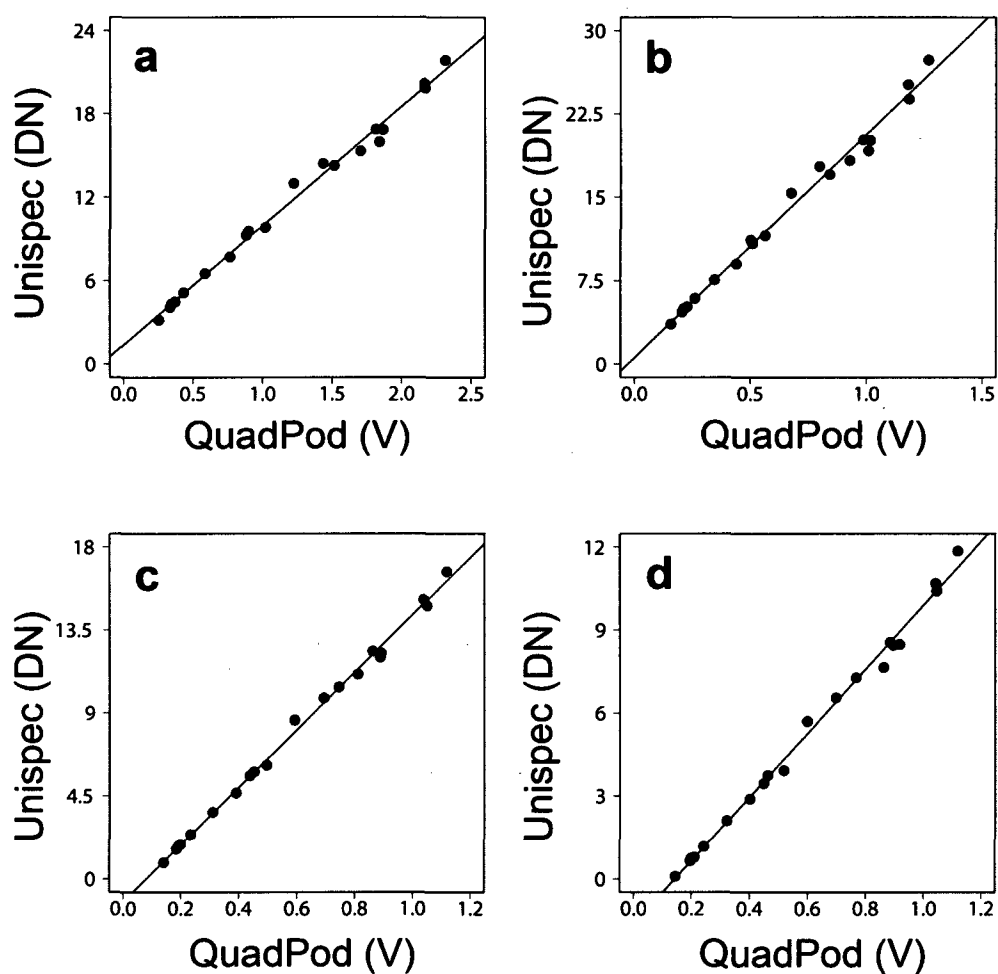


**Figure 8.** Regression between UniSpec instrument and the QuadPod at (a) 532 nm, (b) 568 nm, (c) 676 nm, and (d) 800 nm. Coefficients of determination were 0.992, 0.989, 0.997, and 0.994 respectively. Deviations from a 1:1 relationship are a function of the fixed integration time for the UniSpec instrument.



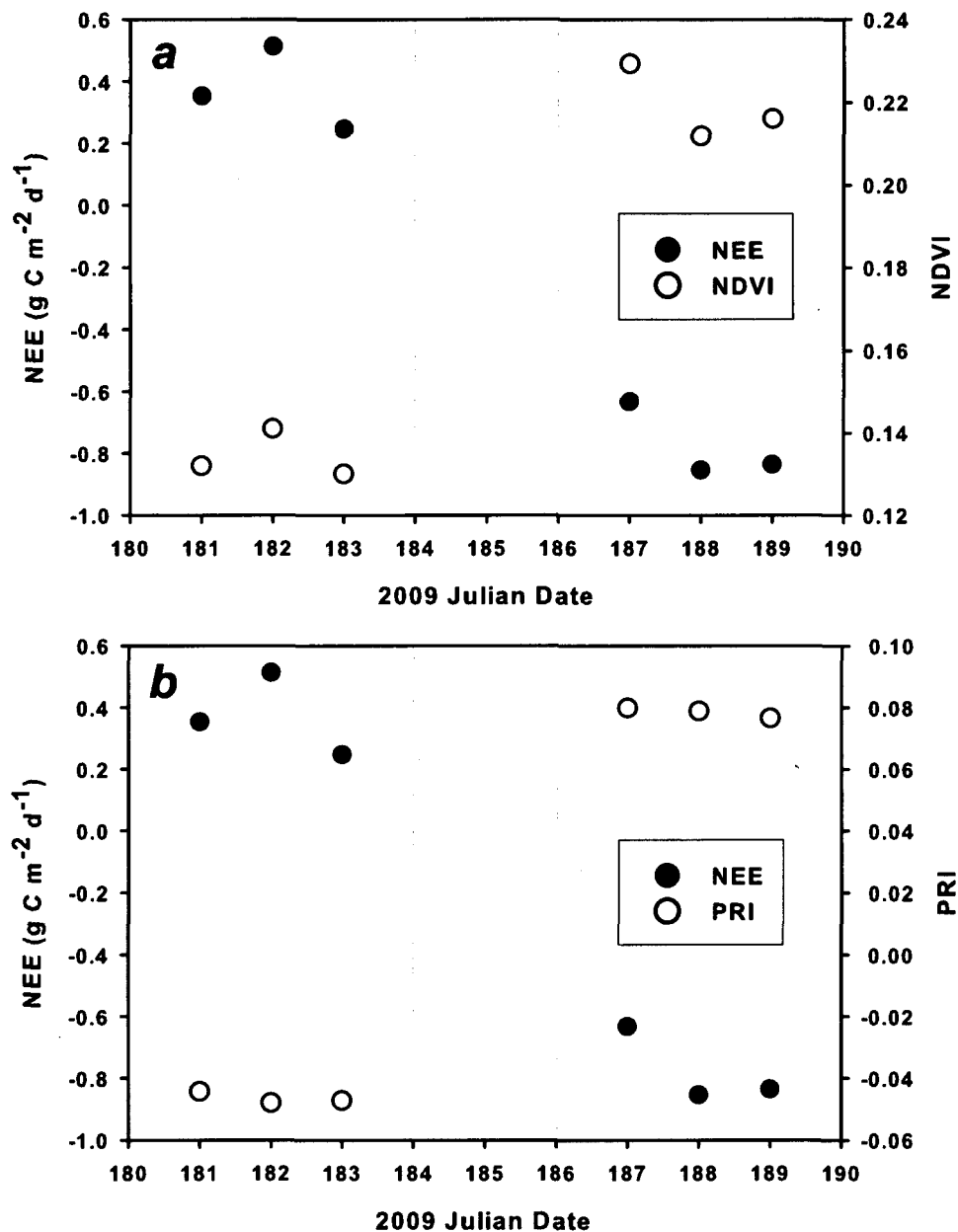


**Figure 9** Comparison of flux-tower measured Net Ecosystem Exchange (NEE) of CO<sub>2</sub> and (a) NDVI and (b) PRI for three days immediately prior to a precipitation event at a desert grassland ecosystem (Julian dates 181-183 of 2009) and three days immediately following the precipitation event (Julian dates 187-189). The sign convention for NEE is such that negative values indicate a net flux to the ecosystem. Data courtesy of M. Litvak and A. Fox.

## CHAPTER 4

### ESTIMATING THE INFLUENCE OF CHANGING SKY DIFFUSE FRACTION ON DECIDUOUS FOREST NET AND GROSS CARBON ASSIMILATION

#### **Abstract**

Long term measurements of global shortwave radiation have shown varying patterns of global dimming and brightening. These dimming and brightening phenomena have been attributed to changes in the amount of atmospheric aerosols and cloud cover due to both anthropogenic and natural activities. Because solar radiation is the key driver of primary productivity, these global changes in solar radiation regime likely have significant consequences for terrestrial carbon cycling. Here, we quantify the effects of the ratio of diffuse to direct radiation on canopy-atmosphere carbon exchange for a northern deciduous forest, and estimate the expected increase/decrease in growing season carbon assimilation for a variety of simulated changes in solar radiation regime. We found that while gross and net canopy carbon uptake were positively affected by moderately diffuse skies, the relationships were inconsistent for different time periods throughout a day. Furthermore, when integrated over the growing season there was no significant difference between carbon assimilation under increased sunny conditions compared to carbon assimilation under partly cloudy conditions. Finally, we found significant changes (~ 4-5%) in total gross and net canopy carbon assimilation for simulated sky diffuse fraction mediated increases and decreases in irradiance of approximately 5%.

## Introduction

Several studies have documented long-term changes in the amount of global shortwave radiation incident at the earth's surface (e.g., Stanhill & Cohen 2001, 2005; Liepert 2002; Pinker et al. 2005; Wild et al. 2005; Wild et al. 2009). The amount and direction of change in radiation has been found to be highly dependent on the time period and location of observation (Stanhill & Cohen 2005; Wild 2009). These global, regional, and local patterns of brightening and dimming are thought to be most strongly influenced by changes in the amount of atmospheric aerosols due to both anthropogenic activities and natural processes as well as changes in the amount and type of cloud cover (Stanhill and Cohen 2001; Kvalevag & Myhre 2007; Wild 2009). Because the quantity and diffuse fraction of solar radiation are important components of canopy photosynthesis (e.g., Gu et al. 2002) and ecosystem respiration (e.g., Alton et al. 2008), changes in global radiation regimes may significantly alter carbon uptake and storage.

The most important impact of global dimming or brightening on terrestrial ecosystem carbon cycling may be the alteration of the ratio of diffuse to direct solar radiation incident at the canopy surface (Gu et al. 2003; Farquhar & Roderick 2003). Studies have consistently reported enhanced canopy photosynthesis, net ecosystem productivity, and photosynthetic radiation use efficiency under moderately diffuse solar radiation conditions compared to conditions where diffuse radiation is either very low or very high (e.g., Sinclair et al. 1992; Hollinger et al. 1994; Baldocchi et al. 1997; Gu et al. 2003; Jenkins et al. 2007; Urban et al. 2007; Knohl & Baldocchi 2008). Several mechanisms have been proposed to explain why this enhancement occurs, including a more uniform distribution of radiation within the canopy (Roderick et al. 2001; Gu et al. 2002), changes in the spectral distribution of photons within photosynthetically active wavelengths (Min 2005; Urban et al. 2007), and modifications of air temperature and humidity resulting in increased stomatal conductance (Matsui et al. 2008; Urban et al. 2007) and decreased ecosystem respiration (Leuning et al. 1995; Schimel et al. 1996; Baldocchi et al. 1997; Urban et al. 2007; Alton 2008). Although there have been many studies reporting enhanced ecosystem productivity associated with diffuse sky conditions, there is still

much debate regarding the magnitude of the enhancement (Alton et al. 2007, Alton 2008). Therefore, a key issue that remains to be resolved is understanding how much ecosystem carbon gain or loss may occur with changes in the solar radiation regime.

The objectives of our study were to:

- (1) understand how the ratio of diffuse to direct solar radiation influences gross and net carbon assimilation for a northern mixed hardwood forest,
- (2) estimate the expected gross and net carbon gain or loss with a simulated uniform brightening or dimming of sky conditions, and
- (3) estimate the expected gross and net carbon gain or loss with changes in the proportion of sunny, partly cloudy, and cloudy sky conditions.

## Materials and methods

### *Site description*

This study was conducted at the University of Michigan Biological Station (UMBS) Ameriflux tower in the northern portion of the lower peninsula of Michigan (45° 33' 35" N, 84° 42' 49" W). The study area consisted of a mixed hardwood forest dominated by *Populus grandidentata* (bigtooth aspen), *Populus tremuloides* (quaking aspen), *Quercus rubra* (red oak), *Acer rubrum* (red maple), *Betula papyrifera* (paper birch), and *Pinus strobes* (eastern white pine). Mean canopy height was ~ 20 m and mean Leaf Area Index (LAI) during the peak of the growing season was 4.1 m<sup>2</sup> m<sup>-2</sup>. Additional site details were given by Gough et al. (2007).

### *Meteorological and CO<sub>2</sub> flux measurements*

Total incident photosynthetic photon flux density (PPFD<sub>t</sub>) was measured above the canopy using a quantum sensor (LI-190SZ, LI-COR Corp., Lincoln, NE) and incident diffuse radiation (PPFD<sub>d</sub>) was measured with a sunshine sensor (BF2, Delta-T Devices,

Cambridge, UK). Sky diffuse fraction (SDF) was calculated as the ratio between  $PPFD_d$  and  $PPFD_t$ . The diffuse condition of incident PPFD was divided into three classes: (1) sunny ( $SDF < 0.35$ ), (2) partly cloudy ( $SDF > 0.35$  and  $< 0.65$ ), and (3) cloudy ( $SDF > 0.65$ ). Air temperature ( $T_a$ ) and relative humidity were measured using a temperature and relative humidity probe (HPO-43, Rototronic Instruments, Hauppauge, NY). Canopy surface temperature ( $T_c$ ) was measured using a 3:1 field of view infrared thermocouple (IRt/c.03, Exergen Corp., Watertown, MA) that was mounted on the top of a 46-m tall flux tower and pointed toward the canopy. Vapor pressure deficit of the atmosphere ( $VPD_a$ ) was calculated using  $T_a$  and relative humidity measurements, whereas canopy vapor pressure deficit ( $VPD_c$ ) was calculated using  $T_c$  and relative humidity (Campbell & Norman, 1998).

Hourly averaged net ecosystem exchange (NEE) of  $CO_2$  was measured from the UMBS Ameriflux meteorological tower during daylight hours (600 – 1800 EST) of the 2008 growing season (days 160-250) using the eddy covariance method (Baldocchi et al. 2001; Baldocchi 2003). Heterotrophic respiration ( $R_h$ ) was derived with an empirical model specifically developed for the UMBS forest (Curtis et al. 2005), using inputs of soil temperature and volumetric soil water content. Gross primary productivity (GPP) was calculated as the sum of estimated  $R_h$  and hourly averaged NEE. Gap-filled estimates of NEE and GPP were used when conditions did not meet the quality control criteria developed by Schmid et al. (2003). In this study, positive values of NEE represent a net uptake of  $CO_2$  by the ecosystem.

Canopy photosynthetic radiation use efficiency (RUE) was calculated as the ratio between GPP and absorbed photosynthetic photon flux density (APPFD). Hourly APPFD was calculated as:

$$APPFD = PPFD_t * (1 - \rho) * (1 - e^{(-K_b(\Psi)*LAI)}) \quad (1)$$

where  $PPFD_t$  was the hourly averaged total incident PPFD measured above the canopy,  $\rho$  was canopy reflected PPFD (%), and  $K_b$  was the hourly averaged canopy extinction

coefficient, which was dependent on solar zenith angle ( $\psi$ ) and canopy leaf angle distribution (Campbell & Norman 1988).

### *Light response curves*

A rectangular hyperbola was used to model the relationship between  $PPFD_t$  and GPP,

$$GPP = \frac{\alpha\beta PPFD_t}{\beta + \alpha PPFD_t} \quad (2)$$

where  $\alpha$  is the canopy quantum efficiency and  $\beta$  is the canopy photosynthetic potential (Ruimy et al. 1993; Gu et al. 2002; Rocha et al. 2004). A generic two parameter rectangular hyperbola was used to model the relationship between  $PPFD_t$  and NEE,

$$NEE = \frac{a PPFD_t}{b + PPFD_t} \quad (3)$$

where  $a$  and  $b$  are empirically derived parameters. Sigma Plot 2004 (Systat Software, Inc.) was used to fit the light response curves.

### *Simulation modeling*

To elucidate diurnal relationships, we fit quadratic curves to the relationship between SDF and GPP or NEE for six daily time periods based on solar zenith angle (SZA) and solar azimuth angle (SAA): early morning (SZA > 50°), mid-morning (SZA >30° & < 50°), midday before solar noon (SZA < 30°), midday after solar noon (SZA < 30°), mid-afternoon ((SZA >30° & < 50°), and late-afternoon (SZA > 50°), where solar noon was determined as SAA = 180°. For each of these time periods, we simulated a variety of global change sky condition scenarios. Each scenario was based upon published observations and trends in irradiance. First, uniform global dimming was simulated by increasing observed hourly SDF values between 1% and 10%. Similarly, global brightening was simulated by decreasing hourly SDF values within each time period by

1% and 10%. We constrained simulated SDF values by not allowing change scenario values to be greater than 1.0 or less than the observed minimum SDF, 0.11. The quadratic model fits to the observations were used to predict NEE or GPP for each dimming or brightening scenario per time period. Total gross carbon assimilation ( $A_g$ ) and net carbon assimilation ( $A_n$ ) were calculated as the sum of predicted GPP or NEE across all six time periods for each dimming or brightening scenario.

To simulation potential changes in cloud cover that may accompany altered patterns of atmospheric convection and circulation, the proportion of sky diffuse conditions (classified as sunny, partly cloudy, or cloudy) was increased between 1% and 10%, while the pooled proportion of the remaining two classes were decreased by the same proportion. Gross carbon assimilation ( $A_g$ ) and net carbon assimilation ( $A_n$ ) per time period and scenario was calculated as the sum of the means of 100 simulations. For each scenario, total growing season  $A_g$  or  $A_n$  was calculated as the sum of  $A_g$  or  $A_n$  across each of the six daily time periods.

In order to statistically assess the effects of dimming, brightening, or changed proportion of sky diffuse conditions on carbon assimilation, confidence intervals for the observed values of GPP and NEE were produced by bootstrapping the original data ( $n = 100$ ). The sum of the bootstrapped means were used as a baseline value of  $A_g$  or  $A_n$ . The statistical significance of the difference between simulated and baseline carbon assimilation was determined by comparing 95% confidence intervals.

## **Results**

### *Meteorological variables*

A total of 1092 hourly flux and meteorological observations were recorded during the study period. As SDF increased from sunny ( $SDF < 0.35$ ) to partly cloudy ( $SDF > 0.35$  and  $< 0.65$ ) and cloudy ( $SDF > 0.65$ ), significant decreases were observed in diurnal, class-averaged GPP, NEE,  $T_a$ ,  $VPD_a$ ,  $VPD_c$ , and  $PPFD_t$  (Table 1). The only variable that

significantly increased across all diffuse classes was RUE.  $PPFD_d$  significantly increased from sunny to cloudy but decreased from partly cloudy to cloudy. However  $PPFD_d$  under cloudy conditions was significantly higher than  $PPFD_d$  under sunny conditions. The only variable that did not change significantly among diffuse classes was  $T_c$ .

### *Response of NEE, GPP, and RUE to SDF*

Several enhancements in NEE and GPP were observed as SDF increased. The compensation point for NEE was 49% higher when conditions were cloudy ( $SDF > 0.5$ ) compared to when conditions were sunny ( $SDF < 0.5$ ; Fig. 1a). Under cloudy sky conditions  $NEE_{max}$  (NEE at saturating irradiance ( $2000 \mu\text{mol m}^{-2} \text{s}^{-1}$ )) was higher compared to  $NEE_{max}$  under sunny conditions (23.8 versus  $17.6 \mu\text{mol m}^{-2} \text{s}^{-1}$ ; Fig. 1a). For GPP, canopy quantum efficiency ( $\alpha$ ), derived from fitted light response curves (Eq. 2), was significantly higher under cloudy conditions than under partly cloudy or sunny conditions (Table 2). However,  $\alpha$  was not significantly different between partly cloudy and sunny conditions. Although the shapes of the light response curves for GPP were different for sunny, partly cloudy, and cloudy conditions (Fig. 1b), there were no significant differences in canopy photosynthetic potential ( $\beta$ ) among the sky condition classes.

The SDF value at which NEE was a maximum was 0.19 (Fig. 2a), while maximum observed GPP occurred at a SDF of 0.23 for GPP (Fig. 2b) when all daytime data (600-1800 EST) collected during the 2008 growing season were pooled together. The relationship between SDF and RUE was significant and linear across all sky conditions (Fig. 2c) and demonstrated no significant difference in the slope of the regression among SDF classes. Substantial differences were observed in SDF values corresponding to maximum NEE and GPP when they were divided into groups based on solar zenith angle and solar azimuth. For NEE measurements acquired before solar noon optimal SDF values were 0.46 at midday, 0.48 during the mid-morning, and 0.14 during the early morning (Figs. 3a,b,c respectively). For measurements taken after solar noon optimal SDF values were 0.46 at midday and during the mid-afternoon, and 0.16 during the late



afternoon (Figs. 3a,b,c respectively). We found that NEE was significantly higher under partly cloudy conditions as opposed to sunny conditions during midday after solar noon (Fig. 4b), mid-morning (Fig. 4c), and mid-afternoon (Fig. 4d), and was significantly lower only during the early morning (Fig.4e). During all other time periods there was no significant difference in NEE between partly cloudy and sunny sky conditions.

Optimal SDF values for GPP were somewhat different than those observed for NEE. The SDF values corresponding to maximum GPP measurements acquired before solar noon were 0.44 at midday, 0.49 during the mid-morning and 0.14 during the early morning (Figs. 5a,b,c respectively). For measurements acquired after solar noon, optimal SDF values were 0.41 at midday, 0.46 during the mid-afternoon and 0.31 during the late afternoon (Figs. 5a,b,c respectively). During mid-morning (Fig. 6c) and mid-afternoon (Fig. 6d) GPP was significantly higher under partly cloudy conditions relative to GPP acquired under sunny conditions. As with NEE, the only time that GPP under partly cloudy conditions was lower than under sunny conditions was during the early-morning (Fig. 6e).

#### *Variation in carbon assimilation under simulated changes in irradiance*

Simulated total growing season  $A_n$  was significantly higher than the baseline observed  $A_n$  for all simulations where the uniform decrease in SDF was greater than 1% , and was significantly lower than the observed baseline when the uniform increase in SDF was greater than 2% (Fig. 7a). Similarly, simulated total growing season  $A_g$  was significantly higher than the observed baseline observed  $A_g$  when the uniform decrease in SDF was greater than 1%, and significantly lower when the uniform increase in SDF was greater than 1% (Fig. 7b). The percent decline in  $A_n$  due to a uniform dimming of sky conditions was significantly greater than the decline observed in  $A_g$  (Table 3). Conversely, the percent increase in  $A_g$  due to a uniform brightening of sky conditions was significantly less than the increase in  $A_n$  (Table 3).

For simulations where the proportion of SDF classes were altered to represent change in cloud regimes, we found a significant increase of  $A_n$  over baseline conditions when the increase in proportion of observations classified as sunny was greater than or equal to 4% or when the proportion of observations classified as partly cloudy was greater than or equal to 5% (Fig. 8a). A significant decrease in  $A_n$  was observed when the proportion of observations classified as cloudy was greater than or equal to 2%. There were no significant differences in the amount of increased  $A_n$  between sunny and partly cloudy change scenarios.

We found significantly greater  $A_g$  compared to the observed baseline conditions when an increase in the proportion of sunny and partly cloudy observations was greater than or equal to 3%, and a significant decrease in  $A_g$  was found when the increase in proportion of cloudy observations was greater than or equal to 3% (Fig. 8b). Similar to the results for  $A_n$ , there were no significant differences between changes in simulated  $A_g$  for sunny and partly cloudy sky condition change scenarios.

Across all simulations where the proportion of observations in each sky condition class was altered we found that the percent change in  $A_n$  was significantly greater than the percent change in  $A_g$  (Table 4). However, for each sky condition simulation there was no significant difference between the resulting total amount of  $A_g$  or  $A_n$  (data not shown).

## **Discussion**

The results of our study showed that when all daytime hourly fluxes were considered together, there was only a very minor SDF effect on GPP and NEE (see Figs. 2a,b). The SDF values corresponding to the maximum observed GPP and NEE were 0.23 and 0.19, respectively. These ‘optimal’ SDF values were much lower than previously reported in other studies ( $\sim 0.5$ ; e.g., Gu et al. 2003; Rocha et al. 2004, Jenkins et al. 2007; Alton 2008; Knohl & Baldocchi 2008). This difference is most likely due to the fact that these other studies only assessed the relationship between SDF and carbon assimilation for midday time periods. Our results showed that the optimal SDF for NEE and GPP was

dependent on the time of day (see Figs. 3 and 5 respectively). When only considering data collected during midday time periods, our estimates of optimal SDF values for NEE (0.46) and GPP (0.41-0.44) were in close agreement with the studies cited above, but considerably lower than that reported by a study conducted at the same study site (0.57; Rocha et al. 2004). The discrepancy between our results and those of Rocha et al. (2004) may be due to the fact that they relied on modeled estimates of  $PPFD_d$ , whereas in the present study  $PPFD_d$  was measured directly.

We found that for some daily time periods NEE and GPP were significantly greater under partly cloudy conditions compared to sunny conditions (see Figs. 4 and 5). However, for early morning (see Figs. 4e and 6e) and late afternoon (see Figs. 4f and 6f) measurements there was no significant increase under partly cloudy conditions. This is most likely because all measurements during those time periods were acquired under conditions of relatively low PPFD, so that the primary SDF-related modification of the environment was a reduction in non-saturating PPFD ( $\sim 1000\text{-}1200 \mu\text{mol m}^{-2} \text{s}^{-1}$ ) that would be expected to cause GPP and NEE to decline. However, for measurements acquired at midday where PPFD was saturating and optimal SDF values fell within the partly cloudy SDF region (see Figs. 3a and 5a), we recorded significantly higher NEE only during the period after solar noon (see Fig. 4b). Several studies have shown that an increased proportion of light penetration within the canopy under diffuse conditions is the primary reason for observed enhancement of carbon assimilation (Roderick et al. 2001; Gu et al. 2002; Knohl & Baldocchi 2008). The inconsistency that we observed in enhancement under partly cloudy conditions during midday may have occurred because the difference in light penetration characteristics between sunny and partly cloudy conditions might have been less pronounced at lower versus higher solar zenith angles.

Between the 1950s and 1990s, it is estimated that globally averaged shortwave radiation at the earth's surface declined between 4% and 10% (Liepert 2002). For the period between the mid 1990s to the mid 2000s, an increase in shortwave radiation of approximately 4% has been reported (Wild et al. 2009). Our current understanding of the causes of these brightening and dimming trends is that they are due to changes in the

quantity of atmospheric aerosols and cloud cover (Stanhill & Cohen 2001; Wild 2009). Consequently, we simulated the change in  $A_g$  and  $A_n$  for an uniform increase/decrease in SDF of up to 10%, which we calculated to correspond with an increase/decrease in incident  $PPFD_t$  of approximately 5%. Thus, for a dimming of 5% we estimate a decline in growing season  $A_g$  of 3.98% ( $\sim 123 \text{ g C m}^{-2}$ ) and growing season  $A_n$  of 5.28% ( $\sim 106 \text{ g C m}^{-2}$ ; Table 3). For a brightening of 5%, growing season  $A_g$  and  $A_n$  are expected to increase by 4.46% ( $\sim 138 \text{ g C m}^{-2}$ ) and 5.28% ( $\sim 119 \text{ g C m}^{-2}$ ), respectively (see Table 3). These estimates show a somewhat greater sensitivity to both dimming and brightening than a previous study that simulated a 3% increase/decrease in tree or shrub canopy GPP for a 10% increase/decrease in incident shortwave radiation (Alton 2008). Furthermore, although our results demonstrate a larger total increase/decrease in  $A_g$  compared to  $A_n$ , they also show that the proportional change in  $A_n$  is greater than the proportion change in  $A_g$ , suggesting that  $A_n$  is more sensitive to uniform perturbations in sky diffuse fraction.

Based on our simulations, we would expect the growing season carbon assimilation at the UMBS forest to increase as the proportion of partly cloudy conditions increased relative to sunny and cloudy conditions (see Fig. 8). However, this increase would not be expected to be any greater than if there were an increase in sunny conditions relative to partly cloudy and cloudy conditions. This finding is contrary to what we expected because previous studies have reported significant increases in deciduous forest productivity following volcanic eruption (e.g., Farquhar & Roderick 2003; Gu et al. 2003), which they attributed to an increase in diffuse fraction caused by volcanic aerosols. A limitation of our study is that we did not separate the effects of aerosols and clouds. Diffuse light under aerosols is more anisotropic and is backscattered much less compared to water droplets (Farquhar & Roderick 2003). Therefore, aerosols have a more conservative effect on the total amount of light compared to clouds for any given SDF. These effects were shown to significantly reduce RUE enhancement under high levels of aerosols compared to clouds in a deciduous forest canopy (Min 2005). As our understanding of the effect of different atmospheric diffusing mediums increases, future studies should attempt to elucidate differences in the expected change in ecosystem carbon assimilation that occur due changes in either aerosols or clouds.

The results of our study have shown that it is important to consider diurnal radiation-canopy dynamics when attempting to model the influence of SDF on NEE and GPP. In general, our results are consistent with other studies that have reported carbon assimilation enhancement under moderately diffuse skies for middle portions of the day; however this effect was not always present. The differences among diurnal relationships between SDF and canopy productivity were important for determining the effect of changing solar radiation regimes on total gross and net growing season carbon assimilation. For simulations integrated over the entire growing season we did not find any significant advantage of moderately diffuse conditions compared to sunny conditions for carbon assimilation. Our results demonstrated that the UMBS forest is relatively well adapted to the average sky conditions observed during the study period. However, our simulations of global dimming and brightening scenarios suggest that significant decreases/increases in carbon assimilation occur at this forest due to long-term perturbations in the solar radiation regime.

### **Acknowledgements**

This work was supported by the Harold Heady Professorship at the University of Idaho, and by an NSF-ESPCoR grant to the State of Idaho. We would like to thank Peter Curtis, Christoph Vogel, and Danilo Dragoni for providing flux and meteorological data.

### **References**

- Alton PB, North PR, Los SO (2007) The impact of diffuse sunlight on canopy light-use efficiency, gross photosynthetic product and net ecosystem exchange in three forest biomes. *Global Change Biology*, **13**, 776-787.
- Alton PB (2008) Reduced carbon sequestration in terrestrial ecosystems under overcast skies compared to clear skies. *Agricultural and Forest Meteorology*, **148**, 1641-1653.

- Baldocchi DD, Vogel CA, Hall B (1997) Seasonal variation of carbon dioxide exchange rates above and below a boreal jack pine forest. *Agricultural and Forest Meteorology*, **83**, 147-170.
- Baldocchi D, Falge E, Gu L *et al.* (2001) FLUXNET: A new tool to study the temporal and spatial variability of ecosystem-scale carbon dioxide, water vapor, and energy flux densities. *Bulletin of the American Meteorological Society*, **82**, 2415-2434.
- Baldocchi DD (2003) Assessing the eddy covariance technique for evaluating carbon dioxide exchange rates of ecosystems: past, present and future. *Global Change Biology*, **9**, 1-14.
- Campbell GS, Norman JM (1998) *An Introduction to Environmental Biophysics*. Springer, New York.
- Curtis PS, Vogel CS, Gough CM, Schmid HP, Su H-B, Bovard BD (2005) Respiratory carbon losses and the carbon-use efficiency of a northern hardwood forest, 1999-2003. *New Phytologist*, **167**, 437-456.
- Farquhar G, Roderick M (2003) Pinatubo, diffuse light and the carbon cycle. *Science*, **299**, 1997-1998.
- Gough CM, Vogel CS, Harrold KH, George K, Curtis PS (2007) The legacy of harvest and fire on ecosystem carbon storage in a northern temperate forest. *Global Change Biology*, **13**, 1935-1949.
- Gu L, Baldocchi DD, Verma SB, Black TA, Vesala T, Falge EM, Dowty PR (2002) Advantages of diffuse radiation for terrestrial ecosystem productivity. *Journal of Geophysical Research – Atmospheres*, **107**, D64050, doi:10.1029/2001JD001242.

Gu L, Baldocchi DD, Wofsy SC, Munger JW, Michalsky JJ, Urbanski SP, Boden TA (2003) Response of a deciduous forest to the Mount Pinatubo eruption: Enhanced photosynthesis. *Science*, **299**, 2035-2038.

Hollinger DY, Kelliher FM, Byers JN, Hunt JE, McSeveny TM, Weir PL (1994) Carbon dioxide exchange between an undisturbed old-growth temperate forest and the atmosphere. *Ecology*, **75**, 134-150.

Jenkins JP, Richardson AD, Braswell BH, Ollinger SV, Hollinger DY, Smith M-L (2007) Refining light-use efficiency calculations for a deciduous forest canopy using simultaneous tower-based carbon flux and radiometric measurements. *Agricultural and Forest Meteorology*, **143**, 64-79.

Knohl A, Baldocchi DD (2008) Effects of diffuse radiation on canopy gas exchange processes in a forest ecosystem. *Journal of Geophysical Research*, **113**, G02023, doi:10.1029/2007JG000663.

Kvalevag MM, Myhre G (2007) Human impact on direct and diffuse solar radiation during the industrial era. *Journal of Climate*, **20**, 4874-4884.

Leuning R, Kelliher FM, De Pury DGG, Schulze E-D (1995) Leaf nitrogen, photosynthesis, conductance and transpiration: scaling from leaves to canopies. *Plant, Cell and Environment*, **18**, 1183-1200.

Liepert BG (2002) Observed reductions of surface solar radiation at sites in the United States and worldwide from 1961 to 1990. *Geophysical Research Letters*, **29**, 1421, doi:10.1029/2002GL014910.

Matsui T, Beltran-Przekurat A, Niyogi D, Pielke RA, Coughenour M (2008) Aerosol light scattering effect on terrestrial plant productivity and energy fluxes over the

- eastern United States. *Journal of Geophysical Research-Atmospheres*, **113**, D14S14, doi:10.1029/2007JD009658.
- Min, Q (2005) Impacts of aerosols and clouds on forest-atmosphere carbon exchange. *Journal of Geophysical Research – Atmospheres*, **110**, D06203, doi:10.1029/2004JD004858.
- Niyogi D, Chang H-I, Saxena VK *et al.* (2004) Direct observations of the effects of aerosol loading on net ecosystem CO<sub>2</sub> exchanges over different landscapes. *Geophysical Research Letters*, **31**, L20506, doi:10.1029/2004GL020915.
- Pinker RT, Zhang B, Dutton EG (2005) Do satellites detect trends in surface solar radiation? *Science*, **308**, 850-854.
- Rocha AV, Su H-B, Vogel CS, Schmid HP, Curtis PS (2004) Photosynthetic and water use efficiency responses to diffuse radiation by an aspen-dominated northern hardwood forest. *Forest Science*, **50**, 793-801.
- Roderick ML, Farquhar GD, Berry SL, Noble IR (2001) On the direct effect of clouds and atmospheric particles on the productivity and structure of vegetation. *Oecologia*, **129**, 21-30.
- Ruimy A, Jarvis PG, Baldocchi DD, Saugier B (1995) CO<sub>2</sub> flux over plant canopies and solar radiation: A review. *Advances in Ecological Research*, **26**, 1-63.
- Schimel DS, Braswell BH, McKeown R, Ojima DS, Parton WJ, Pulliam W (1996) Climate and nitrogen controls on the geography and timescales of terrestrial biogeochemical cycling. *Global Biogeochemical Cycles*, **10**, 677-692.



- Schmid HP, Su H-B, Vogel CS, Curtis PS (2003) Ecosystem-atmosphere exchange of carbon dioxide over a mixed hardwood forest in northern lower Michigan. *Journal of Geophysical Research-Atmospheres*, **108**, 4417, doi:10.1029/2002JD003011.
- Sinclair TR, Shiraiwa T, Hammer GL (1992) Variations in crop radiation-use efficiency with increased diffuse radiation. *Crop Science*, **32**, 1281-1284.
- Stanhill G, Cohen S (2001) Global dimming: a review of the evidence for a widespread and significant reduction in global radiation with discussion of its probable causes and possible agricultural consequences. *Agricultural and Forest Meteorology*, **107**, 255-278.
- Urban O, Janous D, Acosta M *et al.* (2007) Ecophysiological controls over the net ecosystem exchange of mountain spruce stand. Comparison of the response in direct vs. diffuse solar radiation. *Global Change Biology*, **13**, 157-168.
- Wild M, Gilgen H, Roesch A, Ohmura A, Long C, Dutton E, Forgan B, Kallis A, Russak V, Tsvetkov A (2005) From dimming to brightening: decadal changes in solar radiation at Earth's surface. *Science*, **308**, 847-850.
- Wild M, Truessel B, Ohmura A, Long CN, Konig-Langlo G, Dutton EG, Tsvetkov A (2009) Global dimming and brightening: An update beyond 2000. *Journal of Geophysical Research-Atmospheres*, **114**, D00D13, doi:10.1029/2008JD011382.
- Wild M (2009) Global dimming and brightening: A review. *Journal of Geophysical Research-Atmospheres*, **114**, D00D16, doi:10.1029/2008JD011470.

**Table 1.** Summary of CO<sub>2</sub> exchange and environmental conditions during the study period. Values are reported as the mean  $\pm$  95% confidence interval of hourly averaged values measured under each sky diffuse fraction (SDF) classification.

	Sunny (SDF < 0.35)	Partly Cloudy (SDF 0.35 - 0.65)	Cloudy (SDF > 0.65)
GPP (mmol m <sup>-2</sup> s <sup>-1</sup> )	19.68 $\pm$ 0.57	18.03 $\pm$ 0.97 <	12.13 $\pm$ 0.75 <
NEE (mmol m <sup>-2</sup> s <sup>-1</sup> )	13.76 $\pm$ 0.50	12.08 $\pm$ 0.91 <	6.71 $\pm$ 0.75 <
RUE	0.018 $\pm$ 0.0005	0.024 $\pm$ 0.0010 >	0.037 $\pm$ 0.0013 >
T <sub>a</sub> (°C)	21.76 $\pm$ 0.33	20.55 $\pm$ 0.41 <	17.81 $\pm$ 0.40 <
T <sub>c</sub> (°C)	19.67 $\pm$ 0.42	19.09 $\pm$ 0.57	18.63 $\pm$ 0.43
VPD <sub>a</sub> (kPa)	0.92 $\pm$ 0.05	0.76 $\pm$ 0.07 <	0.58 $\pm$ 0.05 <
VPD <sub>c</sub> (kPa)	1.11 $\pm$ 0.04	0.80 $\pm$ 0.05 <	0.45 $\pm$ 0.03 <
PPFD <sub>t</sub> (mmol m <sup>-2</sup> s <sup>-1</sup> )	1434 $\pm$ 42	952 $\pm$ 56 <	458 $\pm$ 32 <
PPFD <sub>d</sub> (mmol m <sup>-2</sup> s <sup>-1</sup> )	314 $\pm$ 11	448 $\pm$ 27 >	385 $\pm$ 25 <

< Indicates that the mean is significantly less than the mean in the preceding SDF class ( $p < 0.05$ ), whereas > indicates that the mean is significantly greater than the mean in the preceding SDF class ( $p < 0.05$ ).

**Table 2.** Estimates of canopy quantum efficiency ( $\alpha$ ), canopy photosynthetic potential ( $\beta$ ), and the coefficient of determination for the least squares regression fit of the light response curve ( $r^2$ ).

Sky condition	$\alpha$	$\beta$	$r^2$	n
Sunny	$0.023 \pm 0.003$	$52.1 \pm 9.97$	0.46	416
Partly Cloudy	$0.027 \pm 0.003$	$69.6 \pm 16.2$	0.77	257
Cloudy	$0.036 \pm 0.003$	$65.1 \pm 11.5$	0.82	419

**Table 3.** Percent change in biosphere-atmosphere exchange of CO<sub>2</sub> that would be expected with uniform brightening or dimming of the sky. Results are reported as the percent change from the baseline. The 95% confidence interval for all estimates is  $\pm$  0.5%.

Change in SDF (%)	$\Delta$ GPP		$\Delta$ NEE	
	Brightening effect (%)	Dimming effect (%)	Brightening effect (%)	Dimming effect (%)
1	ns	ns	ns	ns
2	1.01	-1.16	1.64	ns
3	1.48	-1.67	2.32	-1.90
4	1.94	-2.20	2.98	-2.63
5	2.38	-2.65	3.63	-3.27
6	2.82	-2.99	4.27	-3.78
7	3.25	-3.28	4.90	-4.21
8	3.67	-3.52	5.51	-4.58
9	4.07	-3.76	6.12	-4.94
10	4.46	-3.98	5.94	-5.28

ns = not significant ( $p < 0.05$ )

**Table 4.** Percent change in biosphere-atmosphere exchange of CO<sub>2</sub> with simulated changes in the proportion of each SDF class, where Sunny = SDF < 0.35, Partly cloudy = SDF > 0.35 & < 0.65, and Cloudy = SDF > 0.65. Results are reported as the % deviation from the baseline. The 95% confidence interval for all estimates is ± 0.5%.

Change in sky condition (%)	ΔGPP (%)			ΔNEE (%)			Hours increased
	Sunny	Partly cloudy	Cloudy	Sunny	Partly cloudy	Cloudy	
1	ns	ns	ns	ns	ns	ns	11
2	ns	ns	ns	ns	ns	ns	22
3	ns	ns	-0.78	ns	0.77	-1.53	33
4	0.96	ns	-1.07	1.10	0.95	-1.96	44
5	1.21	1.34	-1.46	1.47	1.41	-2.61	55
6	1.37	1.46	-1.76	1.90	1.59	-3.07	66
8	1.79	2.00	-2.55	2.60	2.06	-4.25	87
10	2.28	2.41	-3.20	3.30	2.74	-5.14	109

ns = not significant (p<0.05)

## Figures

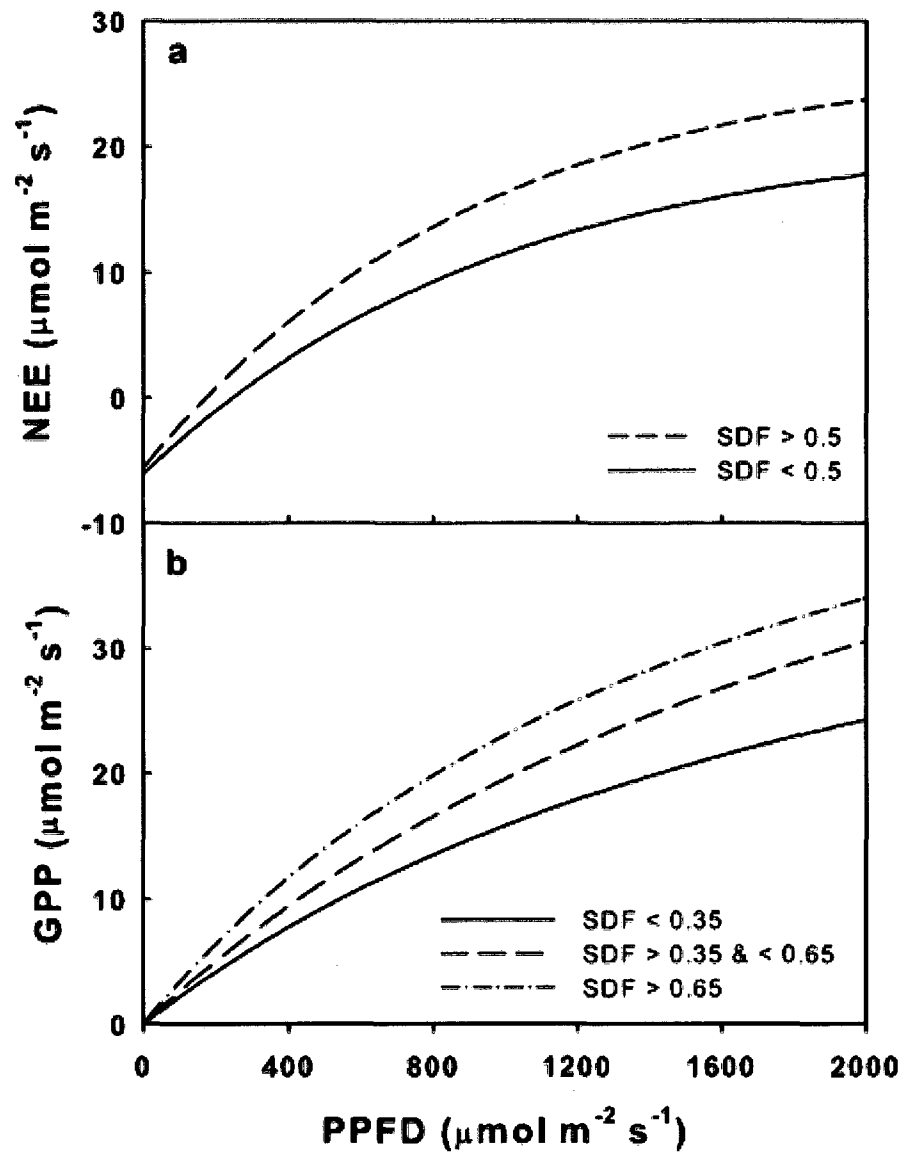


**Figure 1.** Light response curves of (a) NEE under sunny (SDF < 0.5) and cloudy (SDF > 0.5) sky conditions, and (b) GPP under sunny (SDF < 0.35), partly cloudy (SDF > 0.35 and < 0.65), and cloudy (SDF > 0.65) sky conditions.

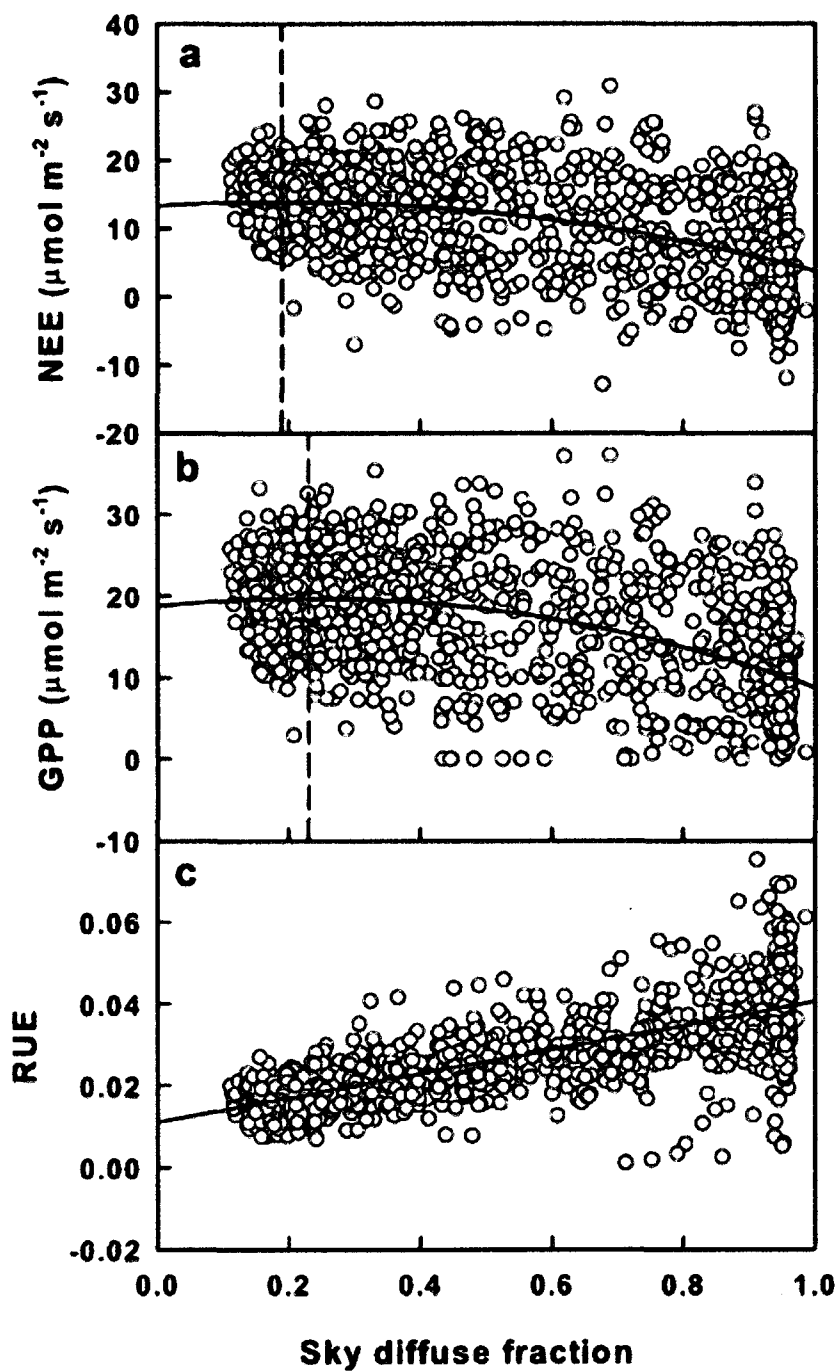


**Figure 2.** Response of hourly (a) NEE, (b) GPP, and (c) RUE to SDF. Data are from daylight hours (600 – 1800) during the growing season.

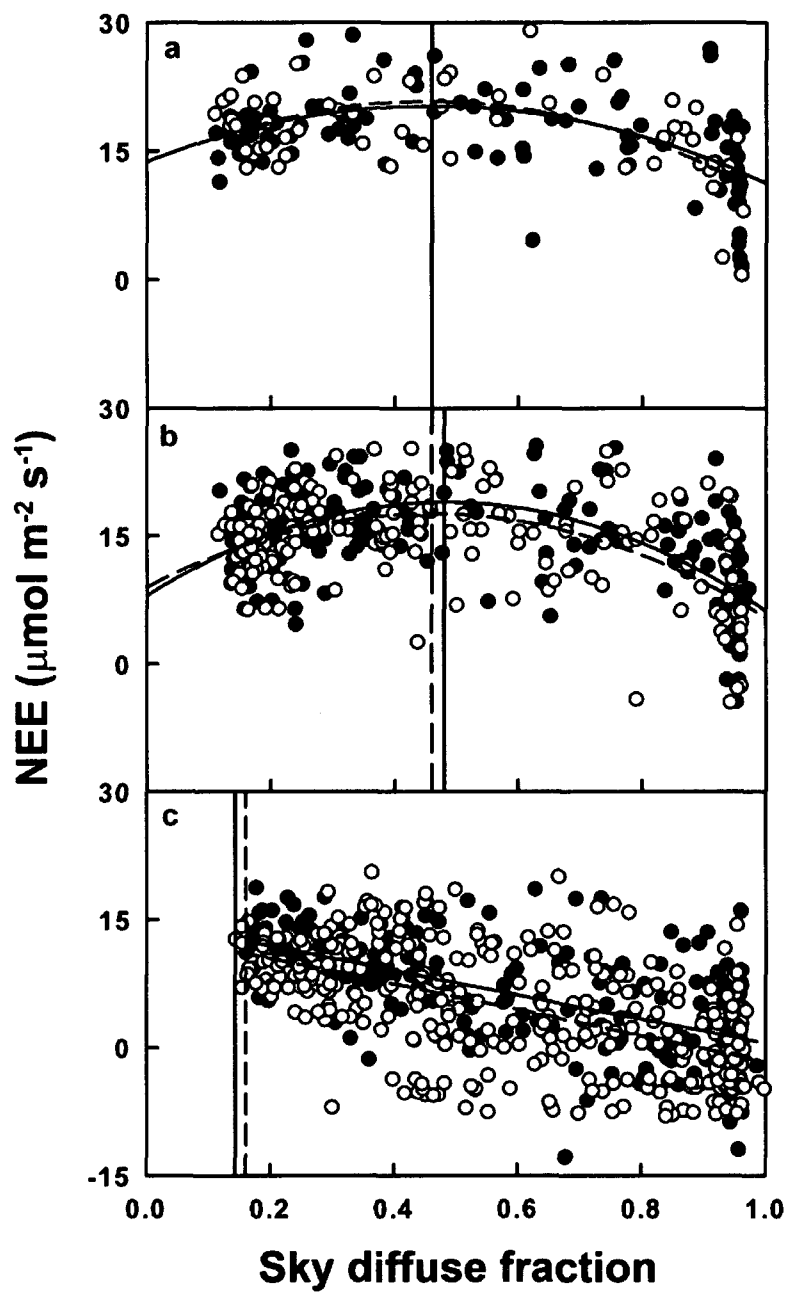


**Figure 3.** The relationship between SDF and NEE during (a) midday, (b) mid-morning and mid-afternoon, and (c) early morning and late afternoon. Solid circles represent data collected prior to solar noon and open circles represent data collected after solar noon. Vertical lines represent the optimal SDF for the time period prior to solar noon (solid line) and after solar noon (dashed line).



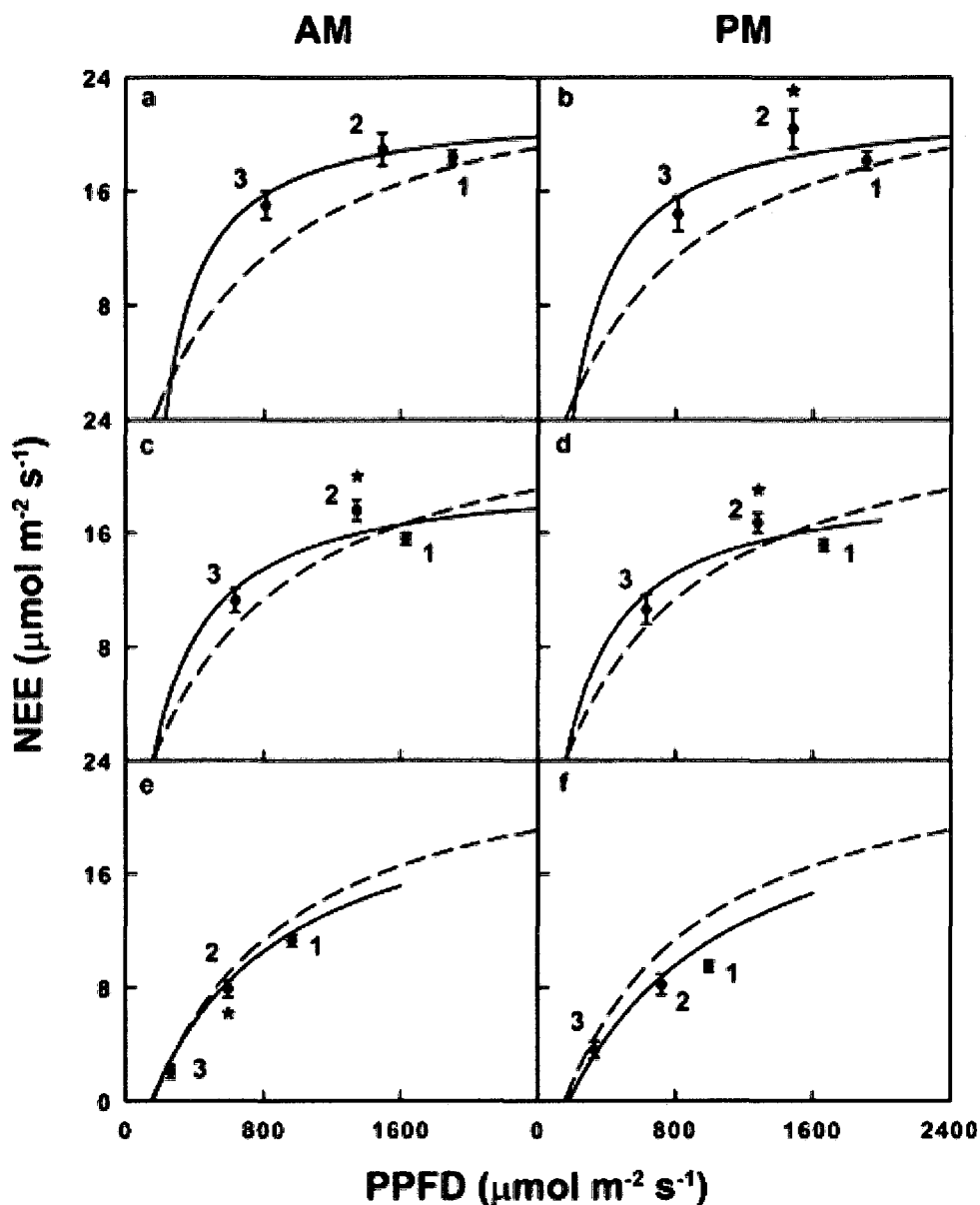


**Figure 4.** The response of sky condition-averaged NEE to incident PPFD during (a) midday prior to solar noon, (b) midday after solar noon, (c) mid-morning, (d) mid-afternoon, (e) early morning, and (f) late afternoon. The numbers beside each data point represent the sky condition class, where 1 = sunny, 2 = partly cloudy, and 3 = cloudy. The solid line is the light response curve fit to the data within each given time period, and the dashed line is the light response curve of all the data pooled together.

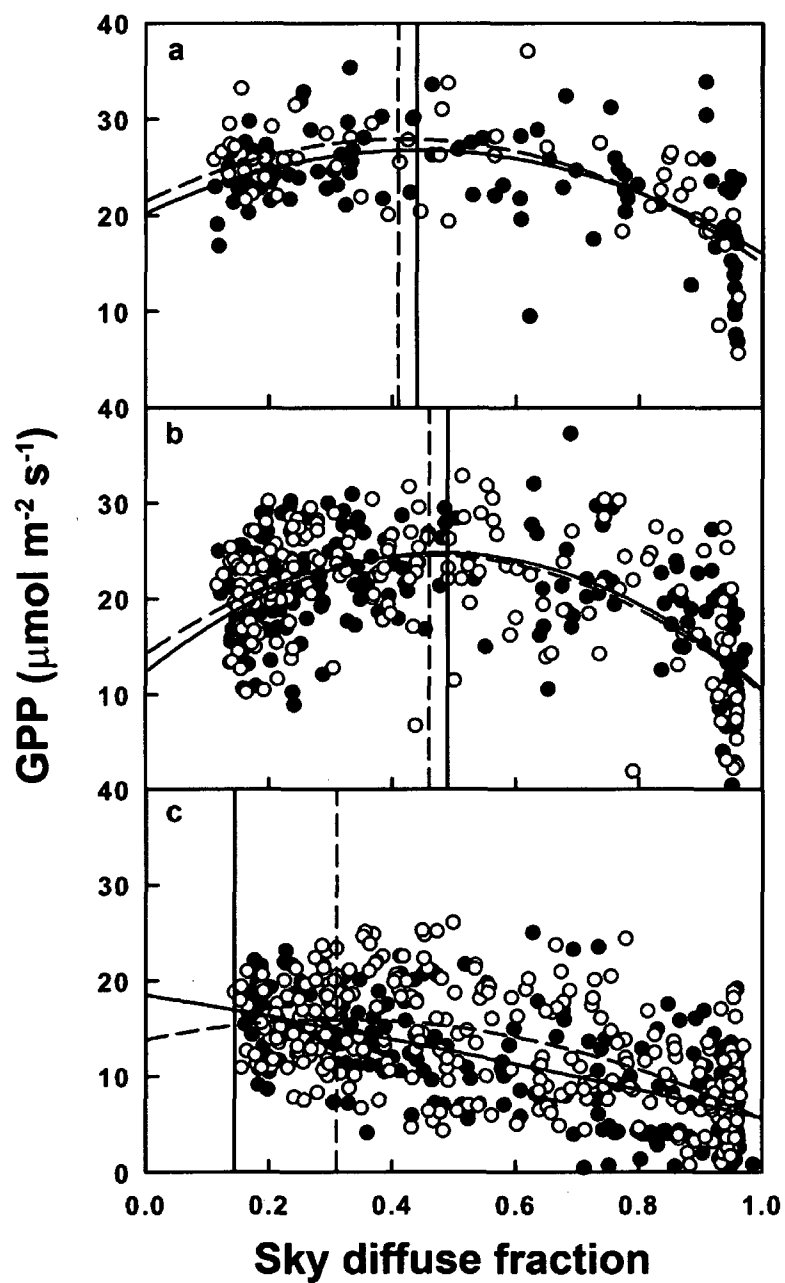


**Figure 5.** The relationship between SDF and GPP during (a) midday, (b) mid-morning and mid-afternoon, and (c) early morning and late afternoon. Solid circles represent data collected prior to solar noon and open circles represent data collected after solar noon. Vertical lines represent the optimal SDF for the time period prior to solar noon (solid line) and after solar noon (dashed line).

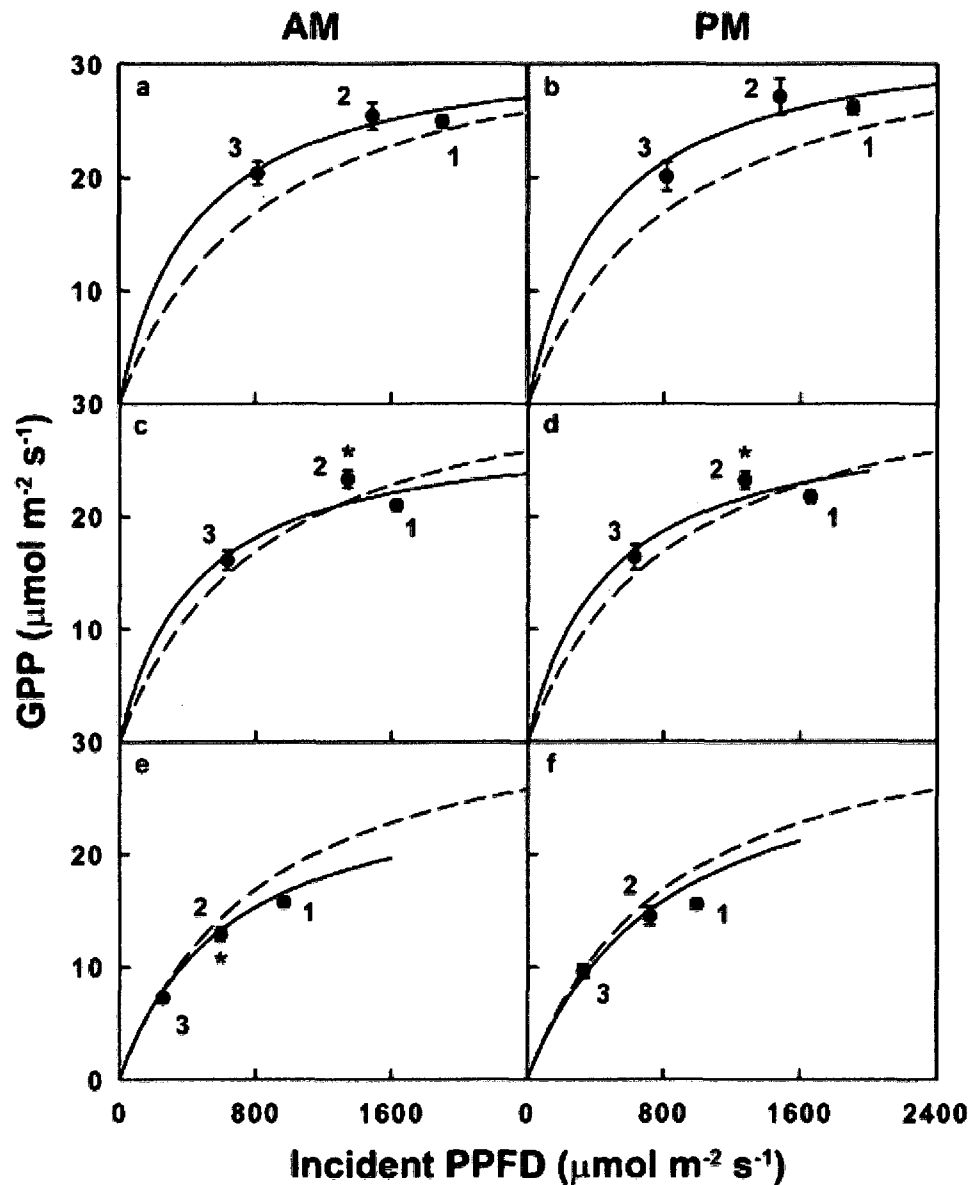


**Figure 6.** The response of sky condition-averaged GPP to incident PPFD during (a) midday prior to solar noon, (b) midday after solar noon, (c) mid-morning, (d) mid-afternoon, (e) early morning, and (f) late afternoon. The numbers beside each data point represent the sky condition class, where 1 = sunny, 2 = partly cloudy, and 3 = cloudy. The solid line is the light response curve fit to the data within each given time period, and the dashed line is the light response curve of all the data pooled together.

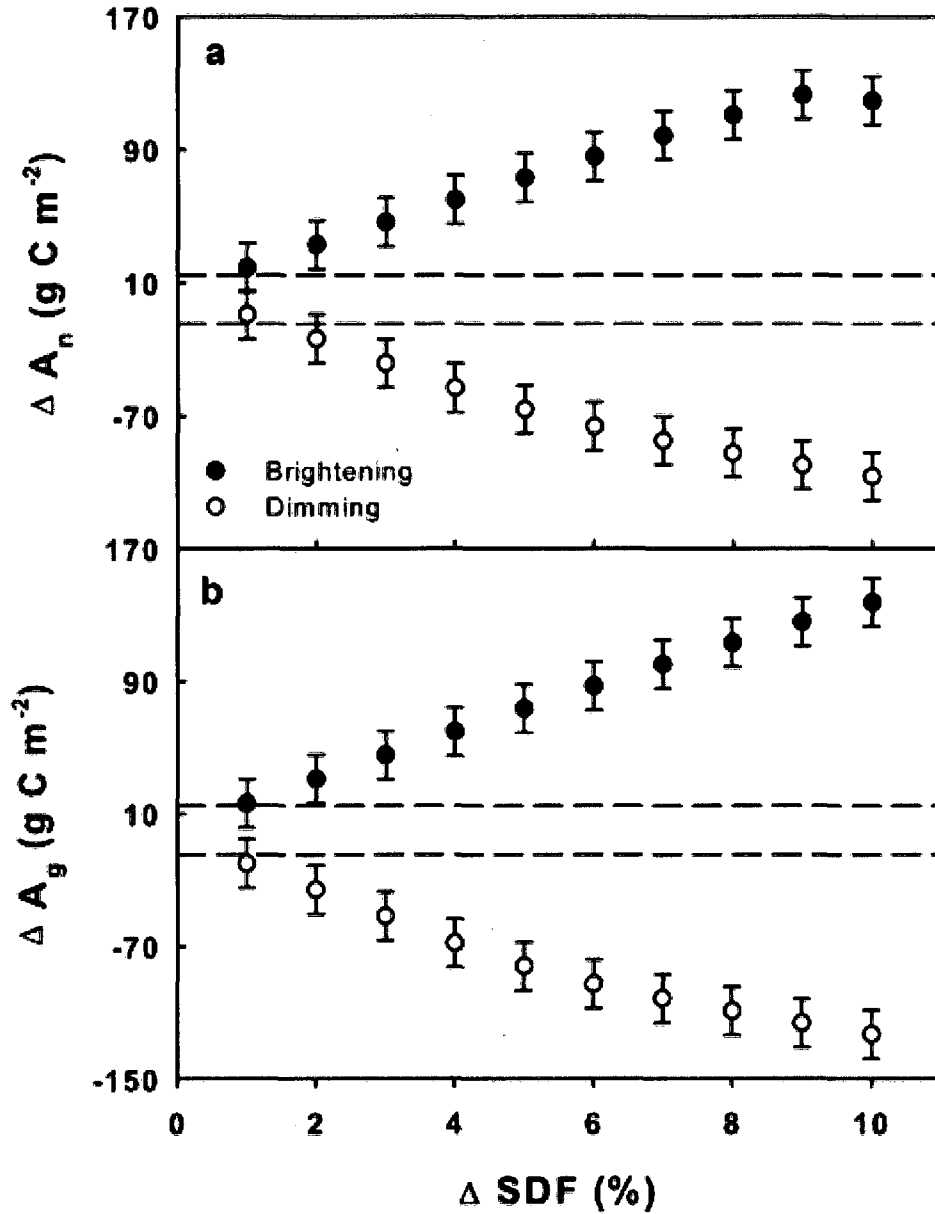


**Figure 7.** Estimated response of total growing season (a)  $A_n$ , and (b)  $A_g$  to simulated uniform brightening (closed circles) and dimming (open circles) scenarios. Data points are the mean from 100 bootstrapped estimates and error bars represent the 95% confidence interval. The horizontal dashed lines represent the upper and lower 95% confidence bounds on the bootstrapped estimate of the mean of the observed data.

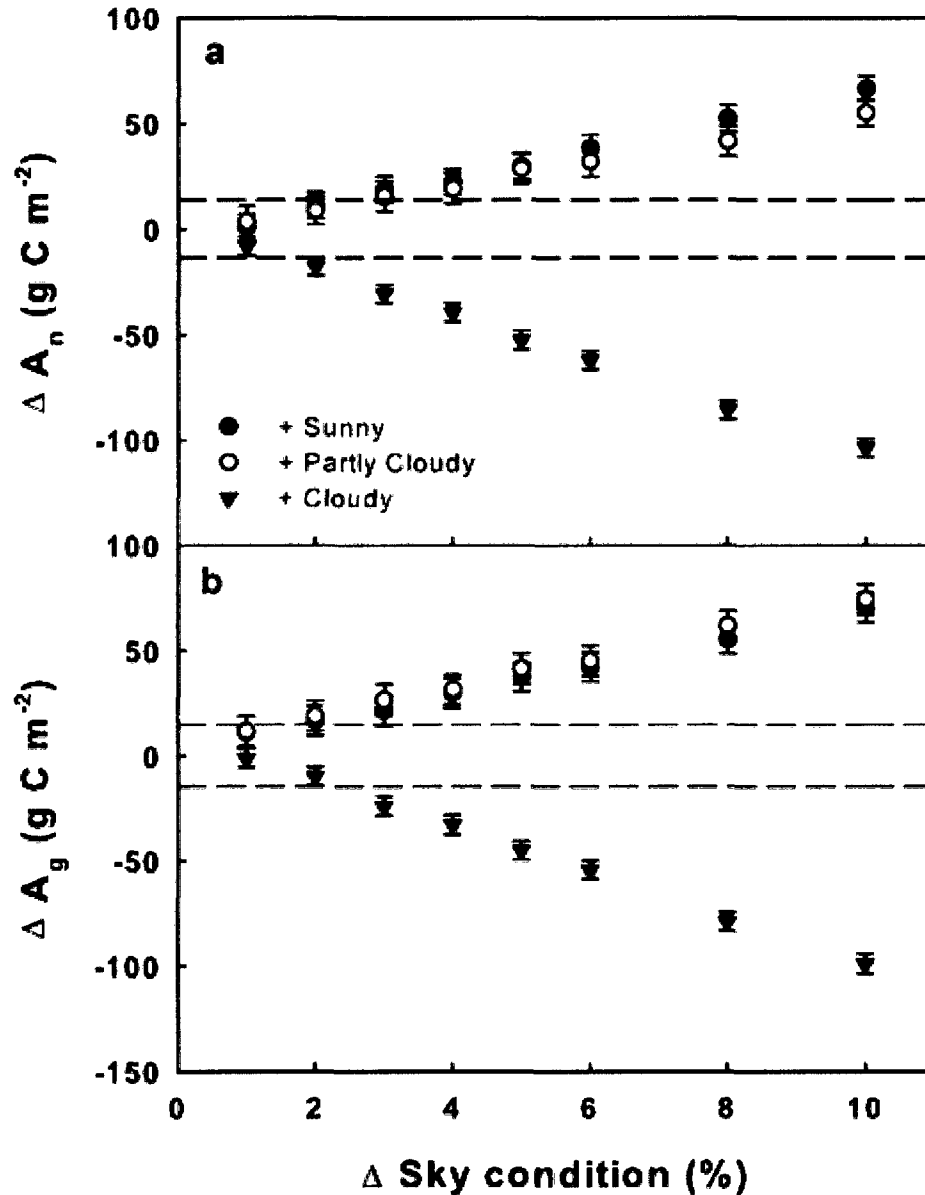


**Figure 8.** Estimate response of total growing season (a)  $A_n$ , and (b)  $A_g$  to simulated changes in the proportion of each sky condition class. Data points are the mean of 100 simulations and error bars represent the 95% confidence interval. The horizontal dashed lines represent the upper and lower 95% confidence bounds on the bootstrapped estimate of the mean of the observed data.

## CONCLUSIONS AND FUTURE WORK

This dissertation primarily focuses on improving our understanding of the response of PRI to leaf pigments and canopy structure and physiology. The research presented herein has made a significant contribution to our understanding of the leaf- and canopy-level features and processes that drive the response of PRI measurements, while demonstrating the utility of PRI measurements for further understanding of these processes. The secondary focus was to describe the relationship among varying diffuse radiation regimes and total growing season forest carbon assimilation.

This research is the first to combine measurements of seasonal changes in canopy-level PRI with leaf optical and radiative transfer simulation modeling. The combined observation-simulation experiments were used to demonstrate that several factors are responsible for seasonal patterns of PRI, including phenological changes in canopy structure and seasonal physiological acclimation. These results corroborated previous studies that observed non-uniformity in the response of PRI to changes in leaf-level RUE, and made significant contribution to our understanding of why these non-uniformities occur. Furthermore, they present a spectroscopic approach for describing the seasonal progression of canopy-level physiological acclimation to the light environment and lend support to the hypothesis that xanthophylls are an integral component of this acclimation process. Further observation-based experiments are necessary to understand how the pool sizes of individual xanthophyll pigments influence the PRI. Results from such studies are necessary to facilitate advances in leaf optical modeling as well as research into the role of canopy-level xanthophyll activity in regulating carbon assimilation.

This research is the first to rigorously test how total pools of chlorophyll and carotenoid pigments influence PRI measurements. The results conclusively demonstrate that the ratio of carotenoid content to chlorophyll content has a significant influence on the PRI. While this will confound the relationship between the de-epoxidation state of the xanthophyll cycle and measurements of PRI that are made across spatial and temporal gradients, it presented a new opportunity for remotely monitoring leaf- and canopy-level dynamics not previously explored. For example, when the PRI was combined with a vegetation index designed for chlorophyll detection, the prediction of carotenoid content

was made possible. Because carotenoids are important for light harvesting and photoprotection, the ability to quantify these pigments may improve our ability to describe the photosynthetic performance of plant canopies. Future research should test the relationship between residuals of the PRIxCI-carotenoid relationship for evidence of xanthophyll biochemistry.

There is currently a high level of interest in national observation of phenological trends in vegetated ecosystems (e.g., National Phenology Network, <http://www.usanpn.org/>). While traditional measures of phenology are well suited for understanding differences in the timing of specific events and for detecting rates of change, they are somewhat limited for being able to describe how shifts in the timing of phenological events influence biogeochemical processes. Based on the research presented here, the PRI may be used for tracking changes in phenologically related properties of plant canopies such as pigment contents, pigment ratios, and photosynthetic acclimation. This may advance our understanding of ‘photosynthetic phenology’, and thus provide a tool for monitoring the influence of climate change on biosphere-atmosphere carbon cycling.

Ultimately, the goal is to use the PRI for operational monitoring of dynamic plant canopy photosynthetic processes in support of efforts to quantify CO<sub>2</sub> fluxes between the biosphere and atmosphere across the globe. A variety of networked observational platforms currently exist that could support such observations, including orbiting satellite-based instruments and tower-based meteorological observation stations. Although satellite-based observations of PRI have been shown to be possible, their use in understanding broad spatial and temporal patterns of vegetation processes has been lacking. The research presented in this dissertation suggests that spaceborne observations could be used to understand global patterns of ‘photosynthetic phenology’, pigment dynamics, and elucidate differences in patterns and rates of canopy-level physiological acclimation to environmental conditions.

The development and of the QuadPod represents an important advance in instrumentation for canopy carbon assimilation research. The main advantages of the QuadPod over other spectroscopic instrumentation include reduced cost, automated data

collection, simplified operation, and deployment flexibility. These features make PRI and other narrowband measurements more widely accessible to scientists that do not have specialized training in spectroscopic instrumentation and measurements. Furthermore, they facilitate the simultaneous deployment of several instruments for understanding spatial and temporal patterns of ecosystem processes, and allow for instrument deployment in areas of plant canopies not typically covered by long-term observational studies. Thus, the QuadPod represents a significant advance to the Spectral Network (SpecNet, <http://spectralnetwork.net/home.htm>) vision of globally networked research locations where optical remote sensing data collection is made in conjunction with intensive meteorological and ecological observations.

Finally, empirical relationships between sky diffuse fraction and canopy carbon assimilation were used to simulate the response of a deciduous forest canopy to changes in the solar radiation regime that may occur due to fluctuations in the amount of atmospheric aerosols and cloud cover. The results of these simulations show that although the UMBS forest is relatively well adapted to the mean solar radiation regime of northern lower Michigan, total growing season carbon assimilation is relatively sensitive to uniform global dimming or brightening scenarios (approximately a 1% increase/decrease in carbon assimilation for a 1% increase/decrease in photosynthetic photon flux density that results from decreased/increased diffuse radiation). A more detailed treatment of the various environmental modifications resulting from changes in sky diffuse fraction will be necessary to more fully understand whether or not the UMBS forest is well adapted to the solar radiation regime. Future research should also distinguish between the radiation scattering effects of aerosols versus clouds to better understand how the forest will respond to various anthropogenic and natural perturbations of the atmosphere.